ATOMISTIC MODELING OF ENERGETICS AND DYNAMICS OF DIFFUSIVE AND FRICTIONAL PHENOMENA IN C_{60}/GRAPHENE-BASED SYSTEMS

MEHDI JAFARY ZADEH

M.Sc. (Hons.), Materials Science and Engineering,

Sharif University of Technology, Iran

A THESIS SUBMITTED FOR THE DEGREE OF DOCTOR OF PHILOSOPHY

DEPARTMENT OF MATERIALS SCIENCE AND ENGINEERING

NATIONAL UNIVERSITY OF SINGAPORE

2013

DECLARATION

I hereby declare that the thesis is my original work and it has been written by me. I have duly acknowledged all the sources of information which have been used for the thesis.

This thesis has also not been submitted for any degree in any university previously.

MEHDI JAFARY ZADEH

2013

Acknowledgments

My Ph.D. research would not be completed without the guidance and support of many people. Firstly, I would like to express my sincerest gratitude to my Ph. D. supervisor Prof. Zhang Yong-Wei and my co-supervisor Dr. Chilla Damodara Reddy for their guidance, inspiration and encouragement during my Ph.D. study. Their strong support and valuable comments helped me overcome lots of difficulties during my research. I would like to thank Dr. Viacheslav Sorkin from Institute of High Performance Computing (IHPC), for all his help and valuable discussions and comments.

I would like to give my thanks to the staffs in IHPC (especially Dr. Palla Murali, Dr. Liu Ping, Dr. Bharathi M. Srinivasan and, Dr. R. Hariharaputran, and Dr. Mark Jhon) and Department of Materials Science and Engineering (MSE, NUS) for their helpful discussions, support and friendship. The computational facilities provided by IHPC, and MSE Department for my research works are greatly acknowledged.

I would like to thank my friends Dr. M. Khazaei and Dr. R. Tavakoli for their kind support and scientific discussions. I have to thank my friend Dr. J. R. Jennings for all his help. I also would like to thank my other friends, especially Lisen, for their friendship and encouragement during my life and study in Singapore.

Last but not least, I would like to thank all my family members, especially my parents, for their concerns, passionate support and encouragement.

Table of Contents

Summary

Understanding the diffusive and frictional mechanisms of adsorbates on periodic or random surfaces is a ubiquitous interest. Surface diffusion is a key to control the rate of self-assembly and growth in bottom-up approaches. Moreover, friction of nanoscale moving objects (nanofriction) is important in development of nanoelectromechanical systems (NEMS), surface probing and tribological devices. Interestingly, surface diffusion and nanofriction are closely related.

Despite numerous experimental and theoretical studies having been performed to illuminate surface diffusion and nanofriction, a comprehensive atomic-scale understanding of these phenomena remains elusive. For example, continuous surface Brownian motion (BM), which is beyond the traditional picture of surface diffusion based on the thermally activated jumps, is largely unexplored. Moreover, conventional tip-based techniques, such as Atomic Force Microscopy which are widely used in nanotribology, can only evaluate the static friction between the adsorbates and their substrates. These techniques are not suitable to determine the kinetic nanofriction of mobile adsorbates. The relation between diffusion and friction of adsorbates may help to address this problem. Additionally, the effect of chemical modification or contamination of the substrate on the mobility of an adsorbate is another intriguing problem.

Computational techniques are powerful tools to address the challenging issues discussed above with the atomic-scale resolution. In this thesis, we employ molecular dynamics simulations to study the surface diffusion of a single C_{60} admolecule on graphene substrate, which is considered as a prototypical physisorbed system. We show that the C_{60} admolecule exhibits two distinct regimes of surface Brownian motion (a

quasi-continuous and a ballistic-like) on graphene. A crossover occurs between these two regimes by merely changing the temperature which alters the mechanism of exchanging the energy between the admolecule and the substrate.

We evaluate the effect of rotational degrees of freedom (DOFs) of the C_{60} admolecule on its surface diffusion. We show that there is an intermediate temperature range in which the rotational DOFs provide alternative routes for the admolecule to overcome the energy barriers and performing a quasi-Brownian motion, which enhances the admolecule mobility. Beyond this intermediate temperature range, the contribution of rotational DOFs to the overall mobility of the admolecule is negligible.

We develop a theoretical framework to study the temperature dependence of kinetic nanofriction. We use the Einstein's theory of Brownian motion to analyze the surface diffusion of the C_{60} admolecule on graphene, and show that the decrease of kinetic nanofriction coefficient with temperature in this system follows an Arrhenius form.

By comparing the diffusion of C_{60} admolecule on both pristine and hydrogenated graphene, we introduce a chemical route to control the molecular mobility. Our results demonstrate that a minute hydrogenation (dehydrogenation) of the graphene (graphane) drastically reduces the mobility of admolecule. We suggest a theoretical model, which takes the effects of both random traps and barriers into account, to predict the diffusion coefficient as a function of temperature and hydrogen coverage. Our findings provide insights into the understanding of the diffusive and frictional phenomena at the nanoscale, and may help to develop future NEMS.

List of Tables

List of Figures

List of Symbols

α	Diffusion exponent
Γ	Effective jump frequency
Γ_0	Effective jump frequency prefactor
γ	Stokes coefficient
Δ	Dissipation parameter
$(\delta N)^2$	Square fluctuation of the number of adsorbed particles
η	Kinetic nanofriction coefficient
θ	Coverage of adsorbates on the surface
μ	Chemical potential
ν_{osc}	Vibrational frequency of the adsorbate
$\boldsymbol{\xi}$	Stochastic force
ρ	Adsorbate concentration
τ_p	Momentum relaxation time of the Brownian particle
$<\tau>_{hom}$	Average dwelling time at the bottom of the energy well of a homogeneous system
$<\tau>_{het}$	Average dwelling time at the bottom of the energy well of a heterogeneous system
Φ	Velocity autocorrelation function
Φ_{Norm}	Normalized velocity autocorrelation function
A	Surface area
a	Lattice parameter
c_t, c_b, c_H	Concentration of energy traps, energy barriers and hydrogen atoms, respectively

D^*, D	Tracer surface diffusion coefficient
D_c	Collective surface diffusion coefficient
D_{hom}	Tracer Diffusion coefficient of a homogeneous system
D_{hett}	Tracer Diffusion coefficient of a heterogeneous system containing traps
D_{hetb}	Tracer Diffusion coefficient of a heterogeneous system containing barriers
D_{Norm}	Normalized tracer diffusion coefficient of a heterogeneous system
d	Spatial dimensionality of the system
E_0	Initial total energy of the adsorbate
E_a	Diffusion activation energy
F	Deposition flux
F_{fric}	Friction force
$\boldsymbol{F_i}$	Force vector acting on the *i*th particle
f	jump correlation factor
J	Flux of the adsorbates
k_B	Boltzmann constant
$< l^2 >$	Mean square jump length
m	Mass
N	Number of particles
$n(t)$	Number of jumps at a given time
$P(\boldsymbol{r}, \boldsymbol{v}, t)$	Phase-space probability distribution
p_b	Distribution density of the barriers
p_t	Distribution density of the traps
$\boldsymbol{r}$	Position vector
$\boldsymbol{r}_i(t)$	Position vector of the *i*th particle at time *t*

$\langle \boldsymbol{R}(t) \rangle$	Mean displacement at a time t
$\langle \boldsymbol{R}^2(t) \rangle$	Mean square displacement at time t
t	Time
T	Temperature
v	Velocity
$\boldsymbol{v}$	Velocity vector
$U(\boldsymbol{r}_1, \ldots, \boldsymbol{r}_N)$	Potential energy function
$V(x)$, $V(r)$	One and two dimensional potential energy surface, respectively

List of Abbreviations

1D, 2D, 3D	One, two and three dimensional, respectively
AFM	Atomic force microscopy
AIREBO	Adaptive Intermolecular Reactive Empirical Bond Order
BLBM	Ballistic-like Brownian motion
BM	Brownian motion
CG	Conjugate gradient
CNT	Carbon nanotube
COM	Center of mass
DFT	Density functional theory
DOFs	Degrees of freedom
EBL	Electron beam lithography
FDT	Fluctuation dissipation theorem
FEM	Field emission microscopy
FFM	Friction force microscopy
FIM	Field ion microscopy
FPE	Fokker-Planck equation
FQM	Fluorescence quenching microscopy
GNR	Graphene nanoribbon
HAS	Helium atom scattering
LAMMPS	Large−scale Atomic/Molecular Massively Parallel Simulator
LE	Langevin equation
LITD	Laser induced thermal desorption
LJ	Long jump

LOD	Linear optical diffraction
MC	Monte Carlo
MD	Molecular dynamics
MSD	Mean square displacement
NEMS	Nanoelectromechanical systems
NR-C_{60}	Non-Rotational C_{60}
PEEM	Photoemission electron microscopy
PSE	Potential energy surface
QCBM	Quasi continuous Brownian motion
QCM	Quartz crystal microbalance
QHAS	Quasi-elastic helium atom scattering
R-C_{60}	Rotational C_{60}
SE	Stokes-Einstein (relation)
SCPM	Scanning contact potential microscopy
SJ	Single jump
STM	Scanning tunneling microscopy
TST	Transition state theory
vdW	van der Waals

1 Introduction

The idea of manipulating matter at the atomic scale was inspired by Richard Feynman's 1959 visionary lecture "There's plenty of room at the bottom" [1, 2]. He predicted the rise of a new era of science and technology that can change people's lives by molecular machinery, denser computer circuits, compact data and energy storage, and nanoscale medical technology. Over the several decades since then, scientists have been trying to miniaturize devices at the atomic and molecular scales (0.1-100 nm). Invention of scanning tunneling microscopy (STM) [3] and atomic force microscopy (AFM) [4, 5] made it possible to observe and manipulate single atoms. Discovery and synthesis of buckyballs [6-8], carbon nanotubes (CNTs) [9-11], graphene [12-17], and quantum dots [18, 19] have provided opportunities to design nanodevices with diverse and extraordinary functionalities. Moreover, the quest for nanoscale devices which can resemble macroscale machinery has stimulated development of a variety of nanoelectromechanical systems (NEMS) [20, 21], such as nanobearings [22, 23], nanogears [24], and nanomotors [25, 26].

Currently, the most popular fabrication method in microelectronics is "top-down" in which the process is basically started with a bulk substance, and then the bulk is modified into smaller structures using chemical, mechanical, optical, or other forms of energy [27]. In nanotechnology, the top-down approach is realized by using electron beam lithography (EBL), writing and stamping [28]. However, the top-down techniques are close to their limits of scaling, and extensive effort and investment are needed to upgrade existing equipment. Moreover, as device features become smaller than 100 nm,

application of conventional techniques and materials, *e.g.* silicon, faces fundamental problems such as a large spread in device characteristics owing to device size fluctuations [29, 30]. Therefore, development of alternative fabrication methods based on a "bottom-up" approach is crucial to address ever-increasing demands for miniaturization of devices [29, 31, 32]. In contrast to the top-down approach, in which the structure is imposed, in the bottom-up approach, a complex structure is synthesized on the surface from atoms or molecules (building-blocks) which assemble themselves by covalent bonds, or by molecular recognition, *i.e.* bonding through non-covalent interactions such as van der Waals forces [33-35] (see Figure 1.1). As an important advantage of the bottom-up approach, at least one critical dimension of the device can be defined and controlled during the synthesis process with near-atomic-scale precision [29]. This precise control goes beyond that is achievable in the top-down approach, and represents a key feature motivating these efforts.

In the bottom-up approach, the building-blocks are deposited on a surface (substrate) at finite temperatures, and the self-assembled nanostructures evolve as a result of spontaneous growth processes [36]. This approach provides an efficient and versatile tool for mass production of nanostructures [37, 38]. In research-scale production, building-blocks can be manipulated to synthesize nanostructures by pushing and pulling them using external driving forces (by employing an AFM or STM tip) [39]. Consequently, a comprehensive understanding of elementary phenomena governing self-assembly and mobility of nanoscale building-blocks on surfaces is necessary to design efficient bottom-up techniques.

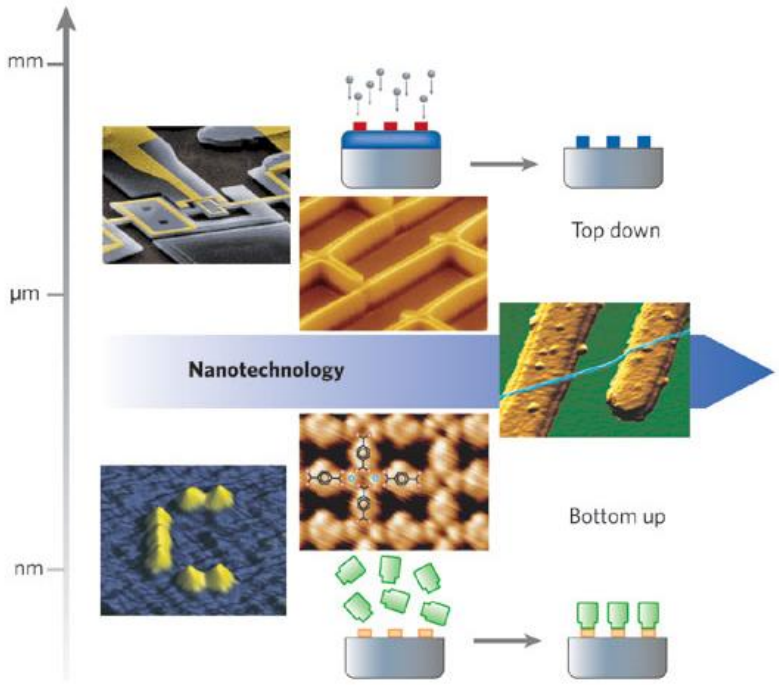

Figure 1.1 Two main approaches of controlling matter and fabricating structures at the nanoscale. In top-down techniques, several methods like lithography, writing, or stamping are employed to form the desirable features from the bulk. Bottom-up approaches rely on self-processes to order atoms and molecules to form the structures. The insets from top left in the clockwise order show a Scanning Electron Microscopy (SEM) of a nanomechanical device fabricated by electron beam lithography (EBL), structured thin film of CNTs, a single CNT connecting two electrodes, a nanoporous metal-organic network consisting of functional molecules and iron atoms, and the letter "C" obtained by manipulating and positioning 7 carbon monoxide (CO) molecules using STM tip [27].

1.1 Surface diffusion controls the self-assembly and growth mechanism

As it is described in the previous section, in the bottom-up approach, the building-blocks are deposited on a surface (substrate) at finite temperatures, and the self-assembled nanostructures evolve as a result of spontaneous growth processes [36]. During self-assembly and growth, adsorbed building-blocks (*adsorbates*) move randomly on the surface, due to thermal fluctuations of the substrate atoms. They may be frequently either trapped on the sites (*potential well*s, or *adsorption sites*) which offer them strong binding,

or may acquire enough thermal energy and escape from these sites. This process is called *surface diffusion*, which is conventionally known as a thermally activated mechanism: the adsorbate overcomes the energy barriers by the means of thermal energy [37]. The diffusion rate is the measure of mobility of the adsorbate, and is commonly quantified by the surface diffusion coefficient, D, defined as the mean square distance travelled by the adsorbate per unit of time [40]. The temperature dependence of D is conventionally described by an Arrhenius law.

The growth mechanism is governed by the energetics and dynamics of the system where the competition between thermodynamics and kinetics may lead to formation of equilibrium or non-equilibrium structures, respectively [41]. If the adsorbates are deposited on the substrate with a given flux, F, then D/F (the ratio of surface diffusion coefficient to deposition rate) is a measure of the average distance that an individual adsorbate can travel on the surface before it meets another adsorbate, either to form a new nucleus or to attach to an existing aggregate [27]. Therefore, the growth mechanism and the final self-assembled structure can be predicted based on the ratio D/F [42, 43]. If surface diffusion of adsorbates is fast compared to their incident flux (large values of D/F), the adsorbates have sufficient time to explore the surface and find the most energetically favorable (equilibrium) configuration. Hence, many aspects of the system can be explained and predicted by employing energetic principles and equilibrium laws of thermodynamics (*i.e.* the process is thermodynamically controlled [41, 44, 45]). In contrast, if the diffusion rate (adsorbate mobility) is limited (D/F is small), the adsorbates do not have the much chance to assemble in an equilibrium manner. This process is controlled by kinetic effects and results in a non-equilibrium structure. To explore and

describe such a process, analysis of only the energetics is not sufficient, and dynamical models such as Monte Carlo (MC) or kinetic MC simulations are required [41, 46-48]. Figure 1.2 illustrates the thermodynamically and kinetically controlled growth scenarios determined by the *D/F* ratio. Therefore, a solid understanding of surface diffusion process is important in all bottom-up approaches since it is a key to control the self-assembly of nanostructures.

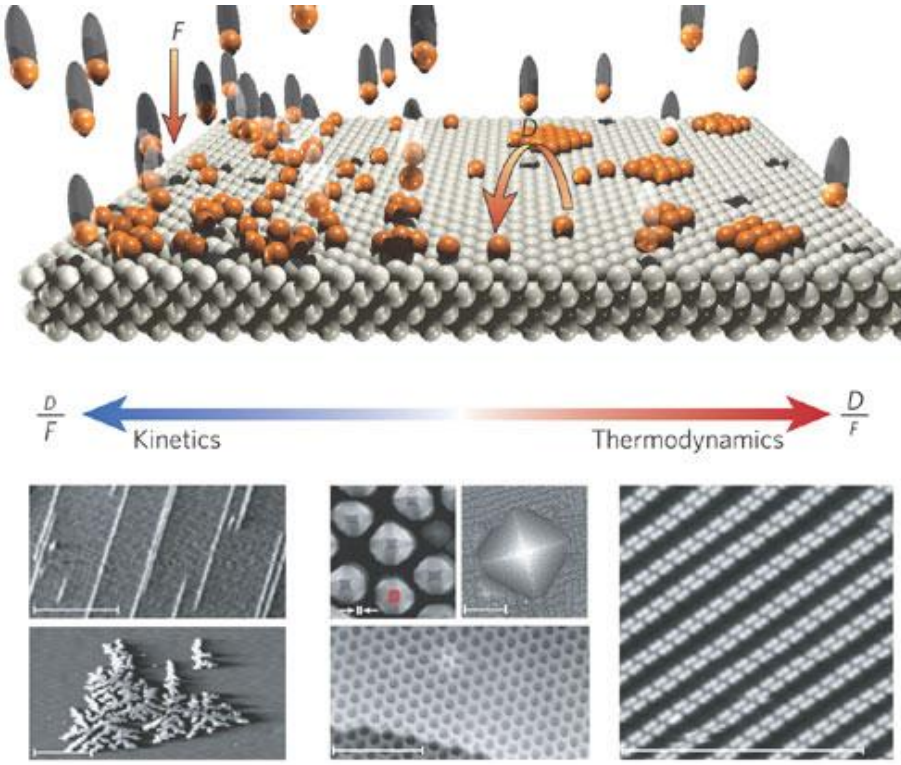

Figure 1.2 Growth processes on a surface at the atomic-scale. The atoms or molecules (building-blocks) are deposited (with flux *F*) on the surface from a vapor phase or an incident beam. The adsorbed building-blocks (adsorbates) diffuse on the surface (with rate *D*) until they meet other adsorbates and form new aggregation nuclei, or attach to other pre-formed islands. The type of growth is strongly dependent on the *D/F* ratio. Metallic islands (micrographs on the left-hand side) are controlled by growth kinetics (small *D/F* values). The super-molecular self-assembly (the micrograph on the right) is based on molecular recognition at equilibrium conditions (large *D/F* values). Semiconductor nanostructures (the micrographs in the centre) are usually grown at intermediate *D/F*, and hence the complex interplay between kinetics and thermodynamics determines their morphology [27].

1.2 Surface diffusion and friction of nanoscale objects

1.2.1 Nanofriction

As it was described above, the basic building-blocks in bottom-up approaches can be manipulated by driving forces to pull, push or slide them on a substrate [49]. The applied driving force must be adjusted to overcome the friction between the adsorbate and the substrate. However, quantification of friction between the building blocks and the substrate at the atomic scale is a challenging issue for both experimentalists and theoreticians [50].

It is common at all length scales that friction dissipates the kinetic energy of moving objects into the surrounding/contact media in the form of thermal energy [51]. At the macroscopic level, friction and lubrication are well-explored phenomena, and various empirical laws have been proposed to describe the frictional behavior of surfaces with different characteristics and chemistries [52]. However, the macroscopic rules of friction such as Amonton's law are not generally applicable to nanosystems [53] due to the significant role of atomic interactions and thermal fluctuations at the nanoscale contacts [51]. Experimental studies of tribological properties of a variety of materials support that adhesion and friction at the nanoscale are strongly system- and size-dependent [54].

A widely used experiment to measure nanofriction is performed by sliding a conical AFM tip on the top of a surface, and measuring the bending torsion of the cantilever induced by the surface frictional forces [55]. Such experiment is known as Friction Force Microscopy (FFM), in which the contact is between the tip apex (with a nominal size of a few nanometers) and the surface. However, the measurements may be significantly affected by the material, size, and shape of the tip [54, 56-58]. Moreover, during the

scanning procedure, the tip shape and/or angle may change and cannot be evaluated independently [58]. Hence, controlling the contact area remains an important problem in FFM measurements. These complexities illustrate that conventional experiments cannot be readily employed to evaluate the frictional forces between nanoscale building-blocks and their underlying substrates.

1.2.2 Surface diffusion and nanofriction

Previously we discussed surface diffusion and friction at the nanoscale. These two phenomena are closely related at the atomic scale, and hence studying surface diffusion may help to elucidate the frictional properties at the nanoscale contacting interfaces. For example, during the pushing of an atom or molecule, or sliding a nanoscale tip along the surface, it has to overcome the energy barriers, which is similar to the surface diffusion process. On the other hand, during the surface diffusion, a nanoparticle experiences friction while it interacts with the energy barriers of the surface. To some extent, surface diffusion can be considered as sliding of the adsorbate affected by infinitesimal driving force in thermal equilibrium [59]. Experimentally, this condition can be realized in Quartz Crystal Microbalance (QCM) measurements [60]. Thus, the dynamics of friction between sliding nanoparticles and the surface can be qualitatively and/or quantitatively studied by measuring surface diffusion (see Chapter 6).

1.3 Motivations of the thesis

1.3.1 Structured graphene-based substrate for mass transport

As discussed in the previous sections, an important goal of nanotechnology is to develop robust techniques to manipulate atoms and molecules at the nanoscale, for example, by

using AFM or STM tips. However, such tip-based techniques are not scalable and are limited to a small number of nanoparticles.

Since carbon nanotubes (CNTs) [9-11] are mechanically robust and chemically inert, they provide sustainable tracks for mass transport. Researchers have successfully conveyed atoms in a certain direction through CNTs by applying a large electric current [61, 62]. If other materials are used, the applied current required to impose the directional motion may destroy the tracks [63].

Similar to CNTs, graphene [12-17] carbon atoms form strong covalent sp^2 bonds. In addition, its electronic conductivity is similar to that of CNTs [64, 65]. Therefore, it is expected that graphene can be used as a mass conveyor. The graphene geometry can be modified using conventional techniques such as lithography. It can be structured to develop complex circuits for mass transport. Recently, the possibility of transport of chemically absorbed (chemisorbed) [66] atoms on graphene has been demonstrated [63]. More elaborated theoretical and experimental studies are required for better understanding of the motion of a variety of molecules on graphene-based substrates, which will be used in future applications.

1.3.2 Physisorption of fullerenes on graphene and the importance of van der Waals interactions

The successful fabrication of molecular structures and devices on a surface strongly relies on understanding the interactions between the adsorbed molecules (*admolecules*) and their underlying substrate, as well as the intermolecular interactions [67]. These interactions play a key role in dynamic processes such as diffusion, friction, conformational changes, and molecular rotation, which play an essential role in

nucleation and growth of self-assembled structures. The van der Waals (vdW) interactions play a prominent role in the structure and properties of physisorbed organic/organic interfaces [68]. Studies have revealed that very weak vdW attractive forces between C_{60} molecule and graphene substrate is the reason for the physisorption in the system [69, 70]. The fact that both C_{60} and graphene exclusively consist of carbon atoms (without any other atoms which may lead to long-range interactions) allows the C_{60}/graphene system to be one of the best adsorbate/substrate systems to study the effect of vdW interactions on dynamic processes occurring in physisorbed systems.

It must be noted that efforts to understand the origins of friction are ongoing, particularly to evaluate the contributions of electronic excitations and thermal vibrations in the systems to the frictional mechanisms [71]. Since in a physisorbed system such as C_{60}/graphene, the effect of electronic excitations on the dynamics of the adsorbate is negligible, studying the dynamics of this system would help evaluate the contribution of lattice thermal vibrations to the friction [72].

Moreover, since the calculation of vdW interaction energies is still a challenging task for the conventional first-principles methods, studying the C_{60}/graphene system may also help to evaluate and develop theoretical frameworks to describe vdW forces [68].

1.3.3 Applications of the C_{60}/graphene system in nanotechnology

Organic molecules adsorbed on graphene may find numerous technological applications [73, 74]. For example, monolayers of C_{60} on graphene, which have been realized recently [75, 76], may be used for molecular bearings [77], spintronics and quantum computing [76, 78]. The exceptionally weak molecule-surface interactions in the C_{60}/graphene system offer possibilities to use this system in photovoltaic devices in which minimal

charge transfer between the functional molecular components and the underlying substrate is desired [79]. Hence, C_{60}/graphene may serve as a model system for better understanding of molecule/surface interactions in graphene-based organic photovoltaic applications.

In addition, it has been shown that three-dimensional (3D) rotation of C_{60} molecule plays a significant role in achieving very low static friction at the graphite/C_{60}/graphite interface [80]. Owing to their spherical shape and 3D rotational degrees of freedom (DOFs), buckyballs such as C_{60} have been suggested as suitable wheels for rolling translation on surfaces [81]. Besides these applications, employment of C_{60} for drug and gene delivery is at an early stage of development in medical field [82, 83]. These promising applications indicate the importance of understanding the mechanisms of motion of C_{60} molecule in a variety of environments.

Surface diffusion of C_{60} on graphene-based substrates has recently received much attention, and theoretical studies have revealed a shallow potential energy surface (PES) due to the very weak vdW interactions between C_{60} and graphene [84]. Therefore, from a scientific point of view, the C_{60}/graphene system is also an ideal candidate to explore the role of pure vdW interactions in dynamic processes such as molecular diffusive and frictional mechanisms in physisorbed systems (see Section 1.3.2).

1.4 Open questions and objectives of the thesis

We chose the C_{60}/graphene system as an ideal prototype model to investigate the energetics and dynamics of molecular surface diffusion and its relation to the nanofriction. Considering this system, the main objective of the thesis is to address a variety of open

questions related to surface diffusion, nanofriction and molecular mobility, as described below.

1.4.1 Diffusive regimes beyond the conventional picture of surface diffusion

The conventional knowledge of surface diffusion is based on the thermally activated jump mechanism (stick-slip motion) [85], and has been commonly described by transition state theory (TST) [86, 87]. However, theoretical studies suggested that increasing the temperature leads to deviations from this model, and a crossover from the low-temperature jump regime to the high-temperature continues Brownian regime might be expected [88]. Although different regimes of continuous BM in systems with high and low friction are theoretically predicted [89, 90], observation of these regimes in real systems is scarce. Only one case of surface BM in a real system with high friction has been reported unequivocally [72]. Due to their scientific and technological importance, various regimes of surface diffusion in different conditions must be mapped and their corresponding physical mechanisms have to be uncovered. However, despite experimental [40] and theoretical studies [90, 91], many problems associated with molecular surface diffusion remain unsolved, especially in the systems with small energy barriers and/or low friction [92].

1.4.2 Effect of rotational degrees of freedom of admolecules on their surface diffusion

In contrast to an adatom, an admolecule occupies a finite space and has rotational degrees of freedom (DOFs), which may play an important role in its interactions with the substrate. Consequently, the surface diffusion of an admolecule is more complex than its atomic counterpart [93, 94]. Hence, understanding the effect of rotational DOFs of

molecules on their diffusive behavior is not only important to understand the different regimes of motion in nano-sized contacting objects, but is also essential to achieve the ability of tuning their dynamics. This ability may allow us, for example, to control the direction of motion of adsorbates [95], or to manipulate the tribological performance of self-assembled thin films [96]. In addition, the complexity of molecular surface diffusion raises questions of applicability of conventional theories of atomic surface diffusion, because these theories do not take the effect of admolecule rotational DOFs into account. Hence, in the current work, we chose C_{60}/graphene as a model system, and used molecular dynamics (MD) simulations to answer several important questions regarding molecular surface diffusion: 1) How do the rotational DOFs alter the diffusion regimes? 2) How to quantify the effect of rotational DOFs on the mobility of admolecules in each regime? 3) What is the role of rotational DOFs in the interactions between the admolecule and the substrate?

1.4.3 Temperature effects on the kinetic friction of nanoscale building blocks

To develop high-performance nanoelectromechanical systems (NEMS) by using bottom-up approaches, understanding frictional mechanisms in different regimes for various basic building blocks is essential [97]. One of the main caveats of NEMS is the reliability and controllability of molecular motion in the presence of nanofriction and thermal fluctuations [98, 99].

Nanoscale imaging and testing techniques, *e.g.* atomic force microscopy (AFM), are conventionally employed to measure nanofriction; however, their results are influenced by the tip-size and shape [56]. During an experiment, evaluating and controlling the real contact area between the tip and the surface remains an important unsolved problem [58]

(see Section 1.2). A possible solution to determine the interfacial friction between a nanoscale adsorbate and its underlying substrate would be to use the "*tip-adsorbate manipulation*" technique [58], which offers measurement of nanofriction at well-defined atomic-size contacts between arbitrary materials. Nevertheless, only static nanofriction between adsorbates and the surfaces has been measured by this technique [50, 58], and it is too slow to determine the kinetic nanofriction of mobile adsorbates [72].

The Einstein's theory of Brownian motion, which is widely applied in microsystems, provides a link between the diffusion coefficient of a Brownian particle and the (kinetic) frictional forces imposed on it from the environment [100]. Therefore, BM of a single nanoparticle on a surface, which was recently found far below room temperature [72], can give us an opportunity to study kinetic nanofriction, and develop reliable and controllable NEMS. Moreover, since these devices are operating at finite temperatures, understanding the relation between friction and temperature becomes crucial.

1.4.4 Controlling molecular mobility by altering the substrate chemistry

How to accurately control the motion of nanoscale building blocks on functionalized/contaminated surfaces is a challenging problem that is crucial for developing high performance NEMS, and for guiding self-organized patterns and structures. Recently, a graphene Moiré pattern was employed to trap and construct arrays of C_{60} molecules for homoepitaxy of graphene nanostructures [101]. Meanwhile, chemically functionalized domains on graphene were demonstrated to trap and pack molecules [102]. However, the theoretical framework for the dynamics of molecular mobility and diffusive behavior on functionalized graphene is still lacking. It is both important and imperative to develop such a theoretical framework.

1.5 Outline of the thesis

The thesis is organized into eight chapters to address the respective problems and open questions discussed in Section 1.4. The main focus of the research is to study the energetics and dynamics of surface diffusion in the C_{60}/graphene system. First we give a brief review of surface diffusion phenomena in Chapter 2. We review some of the most important experimental and theoretical techniques used to study the surface diffusion. Then, in Chapter 3, the computational techniques applied in the present simulations are described. In this chapter, we emphasize the suitability of the molecular dynamics technique (MD) to address different aspects of molecular surface diffusion, which makes it unique among other approaches. In Chapters 4 to 7 we address the main objectives of the thesis that were described as a set of open questions in Sections 1.4.1 to 1.4.4, respectively. In Chapter 4, we describe two distinct regimes of nanoscale BM in C_{60}/graphene system, which are beyond the conventional picture of surface diffusion, and the mechanism of transition between these regimes. In Chapter 5, we address the effect of rotational degrees of freedom on the molecular surface diffusion. In Chapter 6, we provide a framework to address the effect of temperature on the kinetic nanofriction of the C_{60}/graphene system. In Chapter 7, we introduce a chemical route to control molecular mobility by altering the substrate via chemical functionalization. Finally, the thesis is summarized in Chapter 8, where the main conclusions of the present work and future plans are presented.

2 Surface diffusion phenomena: an overview

In this chapter we present an overview of surface diffusion. We discuss experimental and theoretical methods of studying diffusion of atoms and molecules adsorbed on surfaces.

2.1 Basic concepts on the interactions between adsorbate and substrate

On the nanoscale, flat surfaces, which seem to be perfectly smooth, are not structureless, but rather consist of discrete atoms reflecting the crystallographic symmetry of the substrate lattice. These surface atoms exhibit translational symmetry, whose details depend on the particular crystal plane terminated at the surface. An adsorbed atom, molecule or nanoparticle occupies specific positions on the surface called *adsorption sites*, which can be for example on the top of surface atoms, or at bridging sites between two nearest surface atoms, *etc*. These sites are merely the positions offering the lowest potential energy (strongest binding) to the adsorbate/substrate system. However, binding to the surface at sites on other locations of the substrate can be nearly as strong as binding to adsorption sites (see Figure 2.1(a) and Figure 2.1(b)). According to Figure 2.1(c), the *potential energy surface (PES)* of the system, $V(x)$ (or $V(r)$ on two-dimensional (2D) surfaces), represents the potential energy of the entire adsorption system with respect to different lateral positions of the adsorbate while the positions of the substrate atoms are fixed. Indeed, this is an effective potential energy that the adatom experiences during its interactions with the substrate. The adsorption sites reflect the translational symmetry of the surface lattice, and as a consequence, the PES of the system also exhibits a translational symmetry in accordance with the surface lattice (see Figure 2.1).

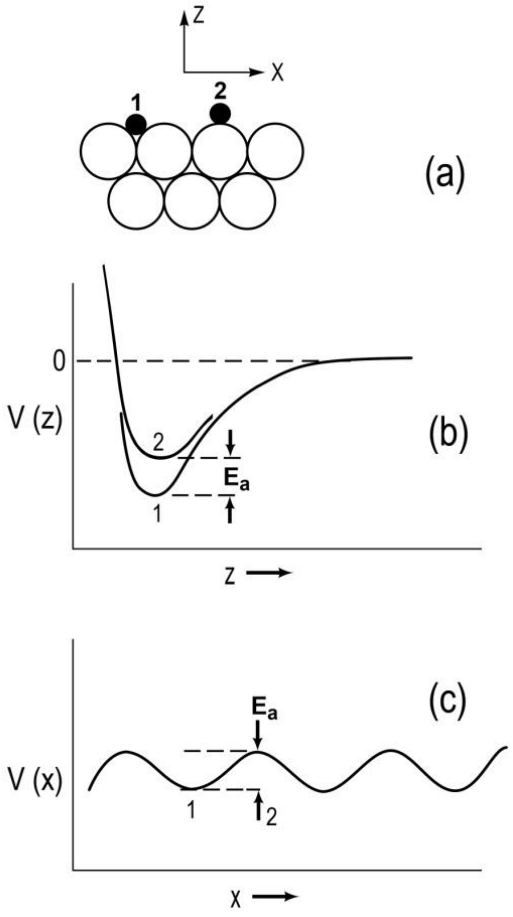

Figure 2.1 (a) Schematic of a substrate (open circles) and two adsorbed atoms (full circles in (1) an equilibrium and (2) a saddle-point configuration. z, distance normal to the surface, x along the surface. (b) Potential energy diagram for the adsorbate moving perpendicular to the surface in x positions 1 and 2 as in (a). (c) Potential energy diagram for the adsorbate moving laterally (parallel to the surface). The activation energy of diffusion E_a, is equal to the energy difference of the minima of curves 1 and 2 in (b) [103].

In the simplest case of surface diffusion, the substrate atoms do not directly participate in mass transport (in contrast to other more complicated cases which involve the exchange of adsorbed and substrate atoms). In this case, substrate atoms just perform small vibrations around their equilibrium positions, and the influences of the substrate on the dynamics of the adsorbate can be separated into two categories: adiabatic and non-adiabatic coupling [91].

2.1.1 Adiabatic coupling of adsorbate to surface

The substrate influences the adsorbate dynamics through the adiabatic PES of the system. The difference between the value of the PES at the saddle point and at the minimum is the classical energy barrier, E_a, for the diffusion process (see Figure 2.1(c)). It is noteworthy that, as it can be seen in Figure 2.1 (b), this energy barrier is smaller than that required for desorption of adsorbate from the surface. At relatively low temperatures ($k_BT<<E_a$, where k_B is the Boltzmann constant, and T is the absolute temperature), the motion of the adsorbate is dominated by the localized oscillations at the bottom of potential well of the system adsorption sites. These oscillations might sometimes lead to a jump, and the adsorbate moves from the adsorption site to the nearest equivalent one providing that it has enough translational energy to overcome the energy barrier of the PES between the adjacent sites. The adsorbate may acquire the energy for the jumping process from the thermal fluctuation of the substrate atoms (i.e. phonon heat bath). Hence, the *jump mechanism (hopping)* is a *thermally activated process*. Similar to all other thermally activated processes, an Arrhenius form separating the rate of jumps into a prefactor and an exponent, $\exp[-E_a/k_BT]$, is often employed to describe the temperature-dependent hopping mechanism.

2.1.2 Non-adiabatic coupling of adsorbate to surface

The substrate also influences the dynamics of the adsorbate through the non-adiabatic coupling of the adsorbate to surface vibrations (excitations). This coupling is responsible for the energy exchange between the adsorbate and the surface, and can alter the diffusion characteristics of the adsorbate, for example, from Brownian to ballistic motion. Through the non-adiabatic coupling, the adsorbate acquires sufficient thermal energy to

jump over the barriers, and then, dissipates this energy and equilibrates at a new adsorption site. Without going to more details in this section, we note that as a simple approximation, the non-adiabatic coupling can be characterized by a simple friction coefficient η [91], where η is the kinetic friction coefficient, which indicates the rate of energy exchange between the adsorbate and the substrate, and plays an important role in the dynamics of the adsorbate.

2.2 A microscopic description of surface diffusion

2.2.1 Single particle (tracer) diffusion

Tracer diffusion refers to migration of a single isolated adsorbate (tracer). Surface diffusion is a stochastic (random) process which mathematically may be described as a random walk whose mean square displacement (MSD) is proportional to the observation time. At sufficiently long time, the scaling of MSD is linearly proportional to the time, and the magnitude of the diffusion rate is described by the *tracer surface diffusion coefficient*, D^*.

2.2.2 Thermally activated jumps

If the temperature is low enough, that is, $k_BT << E_a$, the adatom spends most of its time at its adsorption site, oscillating with a small amplitude. Occasionally, it may receive sufficient energy from the substrate thermal vibrations (heat bath) to make a successful jump over the energy barrier, after which it again thermalizes at another adsorption site. Hence, in this regime, the diffusion is a series of activated microscopic jumps.

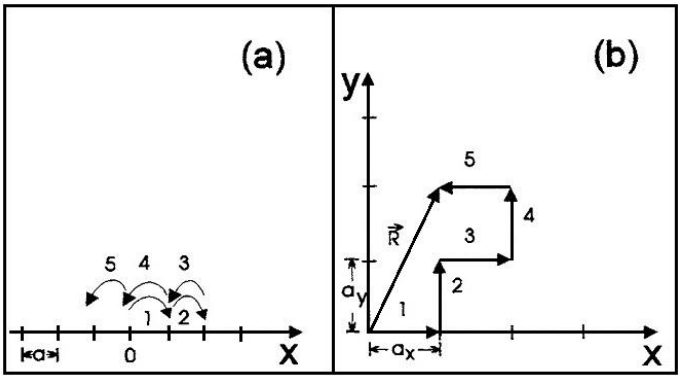

Figure 2.2 (a) One-dimensional and (b) two-dimensional random walks [103].

2.2.2.1 Single jumps: uncorrelated random walk

Providing that the η is large, after the jump the translational energy of the tracer rapidly dissipates into the surface heat bath, and it will equilibrate at the nearest-neighboring adsorption site. Since the jump terminates at a nearest-neighbor site, it is called a *single jump*. After a single jump, the tracer loses all its "memory" about its previous location, and hence, all individual jumps are uncorrelated and identical. For example, in one dimensional (1D) lattice, the tracer makes a new forward or backward jump with equal probabilities (see Figure 2.2). Hence the process can be described as an uncorrelated random walk.

According to the random walk theory, in the case of an uncorrelated random walk in a two-dimensional (2D) lattice, we can write [104]:

$$< \boldsymbol{R}(t) >= 0, \tag{2.1}$$

$$< \mathbf{R}^2(t) >=< l^2 > n(t), \tag{2.2}$$

where $\boldsymbol{R}$ is the displacement vector of the tracer, $n(t)$ is the number of jumps in a given time t, and <.> is the average over a large number of random walks with time duration of t, and mean square jump length is $<l^2>$. $<\boldsymbol{R}^2>$ is the *mean square displacement* of the

tracer. In the case of uncorrelated random walk on a uniform lattice (see Figure 2.2), all jump lengths are equal to the lattice parameter, a, and hence: $<l^2>=a^2$. The effective jump frequency, Γ, can be defined as:

$$\Gamma = n(t)/t. \tag{2.3}$$

Consequently, the mean square displacement of the tracer particle can be written as:

$$< \boldsymbol{R}^2(t) >=< l^2 > \Gamma t. \tag{2.4}$$

Indicating that:

$$< \boldsymbol{R}^2(t) > \propto t. \tag{2.5}$$

The tracer diffusion coefficient, D^*, is defined independent of characteristics of the medium as [103]:

$$D^* = lim_{t\to\infty}[\frac{< \boldsymbol{R}^2(t) >}{2td}], \tag{2.6}$$

where d is the spatial dimension. For the surface diffusion, d=2. Hence, the tracer diffusion coefficient of an isolated adsorbate can be written as:

$$D^* = \frac{1}{2d}\Gamma < l^2 > . \tag{2.7}$$

The two most important quantities to describe the jump diffusion are the total jump rate Γ and the mean square jump length $<l^2>$. The definition of D^* in Equation (2.6) does not depend on the nature of jumps, implying that this definition can be used regardless the jump mechanism is thermally activated, or the jumps take place by quantum mechanical effects such as quantum tunneling [105].

Considering the thermally activated jump mechanism, the temperature dependence of the jump rate, Γ, can be written with the Arrhenius form [106, 107]:

$$\Gamma = \Gamma_0 \exp\left(-\frac{E_a}{k_B T}\right), \tag{2.8}$$

where Γ_0 is the prefactor, E_a is the activation energy, k_B is Boltzmann constant, and T is the temperature. Equation (2.8) can be derived from a microscopic theory of surface diffusion at low temperatures, *i.e.* $k_BT << E_a$ [85, 90], or from the more phenomenological Transition State Theory (TST) [107] (also see the discussion on TST in Section 2.4.1). In the limit of high friction and very low temperatures, the activation energy, E_a, coincides precisely with the energy barrier of the diffusion in the PES of the system [90], which is the difference between the potential energy value of the system at the lowest saddle point between the adjacent adsorption sites, and the value at the bottom of the adsorption site potential well (see Figure 2.1). The prefactor Γ_0 is given by [91]:

$$\Gamma_0 = n_s \nu_{osc}, \tag{2.9}$$

where ν_{osc} is a typical vibrational frequency of the adsorbate at the adsorption site, and n_s is the number of equivalent sites in the neighborhood of the original position (n_s = 4 and 6 on square and triangular lattices, respectively). The description of surface diffusion as a site-to-site hopping process is valid if $\Gamma << \nu_{osc}$, or equivalently, $k_BT << E_a$, which means that the temperature must be low enough to be in the jump regime. From Equations (2.7) to (2.9), the Arrhenius form of surface diffusion coefficient can be written as:

$$D^* = D_0 \exp\left(-\frac{E_a}{k_B T}\right), \tag{2.10}$$

where D_0 is the surface diffusion prefactor:

$$D_0 = \frac{1}{2d} n_s v_{osc} < l^2 > . \tag{2.11}$$

The definition of D^* for a single adsorbate in Equation (2.6) can be generalized for the assembly of N distinguishable adsorbates (which means that the diffusive motion of each adsorbate can be followed individually) as [87]:

$$D^* = lim_{t\to\infty} \frac{1}{2Ntd} \sum_{i=1}^{N} <| \mathbf{r}_i(t) - \mathbf{r}_i(0) |^2>, \tag{2.12}$$

where N is total number of adsorbates, $\mathbf{r}_i(t)$ is the position vector of the ith adsorbate at time t, and $\mathbf{r}_i(0)$ is the position vector of the same adsorbate at time t at time origin, and <.> is the time or ensemble average. It is noted that Equation (2.12) cannot be experimentally measured, because distinguishing and tracing all individual adsorbates is impossible in experimental practices. However, it can be measured by using simulation techniques.

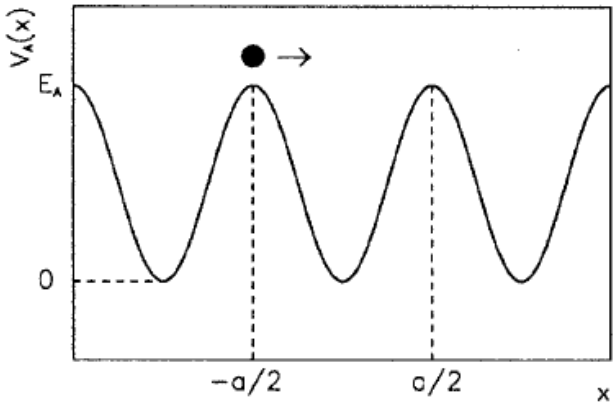

Figure 2.3 Periodic one dimensional potential $V_A(x)$. The particle starts at the saddle point (transition state) with the potential energy of E_A and the kinetic energy of k_BT. It crosses the cell, dissipating energy to the surface due to the friction [91].

2.2.2.2 Long jumps: correlated random walk

The occurrence of long jumps (the jumps in which the adsorbate flies over several adsorption sites), on the other hand, can be discussed qualitatively in the framework of a one-dimensional (1D) model of surface diffusion in a periodic potential $V_A(x)$ (see Figure 2.3), where the adsorbate dissipates its kinetic energy to the substrate with a constant friction coefficient, η. Here, a simple condition for the occurrence of a long jump can be constructed. To this end, the energy dissipated to the surface by the adsorbate while it crosses a lattice cell must be calculated [108]. It can be assumed that the particle starts at the saddle point in the left side of a cell ($-a/2$ in Figure 2.3) with an initial kinetic energy of k_BT, and an initial total energy of $E_0=k_BT+E_a$. Then the particle crosses the cell and the energy is dissipated by the particle, *i.e.* dissipation parameter, Δ, is:

$$\Delta = \int_{-a/2}^{a/2} m\eta v(x)dx, \tag{2.13}$$

where m and $v(x)$ are the mass and velocity of the adsorbate, respectively. If $\Delta < k_BT$, the adsorbate does not dissipate all its kinetic energy during crossing a single cell, and a long jump occurs. Based on this analysis, the low friction regime can be defined by the following condition [108]:

$$\Delta << k_BT. \tag{2.14}$$

Indeed, occurrence of long jumps in surface diffusion has been observed in experiments [109] as well as simulations [110]. Figure 2.4 illustrates an example of a long jump of an adatom observed in molecular dynamics (MD) simulations. Adsorption sites are indicated by the open circles. The initial and final positions of the long jump are indicated by the

arrows. In this jump, the particle has moved over a distance of two unit cells without stopping in the nearest adsorption site.

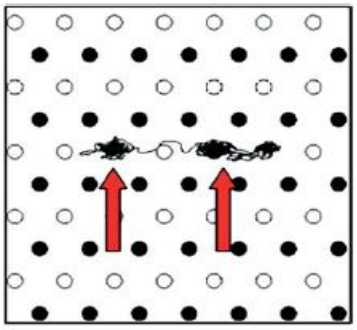

Figure 2.4 Trajectory of an adatom in MD simulations of Cu/Cu system. Open circles indicate the adsorption sites. The arrows indicate a long jump (with length of two unit cells), followed by a single jump (back and forth between two adjacent adsorption sites) [110].

The precise geometry of the PES of two-dimensional (2D) systems has an important role in the probability of the occurrence of long jumps [111]. In fact, numerical solutions of surface diffusion in two dimensional models have shown that the occurrence of long jumps considerably reduces if the minima and the saddle points are not along the same straight line [111, 112]. The reason is that the long jumps are more probable when the most favorable diffusion pathways are straight lines, so that the adsorbate trajectories can easily propagate along them due to the inertial effect. Any geometrical confinement (in the PES of the system), which leads to non-straight diffusive pathways increases the dissipation parameter, Δ (see Equation (2.13)). Therefore, the probability of re-trapping increases, and consequently, the possibility of long jumps is reduced [113]. Experimental and molecular dynamics studies in variety of metal/metal systems have demonstrated the sensitivity of long jumps to the details of the system PES, suggesting that the 1D models

may not be sufficient to appropriately describe the diffusion on real 2D surfaces [114, 115]. Moreover, the probability of occurrence of long jumps can be increased by applying external effects, such as applied field and perturbations of a microscope tip [116, 117].

Occurrence of long jumps, *i.e.* correlated random walks, alters the value of mean square displacement, $\langle \mathbf{R}^2 \rangle$, predicted by the uncorrelated single jump model (see Section 2.2.2.1). To understand this, we rewrite the mean square displacement of the tracer adsorbate as (see Figure 2.2):

$$< \boldsymbol{R}^2(t) >=<((\sum_{i=1}^{n} \boldsymbol{r}_i).(\sum_{j=1}^{n} \boldsymbol{r}_j))>, \tag{2.15}$$

where $\boldsymbol{r}_k$ is the displacement vector of the kth jump, n is the total number of jumps at given time period of t, and the point (.) is the scalar product of the vectors. Assuming that $|\boldsymbol{r}_k| = a$ (the lattice parameter), we will have $\boldsymbol{r}_k.\boldsymbol{r}_k = a^2$, and it is shown that [103]:

$$< \boldsymbol{R}^2(t) >= na^2 < 1 + \frac{2}{n}(\sum_{i=1}^{n-1} \sum_{j=i+1}^{n} \frac{\boldsymbol{r}_i.\boldsymbol{r}_j}{a^2}) > \tag{2.16}$$

Defining the *jump correlation factor*, f, as:

$$f = < 1 + \frac{2}{n}(\sum_{i=1}^{n-1} \sum_{j=i+1}^{n} \frac{\boldsymbol{r}_i.\boldsymbol{r}_j}{a^2}) > . \tag{2.17}$$

The mean square displacement can be rewrite as:

$$< \boldsymbol{R}^2(t) >= na^2 f . \tag{2.18}$$

Now, we can generalize the definition of tracer diffusion, D^*, by using the uncorrelated random walk model as:

$$< \boldsymbol{R}^2(t) >= 2dD^* t = na^2 f . \tag{2.19}$$

The values of f ranges from 0 to n [103, 118]. If we have uncorrelated random walk, $\langle \boldsymbol{r}_i.\boldsymbol{r}_j \rangle = 0$ and $f=1$. In the case of *ballistic motion*, which means the jumps are strongly correlated in such a way that the direction of first jump determines the direction of all subsequent jumps, $\langle \boldsymbol{r}_i.\boldsymbol{r}_j \rangle = a^2$, and $f=n$. When a jump in a certain direction leads to the next jump in the reversal direction, f would approach zero. This case may occur on heterogeneous surfaces leading to subdiffusion (See Chapter 7). Therefore, occurrence of correlated jumps can make D^* time-dependent. Hence, in order to obtain a stable tracer diffusion coefficient, observation time of the tracer mean square displacement must be long enough to eliminate the memory effects, and to reach the normal diffusion regime (f =1).

2.2.2.3 Remarks on thermally activated jump model

The Arrhenius description of surface diffusion presented in Section 2.2.2.1 is the commonly accepted model of the surface diffusion which is traditionally used to analyze and interpret the experimental or simulation results [87, 119]. However, we need to emphasize that the application of Arrhenius analysis in some cases might be arguable and specific considerations must be taken into account.

First, the derivation of the Arrhenius form is possible in special conditions in which the system exhibits thermally activated single jumps [85, 90]. These conditions are usually satisfied at low temperatures. This is because the unique diffusive pathway through the lowest energy saddle point to the next adsorption site dominates only at low temperatures. At higher temperatures, many other diffusive pathways might become accessible for the adsorbate (tracer), and then, the overall activation energy of diffusion is obtained as an average over a distribution of energy barriers which the tracer may overcome. Therefore,

the activation energy extracted by Arrhenius analysis may not coincide with the depth of energy wells in the PES of the system.

Moreover, as it is discussed in Section 2.2.2.2, long jumps are possible during the surface diffusion (especially in the system with low friction coefficient, η). Occurrence of these long jumps causes deviation from the "Arrhenius-like" behavior, thus the explanation of the results becomes difficult. The long jumps cause correlated random walks, which can alter the interpretation of the Arrhenius barrier and/or prefactor [109, 120, 121]. The Arrhenius-like analysis can be adapted for a long jump regime of surface diffusion, by noticing that, on the one hand, different barriers can be associated to jumps of different lengths (since jumps of different lengths need different activation energies [91, 109]. Therefore, the overall Arrhenius activation energy is an average over different activation energies of different jump lengths. On the other hand, the occurrence of long jumps may impose additional temperature dependence in $<l^2>$ and hence the diffusion prefactor [120, 121].

The direct and straightforward application of the Arrhenius analysis may become problematic in the case of surface diffusion on heterogeneous substrates having a random/non-periodic PES rather than a periodic one. This will be described in details in Chapter 7. In such heterogeneous systems, more complicated analysis is needed to describe the simulation/experimental results.

It is important to notice that the models discussed above describe the motion of an isolated adsorbate exhibiting thermally activated jumps between the adjacent adsorption sites. This is a simple picture of surface diffusion. It has been shown that in some systems, *e.g.* homoepitaxial metallic systems, the surface diffusion takes place by more

complex mechanisms such as *exchange process* [122, 123]. In an exchange process, the adatom exchanges with a substrate atom, and that new adatom continues the diffusive motion. The rate of exchange mechanism can be comparable to the rate of simple hopping motion, or even becomes dominant [87]. Other more complicated mechanisms such as multiple exchanges or concerted movements of adsorbates, which involve a large number of atoms, have also been proposed [124].

2.2.3 Collective surface diffusion

The diffusive motion of a single adsorbate was discussed in the previous sections, and the single particle (tracer) diffusion coefficient D^*, was defined. It was shown that D^* is proportional to the product of the rate and the average square length of uncorrelated jumps. This relation is more complicated when the jumps become correlated at finite coverage of adsorbates.

At finite coverage, as long as the trajectory of individual adatoms can be followed, the concept of single particle or tracer diffusion is still useful (see Equation (2.12)). However, in this case a single energy barrier cannot be well defined for the adsorbate. Because of the adsorbate-adsorbate interactions, the actual activation barrier for a single adsorbate also depends on the configuration of all the other particles on the surface. Therefore, the effective activation energy which controls the diffusion is defined as an average over all the fluctuating configurations. In addition, the successive configurations of the adsorbates at finite coverages become correlated, leading to correlated jumps. Obviously, a strict Arrhenius form, as it is described in tracer diffusion for the temperature dependence of collective surface diffusion, no longer exists. Consequentially, at finite coverages, rather

than the single particle (tracer) diffusion coefficient, D^*, a new transport coefficient must be defined, which is called the *collective (chemical) diffusion coefficient*, D_c [87, 91].

D_c is defined through the Fick's first law of diffusion which describes the relation between diffusive flux of the adsorbates, J, and their concentration gradient, $\nabla_r \rho(\mathbf{r})$ [87]:

$$J = -D_c \nabla_r \rho(r), \tag{2.20}$$

where the adsorbate concentration, ρ, is only a function of spatial position, $\boldsymbol{r}$. If ρ is time dependent, the second Fick's law must be used:

$$\frac{\partial \rho}{\partial t} \rho(r,t) = D_c \nabla_r^2 \rho(r,t). \tag{2.21}$$

A general relation between D_c and D^* has been derived as [103, 104]:

$$\frac{D_c}{D^*} = \frac{< N >}{< (\delta N)^2 >} \left[1 + \frac{\int_0^\infty dt \left\langle \sum_{i \neq j} \boldsymbol{v}_i(0).\boldsymbol{v}_j(t) \right\rangle}{\int_0^\infty dt \left\langle \sum_i \boldsymbol{v}_i(0).\boldsymbol{v}_i(t) \right\rangle} \right] \tag{2.22}$$

where the N is the number of particles in the system, $<(\delta N)^2>$ is the mean square fluctuation of the number of adsorbed particles on the surface, $\boldsymbol{v_k}$ is the velocity of kth particle. If the cross-correlations between the velocities of different adsorbates are absent or negligible (which means that the velocities of the adsorbates are independent from each other), a simple relation can be obtained as:

$$\frac{D_c}{D^*} = \frac{< N >}{< (\delta N)^2 >}, \tag{2.23}$$

The relation between $<N>$ and $<(\delta N)^2>$ for the grand canonical ensemble [125], *i.e.* a system with constant volume, chemical potential (μ) and temperature (T), can be written as:

$$\frac{< N >}{< (\delta N)^2 >} = \left[\frac{\partial}{\partial \ln \theta} \frac{\mu}{k_B T} \right], \tag{2.24}$$

where $\theta = N/A$ is the coverage of adsorbates on the surface area of A. Hence, Equation (2.23) becomes:

$$\frac{D_c}{D^*} = \left[\frac{\partial}{\partial \ln \theta} \frac{\mu}{k_B T} \right], \tag{2.25}$$

which is known as the Darken's equation [126].

2.3 Experimental techniques to study surface diffusion

A brief review of experimental techniques used to study surface diffusion is helpful to understand their strength and limitations. This review also highlights the importance of theoretical and computational techniques as complementary or even the only possible approaches to address certain surface diffusion problems. The most important features of the experimental techniques are summarized in Table 2.1. There are several important issues which must be taken into account when the experimental techniques (Table 2.1) are applied. First, these experimental techniques can be classified into two main groups. The first group, which includes STM and FIM techniques, can be used to image and follow the motion of individual adatoms. Consequently, they can measure the single particle tracer diffusion coefficient (D^*). The second group, which includes QHAS, FEM, HAS, LOD, PEEM, LITD, SCPM, and HRLEED, constitutes the majority of the techniques. They can be used to measure either equilibrium density fluctuations (QHAS, FEM, and HRLEED) or the decay of small non-equilibrium density profiles (HAS, LOD, PEEM, LITD, and SCPM). Hence, they measure the collective diffusion coefficient (D_c). However, the experimental techniques with high sensitivity such as QHAS can operate at

very low coverages, the tracer diffusion coefficient D^* can be obtained by measuring $D_c(\theta)$ at small coverages. The D^* can be extracted using the fact that in the limit $\theta \rightarrow 0$, the two diffusion coefficients D_c and D^* become identical ($D_c \rightarrow D^*$). In addition, we note that the STM technique is constantly being improved. Currently, the motion of all the adatoms can be followed in real time with STM, so a time series of the entire configuration can be generated. This in turn can then be used to obtain the collective diffusion coefficient D_c.

Table 2.1 Experimental techniques applied to study surface diffusion (for details, refer to [91, 127] and references therein).

Technique	Abbreviation	Remarks	Coverage (ML)	Length scale
Scanning Tunneling Microscopy	STM	Direct imaging	$\theta \geq 0$	Atomic
Field Ion Microscopy	FIM	Direct imaging	$\theta \geq 0$	Atomic
Quasi-elastic Helium Atom Scattering	QHAS	Density fluctuations	$\theta \geq 0.01$	10 Å
Field Emission Microscopy	FEM	Density fluctuations	$\theta \geq 0.1$	100 - 1000 Å
Helium Atom Scattering	HAS	Density decay	$\theta \geq 0.01$	1 μm
Linear Optical Diffraction	LOD	Density decay	$\theta \geq 0.01$	1 μm
Photoemission Electron Microscopy	PEEM	Density decay	$\theta \geq 0$	0.1-1000 μm
Laser Induced Thermal Desorption	LITD	Density decay	$\theta \geq 0.1$	10-1000 μm
Scanning Contact Potential Microscopy	SCPM	Density decay	$\theta \geq 0.01$	$\geq$ 1 μm

Second, the length scales listed in the Table 2.1 need to be explained. Except for the direct imaging methods (STM and FIM), which probe the atomic length scales, most of the other techniques (except QHAS) have much longer length scale than the lattice constants. For example, LOD method measures at a length scale of a few *mm*. This length scale specifies the maximum wavelength of the decaying density that can be measured. At long wavelength the gradient corrections to Fick's law are negligible and the linear response transport coefficient, D_c, can be truly measured. However, at this length scale surface defects, *e.g.* the steps and impurities, cannot be avoided. The effect of surface

defect must be taken into account to extract the diffusion coefficient from the data. The measured diffusion coefficients could be dramatically different from the diffusion coefficients of a defect-free surface. This effect might be the reason for many inconsistent results of measurements of diffusion coefficients obtained for the same system [128]. The experimental techniques operating at short length scales have the advantages that over a length scale of less than 10 lattice spacings, surface defects (steps or impurities) can be safely ignored, and do not affect the diffusion coefficient.

Third, we note that in some of these experimental techniques, the diffusion coefficients are extracted indirectly. An important example of this is STM measurements in static mode. Using STM in the static mode, the size distribution of islands formed by deposited atoms during growth process can be measured [129]. The diffusion coefficient is extracted using fitting procedure, which is based on assumptions about the nucleation process and the mobility of the adatoms. It has been demonstrated that in some cases (for example in systems with low activation barriers), a small change in other parameters can significantly affect the value of the extracted diffusion coefficient [130, 131]. Therefore, a deep understanding of the fundamentals of each experimental technique helps to have a reliable interpretation of the obtained results.

2.4 Theoretical and computational techniques to study surface diffusion

In order to study surface diffusion, several theoretical approaches have been proposed. In some cases, they may be the only possible method to study certain aspects of surface diffusion. In the following, we provide a brief review of the widely used theoretical approaches, and discuss their strengths and weaknesses.

2.4.1 Transition state theory: conventional model of surface diffusion

As it is described in Section 2.2.2, the standard and conventional model of surface diffusion is based on the combination of the random walk theory and hopping mechanism. In the hopping regime, the adsorbate diffuses through a series of uncorrelated jumps between the adsorption sites on the PES of the system. Therefore, the diffusion coefficient depends on the distance between the adsorption sites (jump length), and the frequency of the jumps (jump rate). These jumps are thermally activated (except in the special case of very light adsorbates, such as hydrogen, at very low temperatures where the quantum effects become important [105, 132]). The transition state theory (TST) [86] describes the jump rate by an Arrhenius form (see Equation (2.8)).

The TST theory provides a very simple and widely used model, since its assumptions are found to be approximately satisfied in experiments [91]. In the framework of TST model, the activation energy of diffusion, E_a, can be extracted from temperature dependence of diffusion rates obtained from experiments or simulations. According to the TST model, E_a can be used to estimate the adsorbate-substrate interaction potential.

However, TST does not provide sufficient insight into the dynamics of the diffusion process. Besides, it is expected that the TST model gives the best estimate of diffusion rate in the limit of high energy barrier ($E_a >> k_BT$) and strong dynamical coupling of the adsorbate to the substrate (high friction). At high temperatures, in the systems with a shallow PES or low friction, a significant deviations from the TST model (this issue will be addressed in Chapter 4) is expected. These limitations of the TST model may be obviated by a more general phenomenological Langevin (or equivalently Fokker-Planck) approach, in which the potential energy barrier and friction coefficient, η, of the system

are included as separate parameters. Indeed, the TST regime (strong energy barrier and high friction) is a special limit of the Langevin approach.

2.4.2 Langevin and Fokker-Planck equations

At the present time, in order to study surface diffusion in details including all degrees of freedom of the adsorbate and substrate, atomistic modeling with empirical or semi-empirical interatomic potentials can be used (see Section 2.4.5), since an entirely first-principles (*ab initio*) simulation is still not possible (see Section 2.4.4). However, a simpler approach is to integrate out the substrate degrees of freedom in the equations of motion of the system, leaving only an effective stochastic equation of motion for the adsorbate [91]. In this case, the dynamics of the adsorbate center of mass (COM) is governed by the Newton's second law in which a stochastic force acts on the adsorbate, taking into account the thermal fluctuations of the surface atoms (heat bath). This is the essence of Langevin equation (LE), which describes the motion of a single adsorbate COM as [111]:

$$m\ddot{\boldsymbol{r}} = -\nabla \boldsymbol{V}(\boldsymbol{r}) - \eta m\dot{\boldsymbol{r}} + \boldsymbol{\xi}(t)\ , \tag{2.26}$$

where m is the adsorbate mass, $\boldsymbol{r}$ is the position vector of its COM, single and double dots are first and second derivatives with respecting to time, $V(\boldsymbol{r})$ is the PES, η is the friction coefficient, $\boldsymbol{\xi}$ is the stochastic force, and t is time.

The LE describes the time evolution of the position $\boldsymbol{r}$, and the velocity, $\boldsymbol{v}=d\boldsymbol{r}/dt$, of the adsorbate. Since the LE is a stochastic equation, it is possible to derive a probabilistic equation for the same system to obtain a probability distribution $P(\boldsymbol{r}, \boldsymbol{v}, t)$, explaining the probability of the adsorbate having the position $\boldsymbol{r}$ with the velocity $\boldsymbol{v}$ at time t. This equation is called Fokker-Planck equation (FPE) [133]:

$$\frac{\partial P}{\partial t} = -\boldsymbol{v}\frac{\partial P}{\partial \boldsymbol{r}} - \frac{\nabla \boldsymbol{V}(\boldsymbol{r})}{m}\frac{\partial P}{\partial \boldsymbol{v}} - \eta\frac{\partial}{\partial \boldsymbol{v}}(\boldsymbol{v}P + \frac{K_B T}{m}\frac{\partial P}{\partial \boldsymbol{v}}). \tag{2.27}$$

$P(\boldsymbol{r}, \boldsymbol{v}, t)$ is called the phase-space probability distribution, and the FPE describes the time evolution of P.

The LE (or equivalently the FPE) is a phenomenological approach, and with an appropriate choice of PES and friction parameter, it provides a powerful tool to study surface diffusion beyond the simple TST model in the systems with shallow energy barriers or weak frictional dissipation [89]. As it is described comprehensively in Chapter 4, the simple LE for the one dimensional surface diffusion has been solved analytically, and different diffusion regimes (beyond thermally activated single jump picture) have been mapped out [108, 134]. Numerical solutions of LE in model 2D systems with a variety of PES shapes and friction coefficients, qualitatively clarify the effects of these phenomenological parameters on the dynamics of surface diffusion [111, 135].

However, it must be noted that the Langevin model is often inadequate to quantitatively describe surface diffusion in real systems [136]. In general, the analytical solution of the LE is not possible for arbitrary systems, and numerical techniques must be employed [137]. Even in the numerical solution of the LE, selection of an appropriate value for the friction coefficient is a challenging task in order to quantitatively describe the diffusivity of a system. Hence, the LE is usually used in the phenomenological studies, or used to extract the friction coefficient of the systems from fitting with experimental results. Another drawback of the LE is that it cannot readily take into account the internal degrees of freedom (DOFs) of the adsorbate.

2.4.3 Monte Carlo simulations

To study the diffusion in dense adsorbed layers of 2D systems, simulations are usually performed based on the lattice-gas model [138, 139]. In the lattice-gas model, the surface is modeled as a 2D lattice with M sites, which is filled by N interacting/non-interacting adsorbates. The adsorbates move on the 2D lattice sites by hopping from site to site. Lattice-gas models are most commonly studied by Monte Carlo (MC) simulations. In the MC simulations, following questions are interesting: how to choose microscopic rates to reproduce experimental data within the lattice gas description? How to extract information about the collective and the tracer diffusion coefficients in an MC simulation?

Nowadays, various MC models have been developed to study surface diffusion [140-142]. But it must be emphasized that the MC simulations were developed to statistically obtain the average quantities of the systems at the equilibrium conditions. The sequence of states generated by the MC method does not correspond to the real dynamics of the system. Therefore; the MC method cannot be applied to study time-dependent properties and dynamic processes. Moreover, the lattice-gas description of the surface diffusion is appropriate only at low temperatures, so that the adsorbates are well localized at the adsorption sites.

2.4.4 First-principles (*ab initio*) methods

First-principles (or *ab initio*) methods are commonly used to calculate the PES of the systems. In the first-principles calculations, the forces between all atoms in the system are calculated quantum-mechanically by applying some approximations, such as density functional theory (DFT) [143]. The great advantage of these methods is that they, in principle, do not need fitting parameters, and almost in all cases (except for strongly ionic

systems and van der Waals forces) can be dealt using the same framework. The first-principles methods have been widely used to calculate the potential energy barriers of the metallic and semiconducting systems [144-147]. However, in order to make first-principles calculations possible, several approximations have to be made [148, 149]. The local density approximation (LDA) [150] is commonly used in bulk calculations (especially for metals), but does not always work well for surface problems [147, 149]. The first-principles calculations are highly computationally expensive, and at present, they are typically limited to adsorbate/substrate systems consisted of about 100 atoms. Moreover, finite-temperature dynamical calculations (for example by using the Car-Parrinello method [151]) are computationally ineffective for the study of surface diffusion, since the simulations typically extend only to 100 picoseconds [152]. Therefore, it is impossible at present, to only use the *ab initio* methods to study surface diffusion especially in large systems. Application of these methods, hence, is mostly limited to small systems and simple ground state (at absolute zero temperature) energetic calculations, such as obtaining the PES of the chemisorbed systems.

2.4.5 Molecular dynamics simulations

Molecular dynamics simulations with empirical or semi-empirical potential energy calculations provide a better picture of surface diffusion (see Section 3.2). In MD simulations, both of the adiabatic potential energy surface (PES) and the non-adiabatic coupling of the adsorbate to the surface (leading to the friction term) are exactly included. From the microscopic viewpoint, the MD simulations are much more detailed compared to the TST, MC and Langevin modeling. Therefore, since today high quality force-fields and computational resources are available, classical MD simulations have been widely

used in surface diffusion studies. Commercial [153-155] and open source [156-158] MD packages provide a wide range of force-fields to study realistic systems.

We note that full MD calculations include only the classical degrees of freedom of the atoms in the system. The non-adiabatic coupling of the adsorbate to the electronic excitations cannot be modeled using this approach, which might be important in surface diffusion of chemisorbed systems. But, in the absence of any feasible first-principles method which can take into account both temperature effects and vdW, MD offers the most powerful tool to study the surface diffusion. MD is especially useful for the physisorbed systems where the vdW forces have the dominant role in the interactions between the adsorbate and the substrate. In the current research, we employed MD simulations to study the energetics and dynamics of diffusive motion of C_{60} on graphene. There details about the MD and its suitability to study molecular surface diffusion are discussed in Chapter 3.

3 Computational techniques

3.1 Why was MD technique chosen for the current study?

3.1.1 Molecular surface diffusion

In contrast to adatoms, the size of the admolecules and adclusters might be larger than the surface unit cells, and hence adsorption sites and transition states cannot be well defined. Furthermore, due to the internal degrees of freedom (DOFs), admolecules can adopt different configurations at adsorption sites. Each of the configurations may correspond to a local minimum of the system PES. Thus, it is possible that the potential energy difference between these local minima to be of the order of the thermal energy of the admolecule. Therefore, the diffusion behavior cannot be considered as thermally activated site-to-site hopping [159].

To stop at the nearest adsorption site, the adsorbate must lose its translational energy before it crosses this site. In many examples of atomic surface diffusion, long jumps are rare especially for metallic adatoms on metals, indicating an efficient exchange of energy (high friction) in such systems [1_{60}-164]. In contrast, molecular surface diffusion mostly can be considered as a sequence of correlated long jumps [165, 166].

3.1.2 Application of MD simulations to study molecular surface diffusion

The conventional TST and lattice gas model, as well as other phenomenological methods like Langevin dynamics cannot be used for accurate quantitative studies of molecular surface diffusion, since they do not distinguish between single atomic and molecular

adsorbates. In MD simulations all the internal degrees of freedom of the system can be taken into account in the simulations of surface diffusion of admolecules. Using MD simulations, the effects of molecular rotation on the surface diffusion can be investigated. Thus, MD is a very powerful method to study the dynamics of molecular surface diffusion.

In the following sections of this chapter, we briefly discuss the principles of MD simulations. Then, the computational techniques and calculation details used in this thesis are explained in detail.

3.2 An overview of MD simulations

In MD simulations, the time evolution of a set of interacting atoms is followed via the solution of Newton's equation of motion:

$$\boldsymbol{F_i} = m_i \frac{d^2 \mathbf{r}_i(t)}{dt^2}, \tag{3.1}$$

where $\mathbf{r}_i(t) = (x_i(t), y_i(t), z_i(t))$, and m_i are the position vector and mass of the ith atom, respectively, and $\boldsymbol{F_i}$ is the force vector acting on the ith atom at time t due to interatomic interactions in the system. The interatomic interactions in MD simulations are prescribed by *potential functions* or *force-fields (*FF*).*

The force-field model describes the systems as collections of atoms kept together by the interatomic interactions such as chemical bonds or vdW forces. The interaction law is specified by the energy function, $U(\mathbf{r}_1, \ldots, \mathbf{r}_N)$, representing the potential energy of the **N** interacting atoms in the system as a function of their positions, $\mathbf{r}_i$. Given the potential energy function, the force acting upon ith atom, $\boldsymbol{F_i}$ in Equation (3.1), is:

$$\boldsymbol{F}_i = -\nabla_{r_i} U(\boldsymbol{r}_1,...,\boldsymbol{r}_N) = -\frac{\partial U(\boldsymbol{r}_1,...,\boldsymbol{r}_N)}{\partial \boldsymbol{r}_i}. \tag{3.2}$$

Finding an accurate potential that can adequately describe the energetics of the system is a nontrivial problem. The atomic FF in the classical MD has a specific functional form with adjustable parameters. The values of these parameters are chosen to provide a good fit to the experimental data (*empirical* FF), or first-principles calculations (*semi-empirical* FF). For the MD simulation of organic materials, including graphene and fullerenes, a typical FF has a functional form as [167]:

$$\begin{aligned} U(\boldsymbol{r}_1,...,\boldsymbol{r}_N) = & \sum_{bonds} \frac{a_i}{2}(l_i - l_{i0})^2 + \sum_{angles} \frac{b_i}{2}(\theta_i - \theta_{i0})^2 + \sum_{torsions} \frac{c_i}{2}[1+\cos(n\omega_i - \chi_i)]^2 \\ & + \sum_{atom\_pairs} 4\varepsilon_{ij}\left[\left(\frac{\sigma_{ij}}{r_{ij}}\right)^{12} - \left(\frac{\sigma_{ij}}{r_{ij}}\right)^{6}\right] + \sum_{atom\_pairs} \kappa \frac{q_{ij}}{r_{ij}}. \end{aligned} \tag{3.3}$$

The first three terms are related to the bonded interactions, and their summations indices run over all bonds, angles and torsion angles defined by the covalent structure of the system. The last two terms are related to the non-bonded interactions, *i.e.* van der Waals and Coulomb electrostatic interactions, respectively, and their summation indices run over all the atom pairs, where $r_{ij} = |\, r_i - r_j \,|$.

To integrate the Newton's equation of motion (Equation (3.1)), which is a second order differential equations, the initial positions and velocities of the atoms as well as the instantaneous forces acting on them are needed. This is a many-body problem, and the equations of motion for all atoms in the system must be solved numerically. The aim of the numerical integration of Newton's equations of motion is to find an expression that defines atomic positions $\boldsymbol{r}_i(t+\Delta t)$ at time $t+\Delta t$ in terms of the already known $\boldsymbol{r}_i(t)$, *i.e.* positions at time t. To this end, the Verlet algorithm is widely used due to its stability and

simplicity. According to this algorithm, $\boldsymbol{r}_i(t+\Delta t)$ can be derived from the Taylor expansions of $\boldsymbol{r}_i(t)$ as:

$$\boldsymbol{r}_i(t+\Delta t) \cong 2\boldsymbol{r}_i(t+\Delta t) - \boldsymbol{r}_i(t-\Delta t) + \frac{F_i(t)}{m_i}\Delta t^2 . \tag{3.4}$$

The exact trajectories correspond to the limit of an infinitesimally small integration step. It is, however, desirable to use larger time steps to sample longer trajectories. In practice Δt is determined by fastest motions in the system, and often is in the order of one femtosecond.

As discussed in this section, the MD simulations explicitly solve the equations of motion for all atoms in the system, and the obtained trajectories allow for studying the dynamics of the system at the atomic level. Moreover, MD simulations have reached a level of accuracy comparable with experimental data, making them a valuable tool to study molecular surface diffusion.

3.3 MD Software

In the current work, LAMMPS (Large−scale Atomic/Molecular Massively Parallel Simulator) package [156, 157] is used to perform MD simulations. LAMMPS is an open source classical molecular dynamics code that can be used to simulate ensembles of particles in liquid, solid, or gaseous states. Using a variety of boundary conditions and force-fields, LAMMPS has been used to model atomic, polymeric, biological, metallic, granular, and coarse−grained systems. It can be run on any parallel machine that compiles C++ and supports the MPI message passing library [168].

3.4 Atomic potential

Adaptive Intermolecular Reactive Empirical Bond Order (AIREBO) potential is used in current work. [169]. This potential is one of the most successful potentials, and has been applied to model both chemical reactions and intermolecular interactions in condensed-phase hydrocarbon systems including graphene [170]. It contains three terms:

$$U = \frac{1}{2}\sum_{i}\sum_{j\neq i}\left[U_{ij}^{REBO} + U_{ij}^{LJ} + \sum_{k\neq i,j}\sum_{l\neq i,j,k} U_{kijl}^{TORSION}\right]. \quad (3.5)$$

The first term, a slightly modified version of Reactive Empirical Bond Order (REBO) [169], is capable to handle short-range interactions (distance between atoms, r < 2 Å), as well as 3-body (angles) and 4-body (torsions) interactions with nearest neighbor atoms in hydrocarbon systems. The second term takes into account the long-range interactions (2 Å< r < cutoff) using the standard Lennard-Jones potential with a cutoff of 12 Å. The third term is an explicit 4-body potential that describes various dihedral angles in hydrocarbon systems. In AIREBO potential, Lennard-Jones and dihedral terms can be switched on or off, depending on the requirement of the users. AIREBO is a distance-dependent many-body bond order potential which is able to model bond breaking/formation in the system.

3.5 Calculation details

The simulation cell used to perform the MD simulations in the current research contains a single graphene sheet with dimensions of 50 Å × 50 Å. We constructed the graphene sheet so that its armchair and zigzag edges were oriented along the X and Y axes corresponding to [100] and [120] crystallographic directions of graphene, respectively. Periodic boundary conditions (PBC) were applied along the in-plane directions to represent an infinitely large substrate. The C_{60} molecule was positioned at the distance of

3.1 Å on the top of substrate in such a way that one of its hexagonal faces was oriented parallel to the graphene substrate (see Figure 3.1). Hereafter, this configuration is referred as “hexagon in phase” (Hex.-In Phase) configuration. As it will be explained later, this is an initial atomic configuration which is energetically close to the equilibrium state (energy minimum). During our MD simulations, the C_{60} admolecule is free to respond to thermal fluctuations, and exhibits both rotational and translational motion. In order to study dynamics of the system, the microcanonical ensemble was used. At the beginning of each simulation, the energy minimization was performed to relax the atomic positions of the system. The Polak-Ribiere conjugate gradient (CG) method implemented in the LAMMPS code was used for the energy minimization. After the energy minimization, the velocities of the C_{60} molecule and the graphene atoms were assigned according to the Maxwell-Boltzmann distribution at a given temperature. The time step of the Verlet integration algorithm was chosen as 1 fs. In each MD simulation, we run at least 50,000 integration steps (50 ps) to reach the thermal equilibrium. Then, we run 10 ns to sample the data.

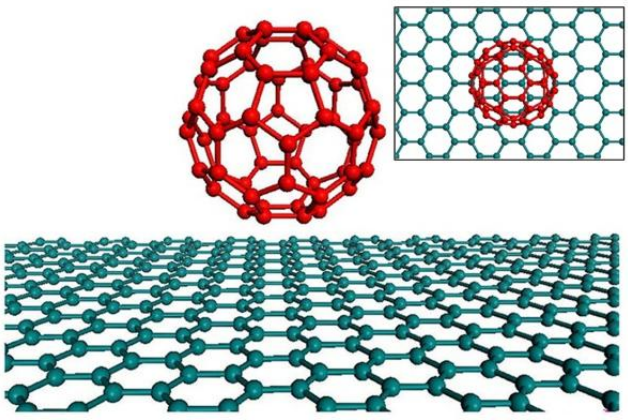

Figure 3.1 Schematics of atomistic model of C_{60}/graphene system, which is used for the present MD simulations of surface diffusion (inset shows the top view of the model).

The trajectories of the C_{60} center of mass (COM) at various temperatures were obtained from the MD simulations. The rotational and translational kinetic energies of the C_{60} were calculated according to the classical mechanics of systems consisted of discrete particles as implemented in LAMMPS code [156, 157]. At a sufficiently long-time, the mean square displacement (MSD) of the C_{60} COM scales linearly with time and the *tracer diffusion coefficient*, D^*, can be calculated using the best linear fit to the MSD curves according to:

$$D^* = lim_{t\to\infty} \frac{\left\langle [\boldsymbol{R}_{COM}(t_0 + t) - \boldsymbol{R}_{COM}(t_0)]^2 \right\rangle}{2td}, \tag{3.6}$$

where, $\boldsymbol{R}_{COM}$ is the two-dimensional position vector of the C_{60} COM, t is the elapsed time from the time origin t_0, <.> denotes time or ensemble average, and d is the dimensionality of the system, which is equal to 2 for the surface diffusion problems. It must be emphasized that our aim in the current thesis is to study diffusion of a single (isolated) C_{60} admolecule, hence for the sake of simplicity, we refer to "traced diffusion coefficient, (D*)" simply as "diffusion coefficient, (D)".

4 Transition from quasi-continuous to ballistic-like Brownian regime

4.1 Introduction

As explained in Chapter 1, atoms, molecules and nanoparticles (such as clusters) are the basic building blocks for many applications in nanoelectromechanical systems (NEMS). When the bottom-up approach is used, these blocks are manipulated through positioning, packing and moving on a surface. Meanwhile, at finite temperature, a building block on a surface may undergo thermally-driven diffusive motion, in which it interacts with its surrounding atoms and experiences kinetic friction [171]. Therefore, there is an intrinsic connection between kinetic friction and surface diffusion at the atomic scale, which has recently attracted considerable attention [72, 172].

Due to the scientific and technological importance of surface diffusion, a great deal of effort has been devoted to understand the microscopic mechanisms by which adsorbates move on a surface [91]. In systems with strong potential energy barriers and at low temperature, surface diffusion occurs through a series of uncorrelated random jumps between neighboring adsorption sites as described by TST (see Section 2.4.1). At sufficiently high temperatures, a crossover from the temperature activated jump regime to the high-temperature Brownian motion (BM) regime was theoretically described [90]. The Langevin equation (LE) provides a remarkably successful technique to study surface diffusion, especially in the case of atomic adsorbates (see Section 2.4.2). It characterizes diffusion by two phenomenological parameters: the strength of the potential energy

barrier E_a, and the kinetic friction coefficient η, which indicates the rate at which energy is transferred between the adsorbate and the surface. Assuming independency between E_a and η, solutions of the one-dimensional (1D) LE describes four distinct regimes of surface diffusion [91, 134]:

Regime I (single jumps): Here, the potential energy barrier (E_a) is high (comparing to the thermal energy (k_BT) of the adparticle) and the friction coefficient η is large, the adsorbate mainly resides inside a local minima of the potential energy surface (PES). The adsorbate moves by hopping from one minimum to an adjacent neighboring minimum. The surface diffusion is described well by the transition-state theory.

Regime II (multiple/long jumps): Here, the potential energy barrier (E_a) is high, and the friction coefficient η is small. The adsorbate moves (hops) from one minimum to a distant local minimum, flying over several sites. In the limit of extremely low friction, the microscopic motion is stick-slip and the trajectory might be characterized as Lévy flight [173].

Regime III (quasi-continuous Brownian motion): Here, the potential energy barrier is low and the friction coefficient η is large. The adsorbate moves continuously without being confined to a single local minimum of the PES. In this case, the adsorbate motion is similar to motion of a Brownian particle in a high-friction (high viscosity) fluid [91].

Regime IV (ballistic-like Brownian motion): Here, the potential energy barrier is low and the friction coefficient η is small. The adsorbate moves continuously without being confined to a single local minimum of the system PES. It travels in trajectories with long linear sections resembling the directional motion of a projectile. In this case, the

adsorbate motion is similar to motion of a Brownian particle in a low-friction (low viscosity) fluid.

Most of the experimental observations of surface diffusion (especially in the chemisorbed systems with high energy barriers) were conventionally described and characterized by the transition-state theory and the single-hop model, although at elevated temperatures, multiple jumps were observed [40]. Characteristics of extremely long jumps (Lévy flight) were observed in systems like gold-cluster/graphite [173], and graphene-flake/graphene [174]. The observation of adsorbates undergoing Brownian motion is relatively rare [72], even though this behavior is theoretically expected at extremely high temperatures [90]. The high-friction Brownian motion (Regime III) was in the benzene/graphite system [72]. To the best of our knowledge, we are unaware of any experimental observation of ballistic-like Brownian motion (Regime IV).

Many issues associated with surface diffusion in the systems with low energy barriers and/or low friction still are not well understood [92]. Therefore, it is necessary to investigate adsorbate/substrate systems with shallow potential energy surface and low friction to study systems which may exhibit nanoscale ballistic-like surface Brownian motion. To this end, we considered the C_{60}/graphene system which is important in current nanoscience research (see Section 1.3.3). It has been shown that a C_{60} monolayer between the graphite plates exhibits ultra-low static friction [77]. Moreover, researchers have reported a shallow potential energy barrier in C_{60}/graphene system [84]. Hence, the C_{60}/graphene system can be an ideal model system to study basic principles of Brownian motion at the nanoscale, and this system is also a promising candidate to exhibit ballistic-like Brownian motion due to its low energy barriers and low surface friction.

In the present chapter, we study the motion of an isolated C_{60} molecule on a graphene substrate, where we identify different surface diffusion regimes, crossover between them, and their underlying mechanisms. We show that the C_{60}/graphene system exhibits both Regimes III and IV, and we reveal a crossover between them by simply increasing the temperature of the system.

4.2 Model and methodology

Our computational model consists of a single C_{60} molecule on graphene. The MD simulations were performed in the temperature range between 5 K and 200 K. Details of our computational model were given in Chapter 3.

4.3 Results and discussions

The trajectories of the center of mass of the C_{60} molecule are plotted in Figure 4.1 for: (a) ultra-low, (b) low, and (c) high temperatures. According to Figure 4.1(a), the single jump mechanism is dominant at the ultra-low temperature of 5 K. With further increasing temperature, our simulations show that multiple jumps gradually dominate. At about 25 K, multiple jumps are dominant, although quasi-continuous motion is also present. Hence, at temperatures below 25 K, C_{60} primarily moves on graphene through the hopping mechanism. At temperatures above 25 K, however, the trajectories suggest that C_{60} no longer undergoes hopping, rather it moves continuously. Qualitatively, as it can be seen in Figure 4.1(b), at temperatures of 40 K, 50 K and 75 K, the trajectories of the C_{60} molecule are consistent with quasi-continuous Brownian motion (Regime III), similar to that observed in the benzene/graphite system [72]. When the temperature is increased above 75 K, the trajectories follow a ballistic-like Brownian motion (Figure 4.1(c)). To

the best of our knowledge, no realistic system has been reported to exhibit the Regime IV, and a crossover between Regimes III to IV.

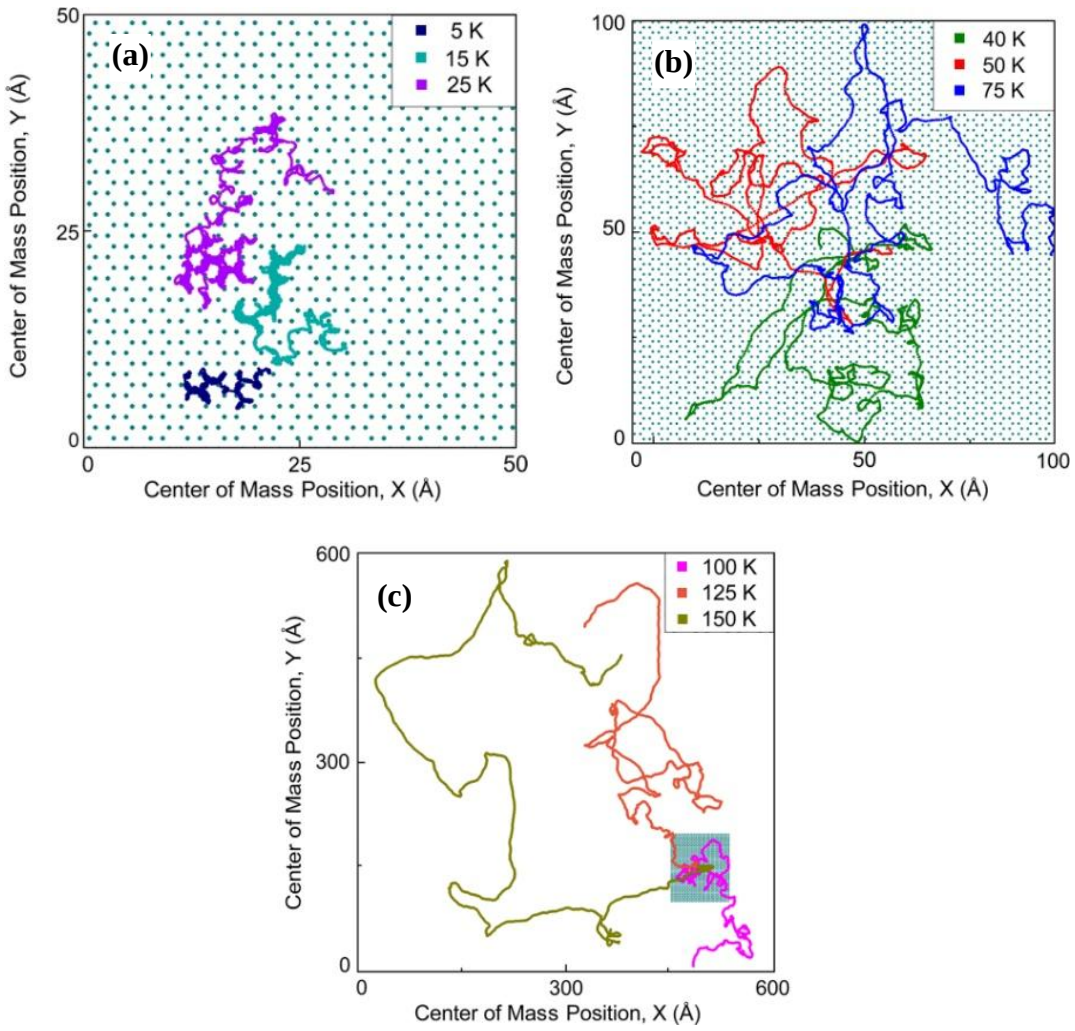

Figure 4.1 Trajectories of C_{60} molecule on graphene surface at (a) ultra-low temperature regime. Single jump motion at 5 K turns to multiple (long) jump motion with increasing the temperature. (b) Low temperature regime, which shows quasi-continuous Brownian motion (Regime III). **(c)** High temperature regime, which exhibits ballistic-like Brownian motion (Regime IV).

We support our above statements through quantitative studies of the time-dependence of mean square displacement (MSD) of the C_{60}'s center of mass, diffusion coefficient, *D*, and the kinetic friction coefficient, η. The diffusion coefficient, *D*, is calculated using the

best linear fit of the MSD at different temperatures. As we discuss in Chapter 6, the surface diffusion coefficient D in the Brownian regimes relates to the kinetic friction η through the Stokes-Einstein theory of Brownian motion: $D= k_BT/(m\eta)$, where m is the mass of the C_{60} molecule. Thus, η, which is identical to the friction coefficient appeared in the Langevin equation (see Section 2.4.2), can be calculated from our simulations.

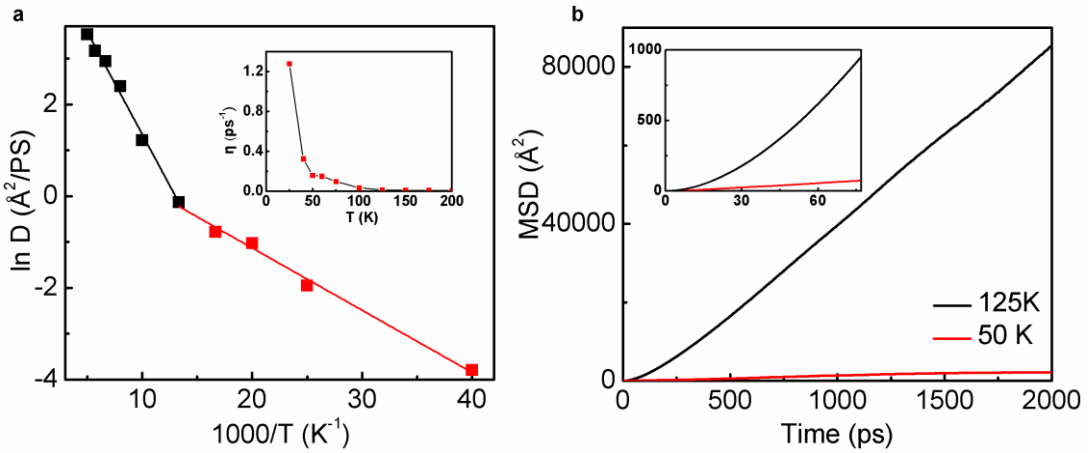

Figure 4.2 Effect of temperature on the diffusion coefficient and kinetic friction of the C_{60}/graphene system. (a) The Arrhenius analysis of the surface diffusion coefficient D of the C_{60} indicates the existence of two diffusive regimes with a crossover around 75 K. The inset of (a) illustrates that the friction coefficient decreases from 1.3 ps-1 to a value of an order of 0.01 ps-1 when the temperature is increased from 25 K to 200 K. (b) Mean square displacement (MSD) of C_{60} motion as a function of time at 50 K and 125 K. Note that at 50 K, the MSD grows linearly with time, consistent with quasi-continuous Brownian motion. At 150 K, the MSD is initially parabolic for time shorter than 1/ η, consistent with ballistic-like Brownian motion.

The variation of diffusion coefficient D with temperature is shown in Figure 4.2(a). From this plot, D appears to follow Arrhenius-like behavior with two different regimes. A crossover between these regimes is observed at about 75 K. The measured activation energies are ~11 meV and ~36 meV for the low and high temperature regimes, respectively. The inset of Figure 4.2(a) shows the calculated kinetic friction coefficient of the C_{60}/graphene system as a function of temperature between 25 K and 200 K. It can be

seen that as the temperature increases, the friction coefficient η drastically decreases as the temperature increases. This indicates that the C_{60} molecule experiences ultra-low kinetic friction at elevated temperatures. The analysis suggests that the kinetic friction coefficient, η, in C_{60}/graphene system is strongly temperature dependent (see Chapter 6). The transition between Regimes III and IV can also be identified by investigating the behavior of MSD of the C_{60}'s center of mass. Figure 4.2(b) shows the MSD curves as a function of time for low (50 K) and high (125 K) temperatures, which correspond to Regime III and IV, respectively. It is clear that at high temperature (125 K), the MSD curve starts as parabolic function and approaches to a straight line after a characteristic time of $1/\eta$, which matches the characteristics of Regime IV [91, 134]. On the other hand, at 50 K, the parabolic part is not observable and the MSD curve is readily rectilinear, indicating the Regime III [91, 134]. In the inset of Figure 4.2(b), we plot the above MSD curves at the short time scale of about 77 ps to clearly illustrate the characteristics of the two regimes of Brownian motion.

Because of the importance of rotational degrees of freedom (DOF) in this system, it is not possible to completely understand the dynamics of the diffusing C_{60} using only the Langevin model for its center of mass. To this end, we examine the interplay between translational and rotational kinetic energies of the C_{60} molecule during its motion on the surface. Figure 4.3(a) and (b) show the distinct energy conversion patterns between rotational and translational modes of C_{60} motion at 50 K (in Regime III) and 200 K (in Regime IV), respectively.

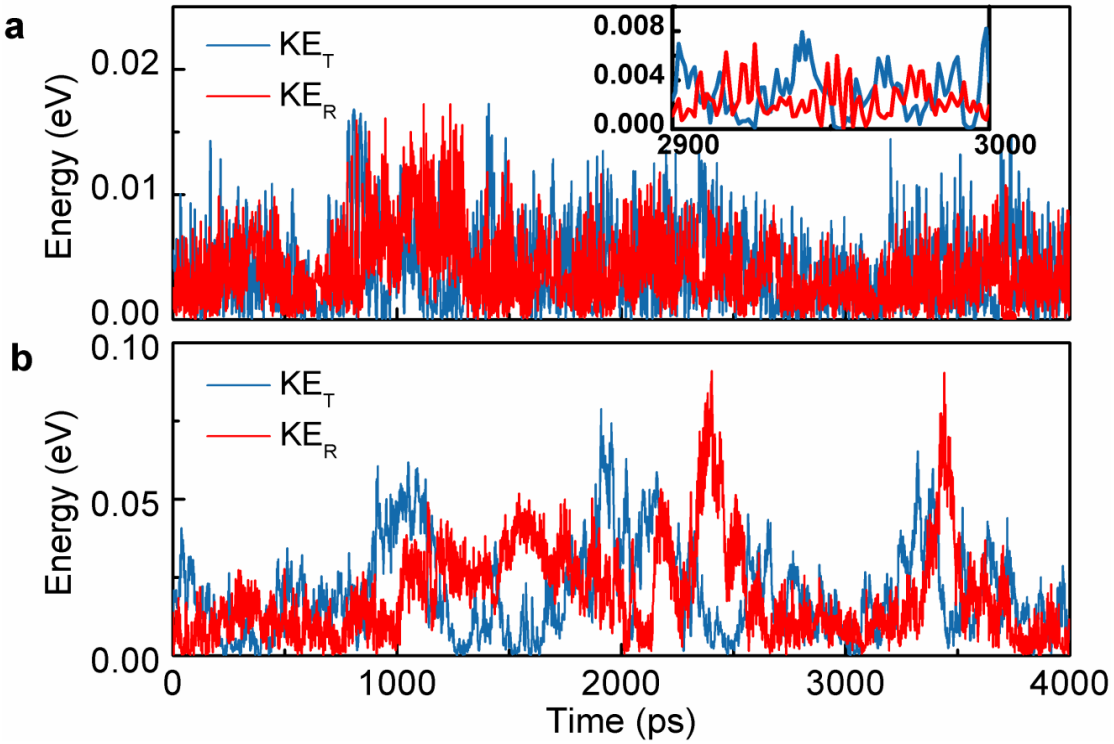

Figure 4.3 Conversion between the translational and rotational kinetic energies of C_{60} during surface diffusion on the graphene at two different temperatures. The temperatures are (a) T=50 K, and (b) T=200 K. The inset in (a) shows the interplay between the translational and rotational energies as a function of time at T=50 K with a higher resolution.

It can be seen that in Regime III (Figure 4.3(a)), that is, at the low temperature regime, the energy transfer occurs with a higher frequency comparing to that in Regime IV (Figure 4.3(b)), that is, the high temperature regime. This pattern suggests that in Regime III, the energy corrugation of the surface (corresponding to the PES) plays an important role in the "push-pull" of the energy between translational and rotational DOF, and the anti-correlation between these DOF occurs with a higher frequency (see Figure 4.3(a)). In contrast, in Regime IV, the overall kinetic energy of the C_{60} is high compared to the shallow PES, and the C_{60} receives extra kinetic energy from the high energy thermally excited graphene atoms in the form of instant kicks. A detailed analysis of thermal vibrations of single-layered graphene is addressed in the literature [172]. Here, it is

noteworthy that the atoms of a defect-free graphene substrate have instantaneous and random thermal corrugations with magnitude $\langle u_z^2 \rangle$ proportional to k_BT. At high temperatures, the role of the PES is negligible in the "push-pull" of the energy between translational and rotational DOF. When the high speed C_{60} moves over the graphene surface, it occasionally collides with the surface thermal corrugations. Due to such collisions, the energy is exchanged between the C_{60} and the graphene, as well as between the C_{60}'s translational and rotational DOF. Generally, such collisions do not lie on the C_{60}'s center of mass and thus create rotational torques. As a result, translational energy is converted into rotational energy. On the other hand, rotating C_{60} may also hit another thermal bump of the surface and pull kinetic energy back into the translation mode. This process is repeated during motion and exhibits as a clear anti-correlation between translational and rotational kinetic energies of the C_{60} (see Figure 4.3(b)).

The anti-correlation between translational and rotational DOF at high temperatures resembles the "ballistic nanofriction" process recently described by Guerra *et al.* in the gold-cluster/graphite system [172]. The mechanism of ballistic nanofriction in their work appears to be similar to the mechanism of motion in Regime IV reported here in two ways: first, it also exhibits a clear anti-correlation between rotational and translational kinetic energies; second, their damping mechanism is governed by the thermal corrugation, and not the potential corrugation of the substrate. Nevertheless, there is a fundamental difference between our and their work. In their work, the ballistic regime was achieved by applying a large instantaneous external force to the gold cluster to generate an initial kick. Hence the gold particle is not in thermal equilibrium, and the

linear-response theory and the Einstein theory of Brownian motion are no longer applicable to their motion.

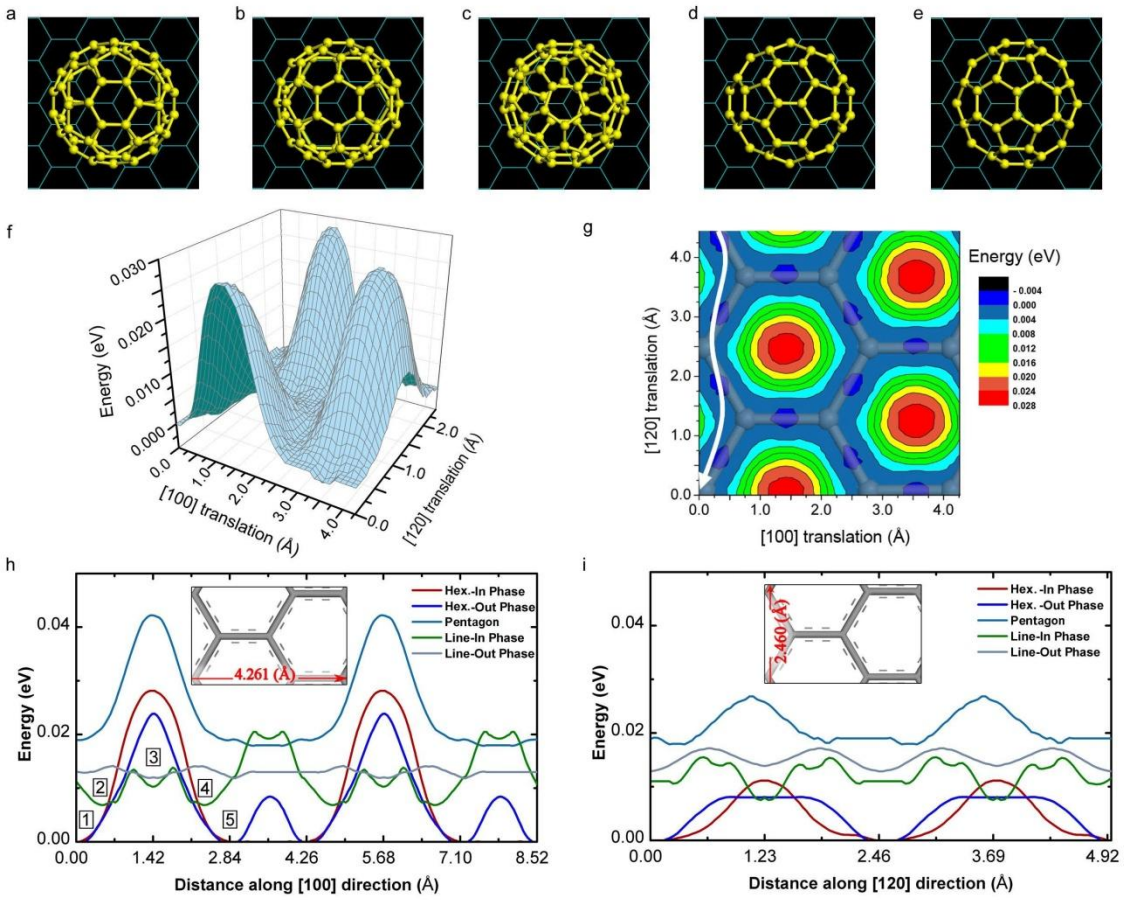

Figure 4.4 The effect of rotational degrees of freedom of C_{60} on the potential energy surface (PES). (a-e) Various configurations are used to examine the PES profiles. These configurations are named as: (a) Hex.-In Phase; (b) Hex.-Out Phase; (c) Pentagon; (d) Line-In Phase; and (e) Line-Out Phase; (f) Three-dimensional PES for the Hex.-In configuration. (g) The contour plot of the PES in (f). The white arrow in (g) indicates the diffusion path with the lowest energy barrier. The arrangement of graphene atoms and their bonds is illustrated in the insets. (h) and (i) show the PES profiles for the C_{60} with different facets as shown in (a-e) during translation along the [100] and [120] crystallographic directions of graphene, respectively.

Since the PES plays an important role in the characteristics of diffusive and quasi-continuous motion of C_{60} on graphene (Regime III), we examine the PES of C_{60}/graphene

system by including the effects of both the facets and finite size of C_{60} (see Figure 4.4). Figure 4.4(f) shows the PES calculated for the Hex.-In Phase configuration of the C_{60} on graphene (see Figure 4.4(a)). According to Figure 4.4(f), the magnitude of PES in C_{60}/graphene system is in the order of a few meV, which is reasonable in a physisorbed system. Such a "flat PES", in the order of a few meV, has been also reported recently in the physisorbed benzene/graphite system [72].

The contour plot of the energy surface of Figure 4.4(f) is presented in Figure 4.4(g), in which a path (indicated by the white arrow) parallel to the [120] crystallographic direction of the graphene is illustrated. This path indicates a smooth diffusive passage with a negligible energy barrier of about 4 meV. Therefore, it might be expected that the trajectories of the C_{60} molecule must be confined in this minimum energy path. However, this is not the case in the temperature range studied in the current work. According to Figure 4.4(h-i), when a C_{60} molecule faces an energy barrier, the molecule can overcome it by rotating to another configuration with an even lower barrier. We illustrate such scenario using Figure 4.4 (h): the C_{60} in the Hex.-In Phase orientation may move from Point 1 to Point 5 along the [100] direction, where it has to overcome an energy barrier of about 26 meV. However, at Point 2, it can partially tilt to the Line-In Phase orientation (see Figure 4.4(d)) and move to Point 3 and then to Point 4 by crossing a lower energy barrier. After passing Point 4, the C_{60} can tilt back to the Hex.-In Phase orientation and continue its way along [100] direction to Point 5. Energetically, this whole process is more favorable. Therefore, we conclude that the rotational degrees of freedom of C_{60} together with its faceted shape offer various possible paths on the graphene substrate with

low energy barriers. Consequently, there is no preferable diffusion path for C_{60} on graphene in Regime III.

It must be noted that chemical modification of graphene, which is widely used to control its electronic properties, may have significant effects on the PES of the C_{60}/graphene system, and cause a drastic change in the diffusive behavior of the C_{60} molecule. This concept will be discussed in Chapter 7.

4.4 Summary

In this chapter, the thermally-induced motion of C_{60} on the graphene surface with a shallow potential energy surface was investigated. We found that the C_{60}/graphene system exhibits two distinct regimes of surface Brownian motion. For the first regime, the C_{60} molecule exhibits a quasi-continuous Brownian motion (Regime III) in the temperature range of 25-75 K. For the second one, the C_{60} molecule follows a ballistic-like Brownian motion (Regime IV) at temperatures above 75 K. These two regimes of Brownian motion imply the existence of two distinct mechanisms of energy exchange between the admolecule and the substrate. In Regime III, the PES of the system, i.e. the potential energy corrugation, has a dominant role in the exchange of energy between C_{60} and graphene. In contrast, the thermal corrugation of the graphene plays a dominant role in Regime IV. The crossover between these two regimes arises from the change in the system temperature. The present findings not only provide insights into controlling the surface mass transport and nanoscale kinetic friction, but also may guide experimentalists to observe and characterize the intriguing diffusive regimes in the C_{60}/graphene system and to explore new materials for nanoscale electro-mechanical applications.

5 Effect of rotational degrees of freedom on molecular mobility

5.1 Introduction

Molecules, nanoparticles and nanoclusters, which are shown to exhibit various fascinating structural, electronic, magnetic and optical properties, are the basic building blocks for constructing functional structures and nanodevices [27, 96, 175]. Under thermal activation and/or external fields, these nanoscale building blocks are often required to perform specified movements. However, how to precisely control their motion to achieve the prescribed trajectory or mobility is an on-going research topic [95, 176, 177]. In contrast to an adatom, these building blocks have rotational degrees of freedom (DOFs) and occupy a finite space, whose dimensions are generally larger than the interatomic spacing. As a consequence, their diffusion behavior is more complex than their atomic counterpart [93, 94]. Hence, understanding the effect of rotational DOFs of these basic building blocks on their diffusion behavior is not only important to control molecular motion, but also essential for many applications such as nanotribology [172], molecular machinery and nanoelectromechanical systems (NEMS) [178].

The diffusive behavior of a molecule (nanoparticle or nanocluster) on a substrate is fundamental in many practical applications. The complexity of molecular surface diffusion raises questions in using existing atomic diffusion theories to interpret molecular diffusion [93]. The conventional and widely used model of surface diffusion is based on the transition state theory (TST), which describes the diffusion of an adsorbate

as the result of a series of thermally activated and uncorrelated random jumps (hopping) between adjacent adsorption sites [91], and the diffusion process is primarily controlled by the profile (shape) of the potential energy surface (PES) of the system (see Section 2.4.1) [90, 91]. Recognizing the importance of rotational DOFs of nanoscale building-blocks, several studies were performed to understand their effect on the diffusion and friction mechanisms [178-183]. For example, theoretical studies [165, 184, 185] showed that even in the simplest case of rigid molecule consisting of only two or three atoms, rotational DOFs can enhance the surface diffusion rate. Molecular dynamics (MD) studies [186] indicated that the energy barrier of lateral diffusion of an admolecule can be overcome by changing the configuration or orientation of the admolecule. MD simulations [187] also revealed that in the absence of rotational DOFs, a benzene molecule performs stick-slip motion which is accompanied by frequent occurrence of long jumps (flights) on a graphite substrate. The correlation between rotation and translation of adsorbed nanoclusters has been reported in different regimes of motion (diffusive and ballistic) [172]. Despite of all theoretical and experimental efforts, several important questions regarding molecular diffusion remain unanswered: 1) How do the rotational DOFs affect the diffusion regimes? 2) What is the role of rotational DOFs in the interaction between an admolecule and substrate? 3) How to quantify the effect of rotational DOFs on the mobility of admolecule in each regime?

Motivated by the intriguing questions discussed above, we chose C_{60}/graphene as a model system to study the effect of rotational DOFs of the C_{60} molecule on its diffusive behavior on graphene. As it is noted in Section 1.3.3, a detailed understanding of the motion of C_{60} molecule in various environments, including on surfaces and membranes,

is crucial for development of promising applications in nanoscience and technology [84, 188]. Hence, the physisorbed C_{60}/graphene is an ideal system for investigating the role of rotational DOFs in molecular surface diffusion. In the current chapter, we present our systematic simulations of the C_{60}/graphene system in a wide range of temperature in the presence and absence of C_{60} rotational DOFs. We then analyze and compare the resulting diffusive regimes and their corresponding mobilities. Our goal is to address the issues raised above, that is, how C_{60} rotational DOFs affect its surface diffusion regimes and their corresponding mobilities.

5.2 Model and methodology

The computational model consists of a single C_{60} admolecule and a graphene substrate. Following the procedure described in Chapter 3, the MD simulations were performed at the temperature range of 5 K to 200 K. The trajectories of the C_{60} center of mass (COM) at different temperatures were obtained from the simulations. Based on the MD technique used in the current work, all degrees of freedom of the system, including the C_{60} rotational DOFs, were explicitly taken into account. In order to study the effect of rotational DOFs on the dynamics of surface diffusion and mobility of C_{60}, a second series of simulations were also performed at the same temperature range, in which, however, the rotational DOFs of the C_{60} were frozen based on the energy separation technique and routines provided by LAMMPS package [189, 156, 157]. It is noteworthy that in these simulations, only the rotational DOFs of the C_{60} were frozen while all other DOFs of the system remained untouched. The results of two different sets of simulations (in the presence and absence of C_{60} rotation) were analyzed and compared with each other to examine the effect of rotational DOFs on the surface diffusion of the C_{60} admolecule. For

simplicity, hereafter, the C_{60} admolecule in the presence and absence of rotational DOFs are referred to as R-C_{60} and NR-C_{60}, respectively.

5.3 Results and discussion

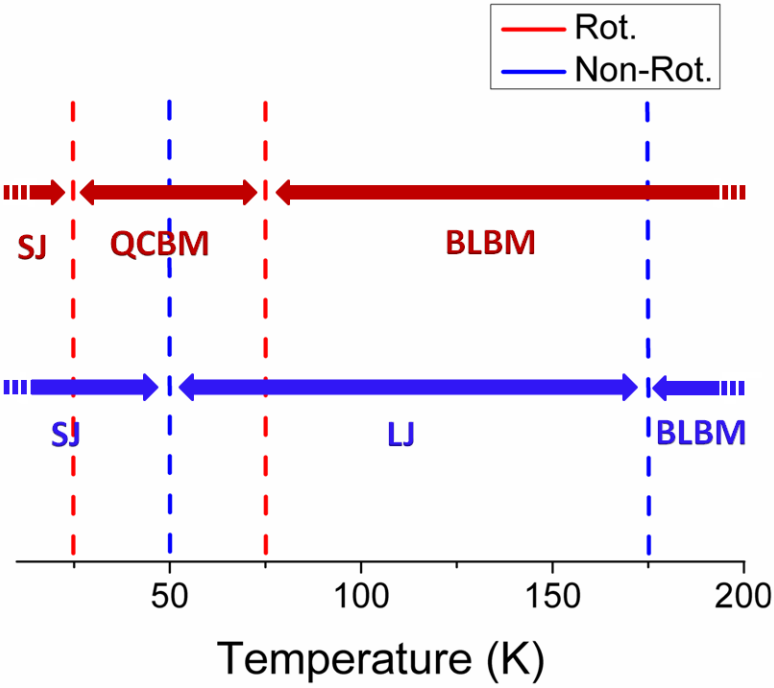

Figure 5.1 Different regimes of surface diffusion in C_{60}/graphene system according to the effect of temperature and rotational degrees of freedom (DOFs) of the admolecule. In the case of rotational C_{60} (the set of arrows in red), the single jump (SJ) regime dominates below 25 K. Between 25 K and 75 K, there is a quasi-continuous Brownian motion (QCBM) regime, which turns into the ballistic-like Brownian motion above 75 K. On the other hand, in the case of non-rotational C_{60} (the set of arrows in blue), the single jump regime (SJ) extends up to 50 K, and then turns into Long Jump (LJ) regime above 50 K. The LJ regime extends up to 175 K and finally there is a BLBM regime at elevated temperature similar to the case of rotational C_{60}.

The simulations were performed to identify and characterize different diffusion regimes in both R-C_{60} and NR-C_{60} systems. The qualitative studies of spatial and temporal trajectories of the admolecule as well as quantitative analysis of its mobility (surface diffusion coefficients, *D*, were carried out and compared. Figure 5.1 summarizes the different diffusion regimes of both systems as a function of temperature. From the upper

set of arrows (red color) of Figure 5.1, it is seen that the R-C_{60} at temperatures below 25 K exhibits the thermally activated hopping motion (stick-slip motion) dominated by single jumps (SJ regime). An increase in temperature leads a transition to Brownian motion (BM) with two distinct regimes: the quasi-continuous Brownian motion (QCBM) between 25 K and 75 K, and the ballistic-like Brownian motion (BLBM) above 75 K. It is noted that the crossover from thermally activated jump regime to Brownian motion by increasing temperature was theoretically predicted [90]. In reality, however, observation of an adsorbate undergoing Brownian motion is relatively rare [72], and the existence of these two distinct regimes of Brownian surface diffusion in the R-C_{60}/graphene system was just recently reported [188]. The lower set of arrows (blue color) in Figure 5.1 shows that the NR-C_{60} exhibits the SJ motion with temperatures up to 50 K. At temperatures between 50 K and 175 K, the NR-C_{60} still performs stick-slip motion; however, its dynamics is dominated by frequent occurrence of very long jumps (flights). At temperatures above 175 K, the NR-C_{60} also undergoes BLBM regime. Clearly, the rotational DOFs are able to alter the regimes of surface diffusion. In the following, we present our qualitative and quantitative analyses of these diffusive regimes.

To qualitatively demonstrate the diffusive regimes of C_{60} admolecule appeared in Figure 5.2, we plot the spatial (x-y) trajectories (4 ns) for each regime in Figure 5.2. This figure presents the trajectories of R-C_{60} and NR-C_{60} in top and bottom rows ((a) and (b) series), respectively. In the case of R-C_{60} (Figure 5.2(a) series), it is seen that the single jump (SJ) motion is dominant at low temperature of 5 K (Figure 5.2(a1)). With increasing temperature, multiple jumps gradually kick in. It is well-known that in the thermally activated jump regime, trajectories of an admolecule might be correlated with the profile

of the PES of the system [90, 190]. Above 25 K (Figure 5.2(a2)), the C_{60} admolecule no longer performs random hopping, rather it moves continuously at temperatures up to 75 K, and its trajectory is consistent with quasi-continuous Brownian motion (QCBM regime), similar to that observed in the benzene/graphite system [72]. With further increasing temperature above 75 K (Figure 5.2(a3)), the trajectories follow a ballistic-like Brownian motion (BLBM). A comparison between Figure 5.2(a2) and 2(a3) implies that in the QCBM and BLBM regimes, the trajectories of R-C_{60} admolecule resemble a Brownian motion in high friction (high viscosity) and low friction (low viscosity) regime, respectively [91].

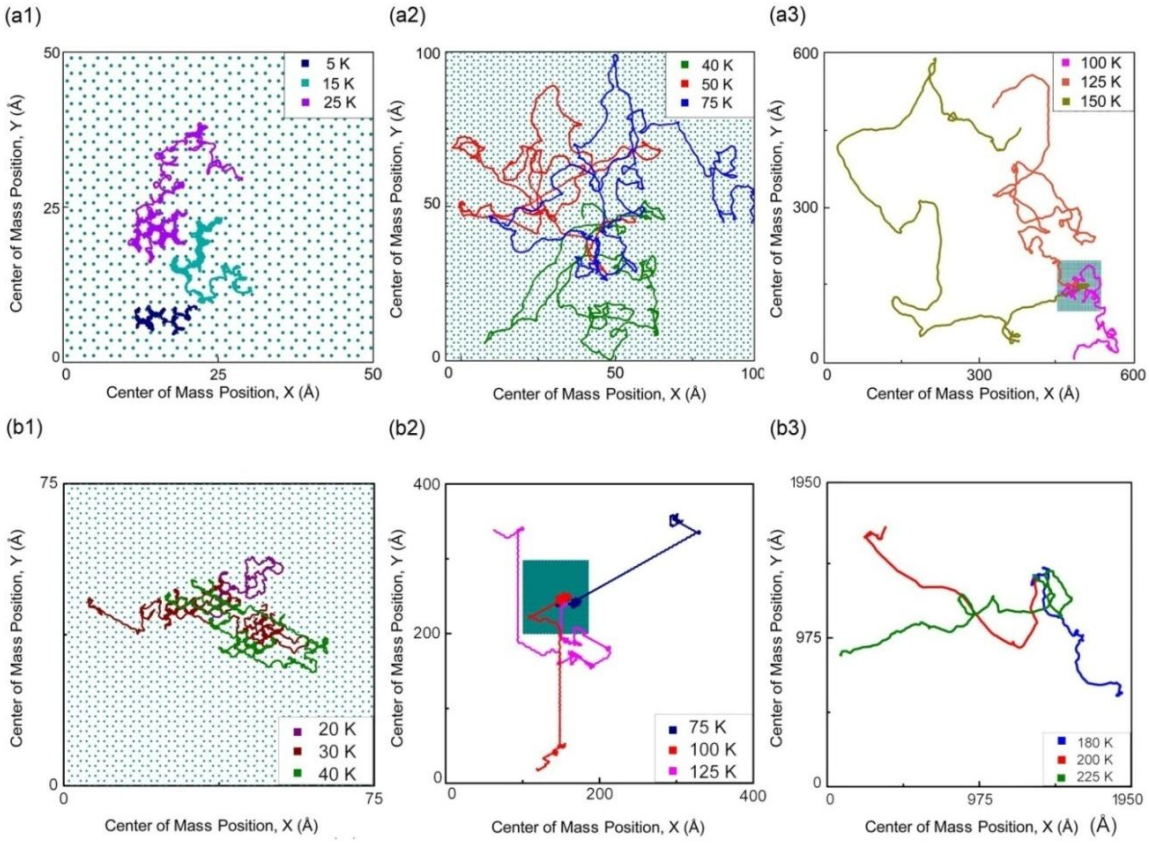

Figure 5.2 Typical trajectories of C_{60} admolecule on graphene illustrate various surface diffusion regimes in the system at different conditions: (a) in the presence of rotational DOFs (a1: SJ, a2: QCBM, a3: BLBM), and (b) in the absence of rotational DOFs (b1: SJ, b2: LJ, b3: BLBM).

According to Figure 5.2(b1), for NR-C_{60} at low temperatures below 50 K, the admolecule exhibits thermally activated hopping mechanism dominated by single jumps. Increasing the temperature leads to increasing the length of random jumps. Figure 5.2(b2) shows the typical trajectories of NR-C_{60} in the LJ regime. Comparing Figure 5.2 (b1) and Figure 5.2(b2) reveals that the anisotropic stick-slip motion, *i.e.* thermally activated jumps in certain crystallographic directions, is a common feature of the trajectories in the SJ and LJ regimes for NR-C_{60}. However, once the NR-C_{60} in the LJ regime acquires enough translational energy towards a specific direction, it performs relatively very long jumps (flights) in comparison with the lattice parameter of the graphene. A visual inspection of trajectories in Figure 5.2(b2) reveals that the stick-slip motion of NR-C_{60} in LJ regime resembles a Lévy flight [191] pattern of diffusion. Similar Lévy flight pattern was also reported in a few other systems, such as gold-cluster/graphite and graphene-flakes/graphene [173, 174, 192]. Figure 5.2(b3) presents the typical trajectories of NR-C_{60} in the BLBM regime, which is similar to the BLBM in the rotational case.

From Fig. 2, it is seen that the trajectory of SJ regime of R-C_{60} (Figure 5.2(a1)) is similar to that of NR-C_{60} (Figure 5.2(b1)). However, in the absence of rotational DOFs, the SJ regime extends up to about 50 K. Moreover, in the SJ regime, the trajectories of both R-C_{60} and NR-C_{60} are anisotropic following certain crystallographic pathways on the graphene substrate. Additionally, in the BLBM regime, the trajectories of both R-C_{60} and NR-C_{60} (Figure 5.2(a3) and 2(b3), respectively) are alike, since in both cases, the admolecule moves continuously, similar to a free Brownian particle without confining to any pathway.

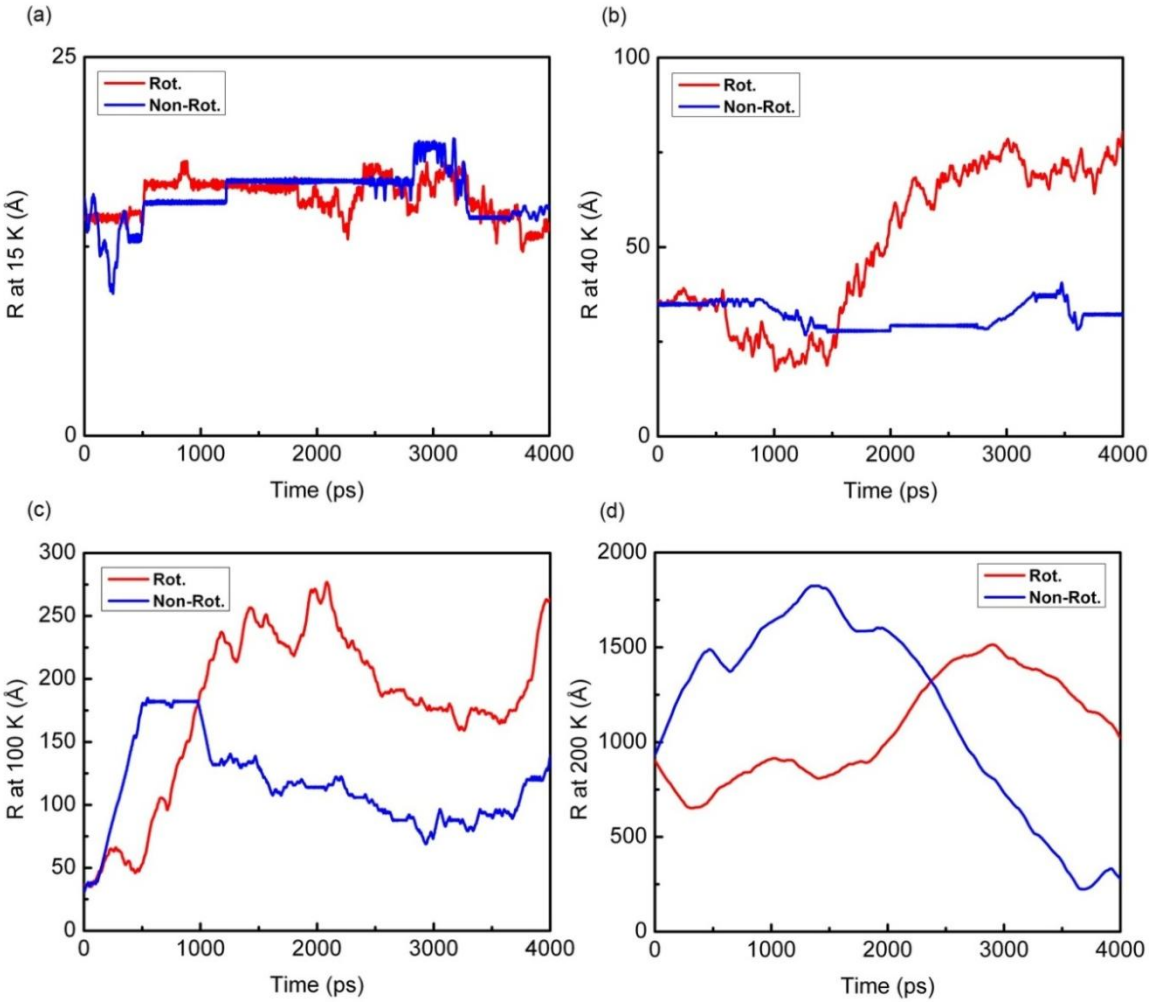

Figure 5.3 Temporal evolution of the position of C_{60} COM, R, in the presence (red curves) and absence (blue curves) of rotational DOFs at different temperatures: (a) 15 K, (b) 40 K, (c) 100 K, (d) 200 K. (a) At very low temperature of 15 K, the C_{60} molecule exhibits a stick-slip (hopping) pattern of motion (the sticking intervals separated by jump events) even in the presence of rotational DOFs. (b) At 40 K, in the absence of rotational DOFs, the C_{60} admolecule still moves by hopping mechanism (dominated by single jumps). However, in the case of rotational admolecule, there are no sticking intervals and the molecule performs Brownian motion (QCBM regime). (c) At 100 K, the rotational C_{60} clearly performs a Brownian motion, where in the absence of rotational DOFs, it still exhibits stick-slip motion during which very long jumps (flights) are observable. (d) At 200 K, in the presence and absence of rotational DOFs, the C_{60} molecule does not stick to a certain absorption site on the surface, and in both cases it performs a free Brownian motion.

To have a clearer qualitative comparison between surface diffusion of C_{60} admolecule in the presence and absence of rotational DOFs, we further analyze the evolution of C_{60} position in time (temporal trajectories), *i.e.* $R_t=[(x_t)^2+(y_t)^2]^{1/2}$, where x and y are the coordinates of the C_{60} COM at time t. The variation of R_t in time as shown in Figure 5.3 is able to reveal the occurrence of trapping in local energy minima, and discriminate between stick-slip and Brownian motion. From Figure 5.3(a), it can be seen that at very low temperature of 15 K, the C_{60} molecule exhibits a stick-slip (SJ) motion with localized vibrations at adsorption sites both in the presence and absence of rotational DOFs. The sticking intervals are separated by hopping events. At 40 K (Figure 5.3(b)), NR-C_{60} still diffuses by hopping mechanism which is dominated by single/short jumps (SJ regime); whereas R-C_{60} moves almost continuously without trapping at adsorption sites (QCBM regime). At 100 K (Figure 5.3(c)), R-C_{60} exhibits continuous BM; whereas NR-C_{60} still exhibits stick-slip diffusion with frequent occurrence of long jumps (similar to Lévy flight). Comparing the R_t curves of NR-C_{60} in Figure 5.3(a, b and c) indicates a crossover in the surface diffusion of NR-C_{60} from the SJ to LJ regime. At 200 K (Figure 5.3(d)), the temporal trajectories of R-C_{60} and NR-C_{60} are almost identical and the admolecule undergoes a Brownian motion, corresponding to the BLBM regimes in Fig. 1.

The quantitative analysis was also carried out to characterize the diffusive regimes of C_{60}/graphene system for both R-C_{60} and NR-C_{60}. The diffusion coefficient, D, was calculated using the best linear fit to the MSD curves for the temperature range of 10 K to 200 K. The variation of the logarithm of D versus the inverse of the temperature is plotted in Fig. 4 for both R-C_{60} and NR-C_{60}. To analyze the temperature dependence of

the diffusion coefficient, *D*, we employed the widely used Arrhenius form consisting of a prefactor, D_0, and an exponential term as:

$$D = D_0 \exp\left(-\frac{E_a}{k_B T}\right), \tag{5.1}$$

where E_a is the activation energy of the diffusion process.

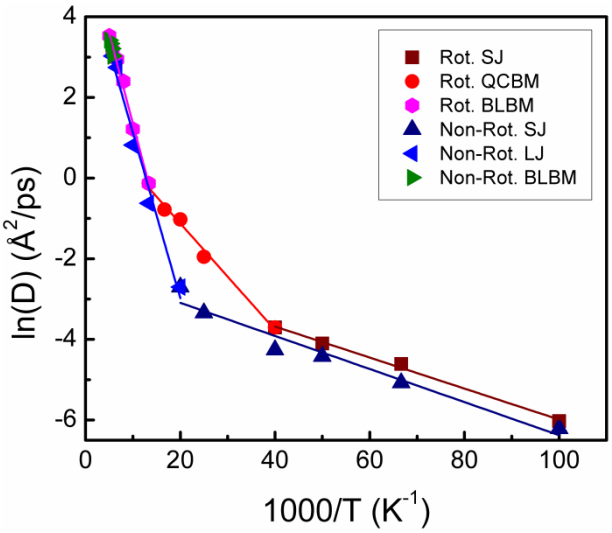

Figure 5.4 Effects of temperature and rotational DOFs on the diffusivity of the C_{60} admolecule on graphene surface. The Arrhenius analysis of surface diffusion coefficient, D, indicates that in the temperature range of 10 K to 200 K, and in the presence or absence of rotational DOFs, the system undergoes distinct regimes of surface diffusion.

If the adsorbate follows the traditional description of surface diffusion based on the single jump mechanism and the transition state theory (TST) at the entire temperature range, the Arrhenius analysis would offer a perfect linear fit, and the resulted activation energy of diffusion would coincide with the potential energy barrier of the diffusion path [91]. However, Figure 5.4 illustrates that at the studied temperature range, the values of *D* for both R-C_{60} and NR-C_{60} deviate from a single linear fit. Hence, a single value of activation energy cannot be assigned to explain the dynamics of the systems, but rather,

D appears to follow several Arrhenius regimes with different activation energies. The corresponding D_0 and E_a values of the Arrhenius regimes and their corresponding temperature ranges are summarized in Table 5.1.

Table 5.1 Arrhenius parameters of different diffusive regimes and their corresponding temperature ranges in the presence and absence of admolecule rotational DOFs (R-C_{60} and NR-C_{60}, respectively).

System	Regime	D_0 (Å^2/ps)	E_a (meV)	Temperature range (K)
R-C_{60}/graphene	SJ	0.12	3.8	< 25
	QCBM	4.6	11.3	25-75
	BLBM	330.3	36.4	> 75
NR-C_{60}/graphene	SJ	0.14	4.1	<50
	LJ	107.2	29.6	50-175
	BLBM	343.9	37.8	>175

In order to illuminate the mechanisms of different regimes of surface diffusion for both R-C_{60} and NR-C_{60}, we would like to address a key question: why does NR-C_{60} follow the same directional pathway in its SJ and LJ regimes (see Figure 5.2(b1, b2))? To answer this question, we study the PES of the C_{60}/graphene system since it plays an important role in diffusion dynamics behind the scene of admolecule motion. The most stable configuration of C_{60}, that, is, one of its hexagons is oriented parallel to the hexagons of the graphene substrate [193, 194], was used to generate the PES of the system. We refer to this atomic configuration (see Figure 3.1) as "hexagon in phase" (Hex.-In Phase), and the same configuration was used in diffusion simulations of NR-C_{60}. The 3D PES is presented in Figure 5.5(a), and its corresponding contour plot is presented in Figure 5.5(b).

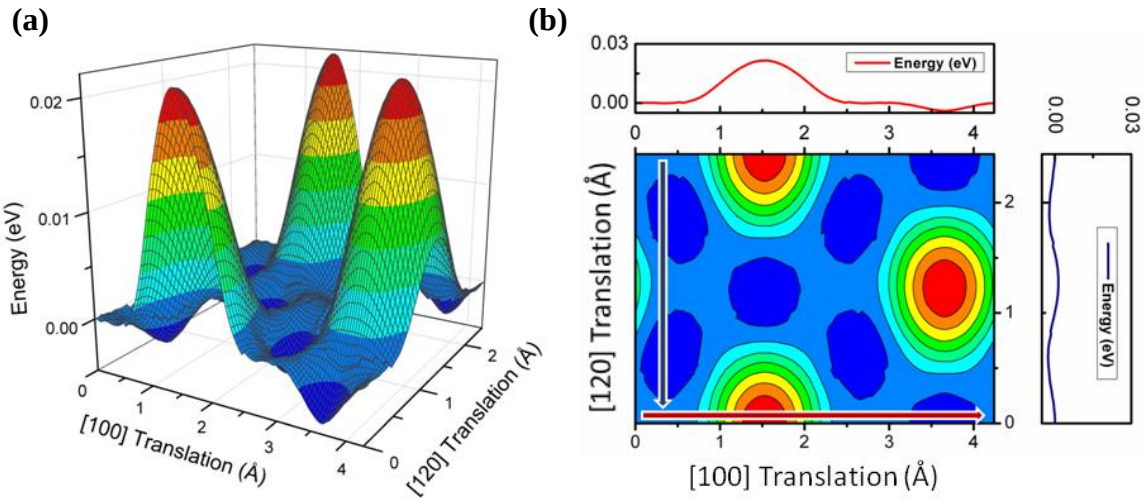

Figure 5.5 Three dimensional potential energy surface (PES) of the C_{60}/graphene system for the Hex.-In Phase configuration. (b) The corresponding contour plot of the PES. The potential energy profile of the path in the [100] crystallographic direction of graphene (the horizontal red arrow), is plotted on the top inset; while the potential energy profile of the path in the [120] crystallographic direction of graphene (the vertical blue arrow), is plotted on the right inset.

The PES of the C_{60}/graphene system has a global minimum and maximum when the vertical projection of the C_{60} COM coincides with the center of sp^2 bonds of the graphene carbon atoms, and with the geometrical center of the graphene hexagons, respectively. The difference between minimum and maximum values of the potential energy is about 26 meV. This relatively shallow PES is due to the weak van der Waals interactions between the physisorbed C_{60} admolecule and the graphene substrate. In addition, the PES of the C_{60}/graphene system has an interesting feature: there is a pathway parallel to the [120] crystallographic direction of the graphene (indicated by the vertical blue arrow in Figure 5.5(b)), along which there is a minimum energy barrier of about 4 meV (as illustrated by the potential energy profile in the right inset of Figure 5.5(b)). This pathway implies an energetically smooth channel for C_{60} to diffuse on graphene. Note that the energy barrier along the [100] crystallographic direction of the graphene, which is

indicated by the horizontal red arrow in Fig (5b), is about 6 times higher than that along the [120] direction (see the corresponding potential energy profile in the top inset Figure 5.5(b)). Hence, it can be expected that the trajectories of the NR-C_{60} admolecule should be confined in the diffusion channels parallel to the <120> family of graphene crystallographic directions. Indeed, this expectation is in good agreement with the directional trajectories of the NR-C_{60} in its SJ and LJ diffusive regimes since they follow the <120> directions. At elevated temperatures, the NR-C_{60} transits to the BLBM regime, since the admolecule thermal energy is comparable with the height of the diffusive channels. Hence its diffusion should no longer be confined by the profile of the PES of the system, and thus the admolecule performs a free Brownian motion as seen in Fig. 2(b3).

According to the Figure 5.2 and Figure 5.3, the R-C_{60} exhibits continuous motion in its QCBM regime and it is not localized in any adsorption site or confined in a certain pathway, whereas at the same temperature range, the NR-C_{60} exhibits stick-slip motion along the diffusive channels in <120> direction. To uncover the origin of this difference between two systems, we consider the effects of C_{60} rotational DOFs together with the finite-size facets on the PES of the system. In Chapter 4 we show that when the R-C_{60} admolecule faces an energy barrier on the PES of the system, it can overcome the barrier by rotating/tilting to another configuration with a lower energy barrier. Therefore, in the QCBM regime, the rotational DOFs of C_{60} provide a variety of low energy pathways for the admolecule to surpass the energy barriers, and consequently, there is no preferable diffusion pathway as the case of NR-C_{60}. However, at elevated temperatures, both R-C_{60} and NR-C_{60} undergo BLBM, which is independent of the PES of the system.

The mechanisms described above together with our quantitative analysis of diffusion coefficients for both R-C_{60} and NR-C_{60} can be used to explain the overall effect of rotational DOFs on the mobility of C_{60} admolecule and the temperature range at which this effect is more pronounced. From Figure 5.4 it can be seen that the diffusion coefficient of both systems (R-C_{60} and NR-C_{60}) are almost identical in the SJ and BLBM regimes. In the SJ regimes, the activation energy of diffusion for both R-C_{60} and NR-C_{60} is about 4 meV. This is in agreement with the dynamics of surface diffusion of the C_{60} in the SJ regime, which is dominated by hopping between nearest shallow adsorption sites (~ 4 meV) along the diffusion channels parallel to the <120> crystallographic directions of graphene. As it is seen in Figure 5.4, the rotational DOFs clearly enhance the mobility of admolecule in the QCBM regime; while at the same temperature range, the NR-C_{60} still performs stick-slip motion along the confined diffusive channels. Therefore, it can be concluded that the role of rotational DOFs is to enhance the mobility of C_{60} admolecule by helping it to overcome the energy barriers of the PES in the temperature range of QCBM regime (25 K-75 K).

Nanoscale devices such as molecular motors often operate at finite temperatures [22, 81, 195]. Clearly at different temperature regimes, the rotational DOFs of an admolecule can have different impacts on the mobility of the admolecule. The present work provides a framework to control the mobility of these nanoscale building-blocks. Moreover, it is known that surface BM is independent of the PES profile of the system, and the dynamics of motion in the Brownian regime is dominated by kinetic friction [72, 186, 190]. Therefore, there is a natural link between molecular diffusion and frictional forces in the Brownian regime. Hence the presented results provides an opportunity to study the

molecular kinetic friction in two different Brownian regimes (QCBM and BLBM), which is investigated in Chapter 6.

5.4 Summary

In this chapter, we studied the effect of rotational DOFs on the surface diffusion behavior of an admolecule. The C_{60}/graphene was used as a prototypical physisorbed system. We showed that at very low temperature limit, that is, T < 25 K, the dynamics of surface diffusion in both R-C_{60} and NR-C_{60} follows the stick-slip motion dominated by jumps between nearest adsorption sites, which is in agreement with the traditional picture of surface diffusion. At elevated temperatures (T > 175 K) both R-C_{60} and NR-C_{60} are in the BLBM regime and their mobility becomes almost identical. The most pronounced effect of rotational DOFs on the surface diffusion of the admolecule appears in the QCBM regime of the R-C_{60} (at about 25 K and 75 K). In this regime, the rotational DOFs enhance the mobility of C_{60} by providing alternative routes for the admolecule to overcome the energy barriers of the PES so that it performs nearly continuous Brownian motion on the surface; while in the absence of rotational DOFs, the NR-C_{60} still performs a confined stick-slip motion in the diffusive cannels along the <120> crystallographic directions of the surface. Our work provides insights and guidelines for controlling molecular motion.

6 Effect of temperature on kinetic nanofriction of a Brownian adparticle

6.1 Introduction

In developing high-performance mechanical-electrical nanodevices using bottom-up approaches, understanding frictional mechanisms in different regimes for various basic building blocks is essential [194, 196, 197]. Such understanding allows us to quantify the frictional forces at single-atomic/molecular level, offering possibilities to precisely manipulate these building blocks by controlling their driving forces. To this end, various advanced nanomechanical testing techniques, such as scanning tunneling microscopy (STM), atomic force microscopy (AFM), and friction force microscopy (FFM) have been employed to examine surface molecular mobility and measure their frictional forces [49, 50, 198]. However, it is still a challenge to track the motion of individual admolecules and measure the kinetic frictional forces imposed on them by the substrate [72].

In Chapters 4 and 5, we discussed that admolecules might exhibit continuous Brownian motion (BM), which is distinct from the traditional picture of surface diffusion described by thermally activated jump mechanism between neighboring adsorption sites [72, 90, 186]. The dynamics of such admolecules is dominated by a kinetic friction term resembling the BM of a microscale solute particle suspended in a solvent fluid [72, 190]. Hence, experiments and simulations have been conducted to establish the connection between molecular diffusion/drift and kinetic friction at thermodynamic equilibrium [190, 199]. In the microscale systems, Einstein's theory of BM [200] has been widely

employed to characterize the physical properties of the Brownian particle environment such as viscosity or surface forces based on the single particle tracking techniques [100, 201-203]. In the Einstein theory, the tracer diffusion coefficient of a Brownian particle, D, is related to the frictional forces acting on the particle by its surrounding media according to the Stokes-Einstein (SE) relation with a general formulation of [204]:

$$D = k_B T / \gamma, \tag{6.1}$$

where k_B is the Boltzmann constant, T is absolute temperature, and γ is the Stokes coefficient described by:

$$\gamma = F_{fric} / v, \tag{6.2}$$

where F_{fric} is the friction force acting against the motion of the particle, and v is its velocity. Hence, the frictional force is related to Stokes coefficient, γ, which is system- and temperature-dependent. When a solute particle exhibits Brownian motion in a solvent fluid, γ tends to fall by increasing temperature [205]. In gaseous state, however, it increases with increasing absolute temperature (T) and is found to be proportional to $T^{1/2}$ [205, 206]. In liquids, a variety of empirical models have been proposed to predict the temperature dependency of liquid viscosity. A common prediction of these models is that the viscosity of a liquid follows an exponential or Arrhenius-like decay by increasing the temperature [205, 207].

At the nanoscale, BM of admolecules appears in a variety of NEMS applications. A few examples to name are protein motors [208], molecular cargoes [209], nanobearings [194, 210], and building block or precursor materials such as C_{60} or aromatic molecules on graphene/graphite substrates [72, 84, 188, 189]. Consequently, it is both important and necessary to understand the role of γ in the BM of admolecules, and identify the

quantities that influence γ. However, the fundamental understanding of Stokes friction in these nanoscale systems is still limited. Moreover, since the molecular systems are operative in a finite-temperature ambient, how the Stokes friction depends on temperature is largely unknown. In most of the existing phenomenological models, the Strokes coefficient is often assumed to be temperature-independent, and used to study the generic response of the system for a given set of parameters [111, 211]. In a recent effort, Hedgeland *et al.* [72] experimentally measured the diffusion coefficient of a benzene molecule on graphite surface to obtain frictional coefficient of the system in a narrow temperature range around 140 K. The sliding friction force of a gold cluster on graphite at a variety of temperatures was theoretically investigated [$_{60}$]. It was assumed that the gold-cluster diffusion on graphite followed a BM and the SE relation was applicable. However, the actual dynamics of this system was found to be controlled by thermally activated jumps rather than BM. Clearly, the temperature dependence of friction coefficient of a nanoscale molecule exhibiting continuous BM is still unclear. Hence, the main objective of the present study is to understand and further establish the relation between kinetic nanofriction coefficient and temperature.

In the present chapter, we consider the C_{60}/graphene as a prototypical physisorbed system, which has a shallow potential energy surface (PES), to study the kinetic nanofriction in a wide range of temperatures. In Chapters 4 and 5, we show that the C_{60} molecule exhibits continuous BM on graphene substrate at temperatures above 25 K. Consequently, in this chapter we employ the Stokes-Einstein (SE) relation to calculate the friction coefficient of the system from the molecular trajectories and formulate its temperature dependence.

6.2 Model and Methodology

Our computational model consists of a single C_{60} molecule on top of a graphene sheet. The trajectories, energetics and dynamics calculations were performed in the temperature range of 5 K to 200 K. Details of atomic configurations, and MD simulations are provided in Chapter 3. The trajectories of the center of mass (COM) of C_{60} at any given temperature were obtained from the MD simulations. Then, the values of diffusion coefficient *D* were extracted by using the best linear fit to the mean square displacement (MSD) curves at sufficiently long time according to:

$$MSD = < \Delta r^2(t) > = 2dDt, \tag{6.3}$$

where Δr is the displacement of the particle's COM with respect to the origin, *t* is the time, <.> denotes time or ensemble average, *d* is the dimensionality of the system, which is equal to 2 for the surface diffusion problems. Here, it is important to clarify the validity of Equation (6.3). This equation is valid in a sufficiently long timescale where a Brownian particle is in diffusive regime, *i.e.* $t >> \tau_p$, where $\tau_p = m/\gamma$ is the momentum relaxation time of the Brownian particle, where *m* is the particle's mass [212]. At a short time scale ($t << \tau_p$), the particle performs a ballistic motion and its dynamics is dominated by the inertia effect, and as a consequence, its *MSD* diverges parabolically with time. At longer times, there is a transition from the ballistic to diffusive regime.

6.3 Results and discussion

Typical trajectories of COM of the C_{60} admolecule are shown in Figure 6.1, which illustrates thermally activated hopping motion below 25 K (Figure 6.1(a)), and Brownian motion above 25 K (Figure 6.1(b, c)). It is seen that the single jump mechanism is

dominant at the very low temperature of 5 K (Figure 6.1(b)), and with increasing temperature, multiple jumps kick in and gradually become dominant. In the thermally activated jump regime, trajectories of the admolecule are in correlation with the geometry of PES of the system [90, 188]. At about 25 K, multiple jumps dominate, although quasi-continuous motion is also observable. At above 25 K, the C_{60} admolecule on graphene no longer undergoes hopping, rather it moves continuously. Qualitatively, as it can be seen in Figure 6.1(b), at temperatures up to 75 K, the trajectories of the C_{60} molecule are consistent with quasi-continuous Brownian motion (QCBM), similar to that observed in the benzene/graphite system [72]. With further increase in temperature above 75 K (Figure 6.1(c)), the trajectories follow a ballistic-like Brownian motion (BLBM). A comparison between Figure 6.1(b) and Figure 6.1(c) implies that in Brownian regime, the trajectory of the C_{60} molecule resembles a BM with high friction (high viscosity) at temperatures between 25 K and 75 K (Figure 6.1(b)), while this molecule performs a BM with low friction (low viscosity) above 75 K (Figure 6.1(c)).

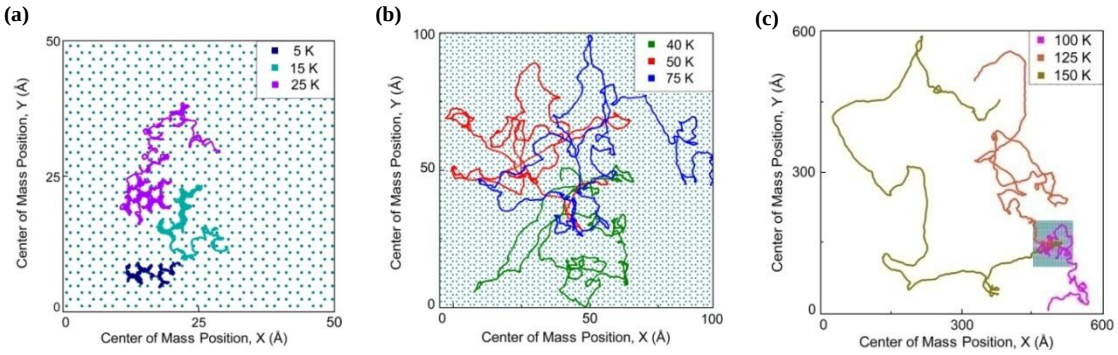

Figure 6.1 Trajectories of C_{60} molecule on graphene surface. (a) Single jump motion at 5 K turns to multiple (long) jump motion with increasing the temperature. (b) Brownian motion of the admolecule resembles high friction (high viscosity) BM below 75 K (QCBM regime), and (c) low friction (low viscosity) BM above 75 K (BLBM regime).

In Figure 6.2, we analyzed the temporal evolution of the C_{60} position, *i.e.* $R_t=[(x_t)^2+(y_t)^2]^{1/2}$, where x and y are the coordinates of the C_{60} COM at time t. The variations of R_t in time can reveal the occurrence of trapping in an adsorption site. From Figure 6.2, it can be seen that the C_{60} molecule exhibits a stick-slip (hopping) motion at very low temperature (see the inset of Figure 6.2, for a better spatial resolution of R at 15 K). In this regime, the diffusive motion of the C_{60} admolecule consists of sticking intervals when the admolecule exhibits localized vibrations at an adsorption site. These sticking intervals are separated by hopping events. However, in Figure 6.2, the sticking intervals are absent at elevated temperatures, indicating the BM of the admolecule.

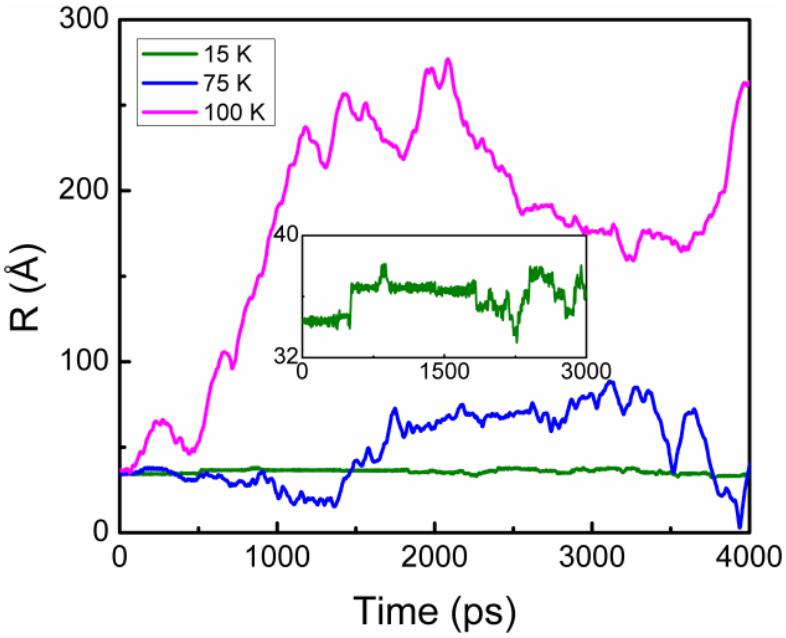

Figure 6.2 Brownian and hopping (stick-slip) surface diffusion. Temporal evolution of positional distance of the C_{60} center of mass from the origin, R, illustrates that at very low temperature of 15 K, the C_{60} molecule exhibits a stick-slip (hopping) pattern of motion (inset: higher spatial resolution of R at 15 K). In contrast, at elevated temperatures, the particle is highly mobile and exhibits a continuous BM.

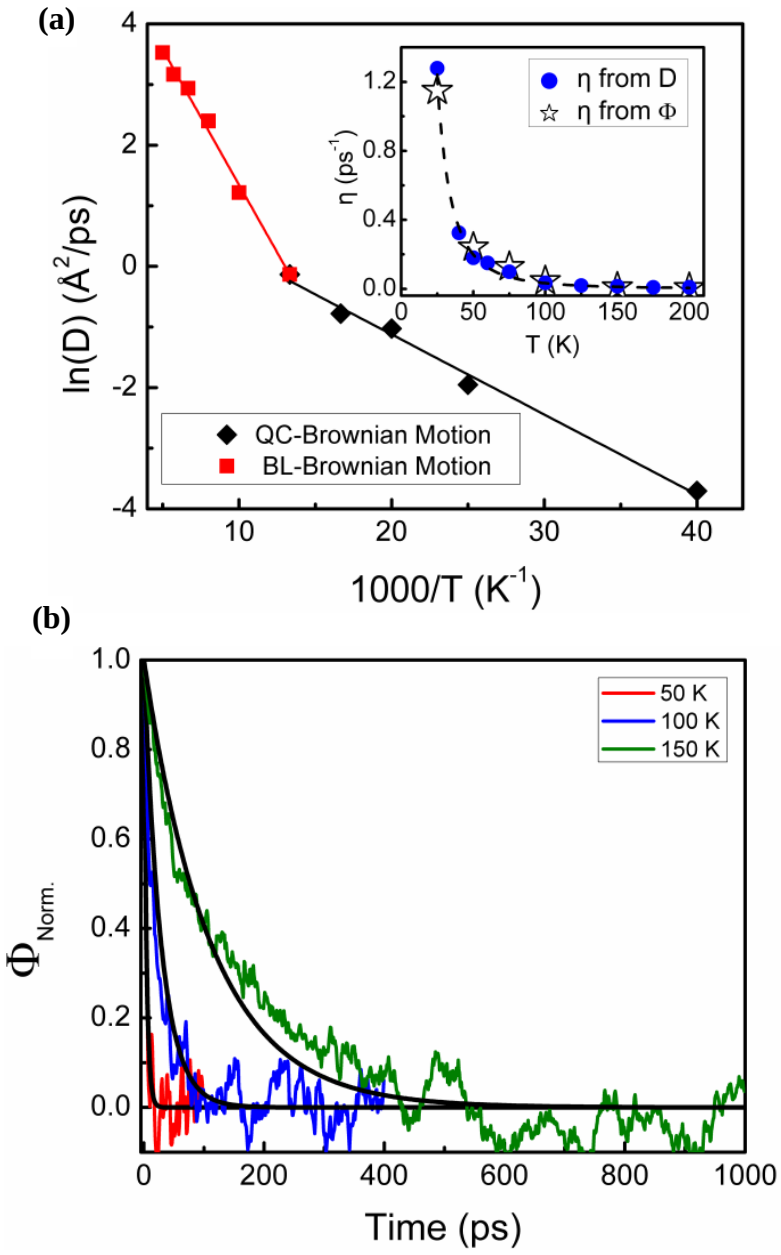

Figure 6.3 Evaluating the temperature effect on the dynamics of surface diffusion and kinetic nanofriction in C_{60}/graphene system. (a) The Arrhenius analysis of surface diffusion coefficient, D, indicates that in the temperature range of 25 K to 200 K, the C_{60} admolecule exhibits two distinct regimes of Brownian motion with a crossover at about 75 K. The inset of (a) shows the kinetic nanofriction coefficient, η, calculated from D and velocity autocorrelation function (VACF), Φ, at different temperatures. (b) Normalized Φ_{Norm} exponentially decays with time. The characteristic time $\tau_p = 1/\eta$ (according to the Equation (6.8)) is extracted at different temperatures.

The diffusion coefficient, D, at different temperatures is calculated using the best linear fit to the MSD curves. The variation of the logarithm of D versus the inverse of temperature is plotted in Figure 6.3 for the temperature range of 25 K to 200 K. An Arrhenius form consisted of a prefactor, D_0, and an exponent is employed to characterize the temperature dependence of diffusion coefficient, D, as:

$$D = D_0 \, exp\left(-\frac{E_a}{k_B T} \right), \tag{6.4}$$

where E_a is the activation energy of the diffusion process. If the adparticle follows the traditional framework of surface diffusion based on the single jump mechanism and the transition state theory (TST), the Arrhenius analysis offers a perfect linear fit, and the resulted activation energy of diffusion coincides with potential energy barrier of the PES of the system [91]. However, from Figure 6.3, it is seen that the values of D at this temperature range in which the admolecule exhibits Brownian motion deviate from a single linear fit. Hence, a unique value of activation energy cannot be assigned to explain the dynamics of the system; rather, D appears to follow two Arrhenius regimes with different activation energies. The crossover between these two regimes occurs at about 75 K. For the low and high temperature regimes, the obtained D_0 values are 4.6 $Å^2$/ps and 330.3 $Å^2$/ps, and E_a values are 11 meV and 36 meV, respectively. These two distinct regimes of the nanoscale BM, which are distinct from the traditional picture of surface diffusion, were recently reported as Quasi-Continuous BM (QCBM) below 75 K, and Ballistic-Like BM (BLBM) above 75 K [188].

Since C_{60} admolecule at the temperature range of 25-200 K exhibits BM, it is valid to explain the dynamics of the system using the SE relation. In the Brownian surface diffusion, the kinetic nanofriction coefficient (η) defined as $\eta = 1/\tau_p$ is often used to

characterize the friction behavior, where τ_p is the characteristic time. Using this definition, the general SE relation can be rewritten for the Brownian surface diffusion as:

$$D = \frac{k_B T}{m\eta} \tag{6.5}$$

Equation (6.5) is used to calculate the kinetic nanofriction coefficient, η, as a function of temperature from D values at 25 K to 200 K. The resulted η values are presented by blue dots in the inset of Figure 6.3. It can be seen that an increase in temperature leads to a decrease in η, indicating a reduction of kinetic friction of a Brownian nanoparticle. The inset of Figure 6.3 also indicates that C_{60} molecule experiences very low kinetic friction at elevated temperatures (around 200 K), which is almost 3 orders of magnitude lower than the kinetic friction at lower temperatures (around 25 K).

From Equations (6.4) and (6.5), the temperature dependence of kinetic nanofriction coefficient can be described as:

$$\eta = \frac{k_B T}{m D_0} \exp\left(\frac{E_a}{k_B T}\right). \tag{6.6}$$

Our analysis indicates that in the considered physisorbed system, the kinetic nanofriction coefficient, η, is strongly temperature-dependent. The inset of Figure 6.3 indicates the existence of two regimes of kinetic nanofriction and their corresponding mechanisms: a high-friction limit at lower temperatures around 25 K, and a low-friction limit at elevated temperatures around 200 K. Their corresponding mechanisms can be interpreted by the frequency of interactions/collisions between the C_{60} and graphene surface at these two regimes. Thus high and low kinetic nanofriction coefficients correspond to the collisions at high and low frequencies, respectively. Recent works [188] showed that at lower temperatures between 25 K and75 K, the C_{60} performs a Brownian motion in which its

rotational degree of freedom plays a vital role in overcoming the energy barriers of the PES (QCBM regime), and the interactions between the admolecule and the energy corrugation of the system (PES) lead to a high collision rate corresponding to the high kinetic friction limit. In contrast, at elevated temperatures above 75 K (BLBM regime), the overall kinetic energy of C_{60} admolecule is high compared to the shallow PES, and the C_{60} exchanges energy with the thermally activated atoms of the graphene substrate with a lower frequency of collisions. Hence, in this regime, the effect of the potential energy corrugations (PES) on the dynamics of the system is negligible [172, 188], and the admolecule exhibits a free Brownian motion on graphene surface with low kinetic friction.

A recent study showed that the nanofriction arises from the aggregate interactions of many vibration modes in the system rather than from a specific vibration mode [213]. Regardless of the complexities, however, the cumulative effect of all interactions/collisions between the admolecule and the surface can be captured by studying the velocity autocorrelation function (VACF) of the admolecule. Hence, to further evaluate the above temperature dependency of single-molecular kinetic friction, we calculate the value of η by analyzing the VACF, Φ, of the C_{60} molecule. At any given elapsed time, t, from the time origin t_0, Φ(t) is described as:

$$\Phi(t) = < v(t_0).v(t_0 + t) >, \tag{6.7}$$

where v is the velocity of the particle COM. The VACF is shown to have an exponential decay with time, and hence can be written as [215]:

$$\Phi_{Norm}(t) = e^{\frac{-t}{\tau_p}}, \tag{6.8}$$

where Φ_{Norm} is the normalized value of Φ at a given temperature. The characteristic time τ_p is the time after which the particle loses the memory of its original velocity due to the frictional drag forces of the substrate, and $\eta = 1/\tau_p$ [214]. Equation (6.8) is used to calculate τ_p from the VACF of the C_{60} COM at different temperatures (see Figure 6.3 (b)). From the calculated values of τ_p at different temperatures, the values of η can be obtained ($\eta = 1/\tau_p$), which are presented in the inset of Figure 6.3(a) by open stars. It can be seen that there is a good agreement between the values of η obtained from two different dynamical aspects of the system, and both methods predict exponential decays of the kinetic nanofriction as a function of temperature.

According to the fluctuation dissipation theorem (FDT) [216], the Einstein relation holds where the particle responds to weak driving forces. Such weak driving forces include the thermal fluctuations at an equilibrium temperature, as well as weak applied driving forces realized in molecular motor [208] and QCM experiments [60]. Hence, within the range of validity of FDT, where the velocity of a drifting nanoparticle (of mass m) is comparable to its thermal velocity ($v_{th} \propto (k_B T/m)^{1/2}$), the kinetic nanofriction force ($F_f = m\eta v_{motion}$) imposed on the particle by the substrate can be evaluated from the diffusion coefficient of its Brownian motion. Therefore, our result can be used to predict the temperature dependence of the required driving force to control a C_{60} admolecule on graphene as a component of molecular devices operating at thermal equilibrium state [171, 208]. Moreover, our findings might help tune the experimental setup for measuring the sliding force in the corresponding QCM experiments, where the required resolution is beyond the temporal/spatial precision of available equipments [60].

6.4 Summary

We used a C_{60} molecule as a Brownian adparticle to understand the temperature dependence of the kinetic nanofriction on graphene substrate. Our analysis revealed the η decreases by increasing the temperature, and its temperature dependence follows an Arrhenius form with two distinct regimes that have a crossover merely by changing the temperature. The velocity autocorrelation analysis further confirmed this finding, which is compatible with the mechanisms of interaction between the admolecule and the substrate. Such temperature dependence of the kinetic nanofriction provides a theoretical framework to study the frictional mechanism and mobility at molecular scale. The C_{60}/graphene is a prototypical physisorbed nanosystem where the dissipation mechanism is dominated by lattice dynamics and thermal vibrations. Similar behavior is expected in many other molecular systems. Therefore, our findings highlight the important role of temperature in nanosystems operating at different temperatures [209, 217], and thus open a possible new route for the development of NEMS.

7 A chemical route to control molecular mobility on graphene

7.1 Introduction

As described in Chapter 1, controlling the motion of nanoscale building blocks on chemically contaminated or modified substrates is a bottleneck in bottom-up approaches to develop high performance. Advances in fabrication at the nanoscale present great opportunities and yet challenges in developing a wide range of Nanoscale Electro-Mechanical Systems (NEMS) [218] such as nanoswitches [219, 220], nanowalkers [221], nanocars [222], and molecular carriers [99, 223]. Effective bottom-up approaches [29], together with efficient computation schemes [224, 225] are crucial to address bottleneck issues that hinder the fabrication, performance and productivity of these NEMS [226]. A closer look at bottom-up approaches reveals that, on the one hand, atoms, molecules and nanoparticles are the basic building blocks to construct NEMS. On the other hand, applications of these NEMS are often at finite temperature, where thermal fluctuations are unavoidable. Therefore, a firm understanding of surface diffusion and mass transport phenomena arising from thermal fluctuations is not only important to reveal new physical insights at the nanoscale, but also to control the basic building blocks, i.e., adsorbates or adparticles, through positioning, packing and moving them for device applications.

Classically, the surface diffusion of an adsorbate is considered as a series of uncorrelated random jumps between neighboring adsorption sites, often described by the transition-state theory (TST). However, at extremely high temperatures, the basic hypotheses of TST are no longer valid, and a crossover from random jump regime to

high-temperature Brownian motion regime takes place [90]. Regardless of mechanism of surface diffusion, its stochastic nature leads to atomic or molecular random motion on substrate surfaces. Consequently, how to precisely control the direction of motion, as well as the mobility of these building blocks becomes an important and practical issue in constructing high-performance NEMS [227]. Although attempts have been made to control the direction and mobility of adparticles on a substrate, for example, by the means of intrinsic guidance on surfaces, such as step edges [228], or by using extrinsic surface templates [229], only limited progress has been achieved [230]. Moreover, regardless of a great deal of theoretical efforts to study the surface diffusion phenomena [91], a universal model which is able to accurately describe the dynamics of the adsorbate/substrate interactions in a variety of systems is still lacking [92]. In addition, at extremely short time scale, for example, at the nanoscale, surface diffusion may exhibit different regimes, i.e., subdiffusion, normal diffusion and superdiffusion. How to identify and control parameters in real systems to achieve a specific diffusion regime is another interesting, and yet challenging issue in designing and constructing NEMS [92, 135].

Motivated by the challenges discussed above we chose C_{60}/hydrogenated graphene, a system promising for various important applications (see 1.3.3) as a model system to study the effect of hydrogenation on the diffusion behavior of C_{60} molecule. In a recent work [101], graphene Moiré patterns have been employed to trap C_{60} molecules for homoepitaxy of graphene nanostructures. Clearly, understanding the energetics and dynamics of such a system is fundamentally important to develop NEMS.

Chemical functionalization of graphene is a well-known approach to manipulate and control its electronic properties [231]. Current theoretical and experimental studies of

functionalized graphene, especially with hydrogen, mainly focus on the chemical, electronic and mechanical properties of the material [231-233]. Although employing chemically functionalized domains on graphene is suggested for molecular packing [102], so far, understanding of the molecular mobility in such a system is lacking. On the one hand, chemically functionalization of graphene may introduce inhomogeneity in the system. This inhomogeneity may lead to specific correlations in the adsorbate motion. On the other hand, although some models have been proposed to describe the motion of an adsorbate on inhomogeneous surfaces, these models cannot treat general cases analytically [234]. Hence, in the present chapter, we aim at understanding the effect of chemical modification of graphene by hydrogen on the diffusive behavior of an adsorbate. To do so, here, we first perform systematic molecular dynamics simulations on the C_{60}/hydrogenated graphene system by changing hydrogen coverage and system temperature. We then propose a theoretical model to predict the diffusive behavior of such a system and compare the model prediction with our molecular dynamics simulations.

7.2 Model and methodology

Our computational model is composed of a single adsorbate and a substrate. A C_{60} molecule was used as the adsorbate, and a hydrogenated graphene sheet used as the substrate. The hydrogen coverage of the graphene sheet varies from 0%, *i.e.* pure graphene, to 100%, *i.e.* graphane. For the hydrogenated graphene substrates, we randomly functionalized the carbon atoms with hydrogen on both sides of graphene according to the coverage. Our technique for the inclusion of hydrogen in the graphene sheet has also been successfully applied to study the mechanical properties of

hydrogenated graphene [233]. The trajectory calculations were performed at temperature ranging from 50 to 300 K**.** Other details of simulations setup is provided in Chapter 3.

Diffusion behavior of the C_{60} molecule can be characterized by the time-dependence of the mean square displacement of its center of mass [234]. At a sufficiently long-time scale, the MSD scales linearly with time, indicating the normal diffusion regime:

$$\mathrm{MSD} = \langle r^2(t) \rangle \propto Dt, \tag{7.1}$$

where $\boldsymbol{r}$ is the displacement vector of the C_{60} center of mass with respect to the origin, t is the time, D, is the diffusion coefficient, and <.> denotes time or ensemble average. Nevertheless, the Equation (7.1) can be generalized as:

$$\langle r^2(t) \rangle \propto t^{\alpha}, \tag{7.2}$$

where α is the diffusion exponent. This exponent determines the diffusive behavior of the adsorbate. At certain time scale, there might exist a transient regime, in which the diffusion is anomalous, depending on the energetics and dynamics of the system. In such scenario, the diffusion exponent can be either $\alpha > 1$, *or* < 1, representing superdiffusive and subdiffusive regimes, respectively [135]. Hence, diffusive behavior also depends on the observation time window. Here, we applied a nanosecond time window to characterize the diffusive behavior of the C_{60}/hydrogenated graphene system since a nanosecond is the typical time scale used in most of the MD simulations, and in a variety of nanoengineering applications [72].

In the normal diffusive regime, *i.e.*, at sufficiently long time scale, the diffusion coefficients, D, can be calculated by using the best linear fit to the mean square displacement (MSD) curves according to:

$$MSD = < \Delta r^2(t) > = 2dDt, \tag{7.3}$$

7.3 Results and discussion

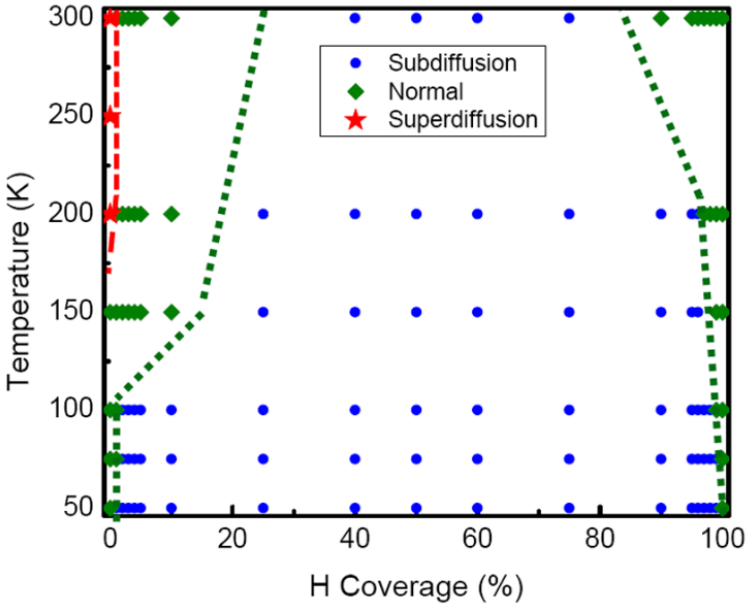

Figure 7.1 Diagram of diffusive behaviors of a C_{60} admolecule on hydrogenated graphene. Temperature and hydrogenation coverage alter the diffusive behavior of the C_{60} admolecule, leading to normal diffusion, subdiffusion and superdiffusion. These regimes are defined based on the MSD behavior of the C_{60} admolecule in a one-nanosecond time window.

In the current chapter, the MD simulations in the C_{60}/hydrogenated graphene system are performed for temperature ranging from 50 to 300 K, and hydrogen coverage from 0 to 100%. The diffusive behavior of the system at a given temperature and coverage is analyzed by examining the mean square displacement (MSD) behavior of the C_{60} molecule over time. The diffusive behaviors at different conditions are summarized as Figure 7.1, which shows a diagram of diffusive behaviors as a function of temperature and hydrogenation coverage. As described in Methods and Model Section, a nanosecond

time window was used to characterize the systems. Figure 7.1 shows the presence of three distinct regimes, namely superdiffusion, normal diffusion, and subdiffusion. Dash lines are drawn to approximately indicate the boundaries between these different regimes. The superdiffusive regime occupies a narrow region of pure/very low hydrogen coverage of graphene at temperatures above 175 K. The normal diffusive regime exists on the left and right sides of the diagram, with either a very low coverage or a very high coverage of hydrogen. At the intermediate coverage of hydrogen, there exists a subdiffusive regime which dominates the diagram. The most important effect of graphene hydrogenation on the diffusive behavior of C_{60} molecule is that minute hydrogenation or dehydrogenation (that is, removal of hydrogen atoms from graphane) leads to a subdiffusive behavior at temperatures ranging from 50 to 100 K. From Figure 7.1, it is seen that at a certain temperature, e.g. 200 K, the motion of the C_{60} molecule transits from superdiffusion, to normal diffusion, then to subdiffusion, and finally to normal diffusion by simply increasing the hydrogen coverage from 0 to 100%. At very low or very high hydrogen coverage, increasing the temperature can change the diffusive behavior from subdiffusion to normal diffusion. However, at an intermediate coverage between 30% and 75%, the system exhibits subdiffusion in all temperatures up to 300 K. Overall, the subdiffusion region is the dominant part of this diagram at the nanosecond time scale.

To demonstrate the diffusive behavior of C_{60} admolecule in three regimes appeared in Figure 7.1, a typical trajectory and MSD curve for each regime at 200K are given in Figure 7.2. This figure shows the trajectories of C_{60} (a1, a2, and a3), and the corresponding MSD curves (b1, b2 and b3) on pure graphene, graphane and partially (50%) hydrogenated graphene, respectively. Figure 7.2(a1 and b1) reveal the typical

characteristics of the trajectory and MSD curve of superdiffusion. Figure 7.2(a1) indicates that at a relatively high temperature, e.g., 200 K, the C_{60} molecule exhibits a ballistic-like Brownian motion on pure graphene. In this case, the adsorbate motion is similar to that of a Brownian particle in a low-viscosity liquid. According to Figure 7.2(b1), the MSD curve of the C_{60} molecule on pure graphene at 200 K exhibits a pronounced parabolic initiation, indicating the ballistic-like motion of C_{60}. For this case, the overall diffusion exponent, α, is about 1.6. Figure 7.2(a2 and b2) show the typical features of normal diffusion: the quasi-continuous Brownian motion of C_{60} on graphane has a readily linear MSD behavior with $\alpha=1$. Nevertheless, the diffusion of C_{60} on partially functionalized graphene is clearly different: The trajectory in Figure 7.2(a3) shows that the C_{60} molecule only vibrates around the local minima of the potential energy surface (PES). Its trajectory, even at relatively high temperature of 200 K, is confined in a small portion of the substrate and the C_{60} molecule does not exhibit any long-range motion. The MSD curve in this case exhibits a sublinear behavior, and has the overall diffusion exponent, α, of about 0.3, which is the signature of subdiffusion. From Figure 7.2 (b1) and Figure 7.2(b2), it is seen that the mobility on pure graphene is approximately one order of magnitude higher than that on graphane. However, the mobility of C_{60} in the subdiffusive regime (Figure 7.2(b3)) is about 5 orders of magnitude lower than its mobility on pure graphene at the same temperature.

In the absence of any external force in our simulations, the physics behind the scene of normal and anomalous diffusive behaviors must be related to the magnitude and topology of the PES of the C_{60} on different substrates. Here, we have calculated the PES for the following three systems: C_{60} on pure graphene, graphane, and partially hydrogenated

graphene (Figure 7.2). If one of the hexagons of C_{60} admolecule is parallel to the hexagons of graphene, energetically, the C_{60} molecule is in the most stable configuration [235]. We refer to this configuration as "hexagon in phase" (Hex.-In Phase) and used it to calculate the PES for each system. (a1, a2 and a3) show the atomic configurations of the three systems, in which carbon and hydrogen atoms are represented by gray and red spheres, respectively. The hydrogen atoms above and below the graphene sheet are denoted by full red spheres and hollow red circles, respectively. Their corresponding PES contour plots are presented in Figure 7.3(b1) to (b3). In these figures, the spectrum of colors from red to blue corresponds to the highest to lowest values.

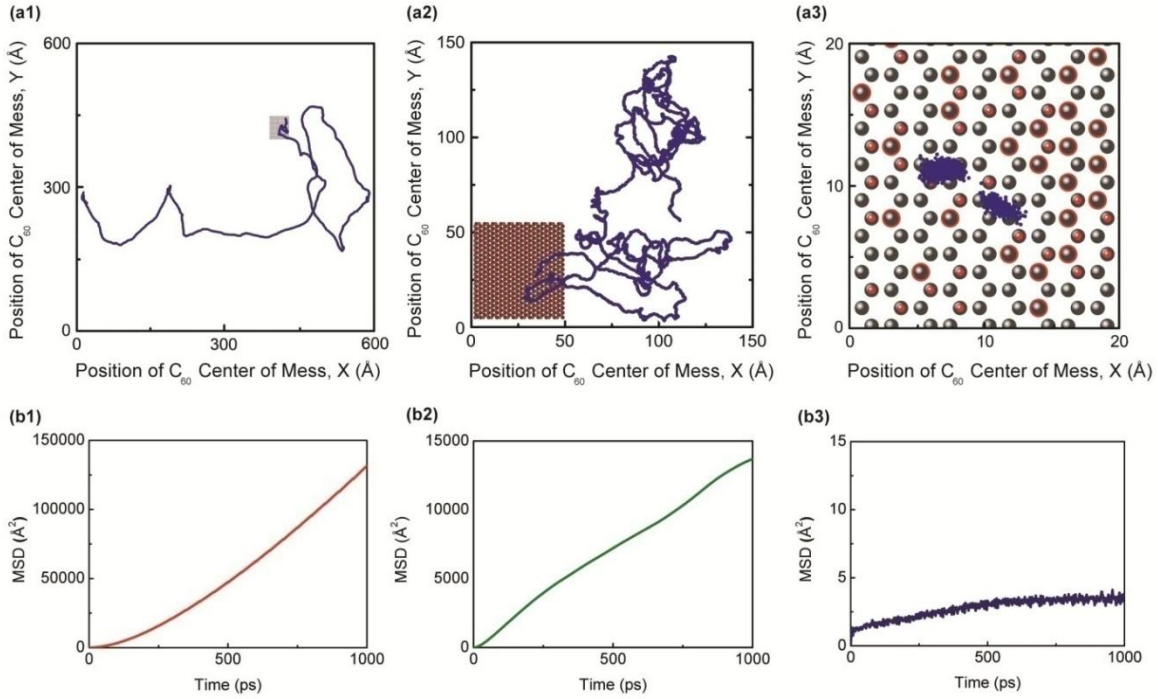

Figure 7.2 The trajectories (a) and MSD curves (b) of the C_{60} admolecule on three different substrates at the same temperature of 200 K. (1) superdiffusion on graphene, (2) normal diffusion on graphane, and (3) subdiffusion on partially hydrogenated graphene (50%). The logarithmic analysis of MSDs (according to Eq. (7.2)) yields the value of α, which is 1.6 in (b1), 1 in (b2) and 0.3 in (b3), corresponding to the superdiffusion, normal diffusion and subdiffusion, respectively.

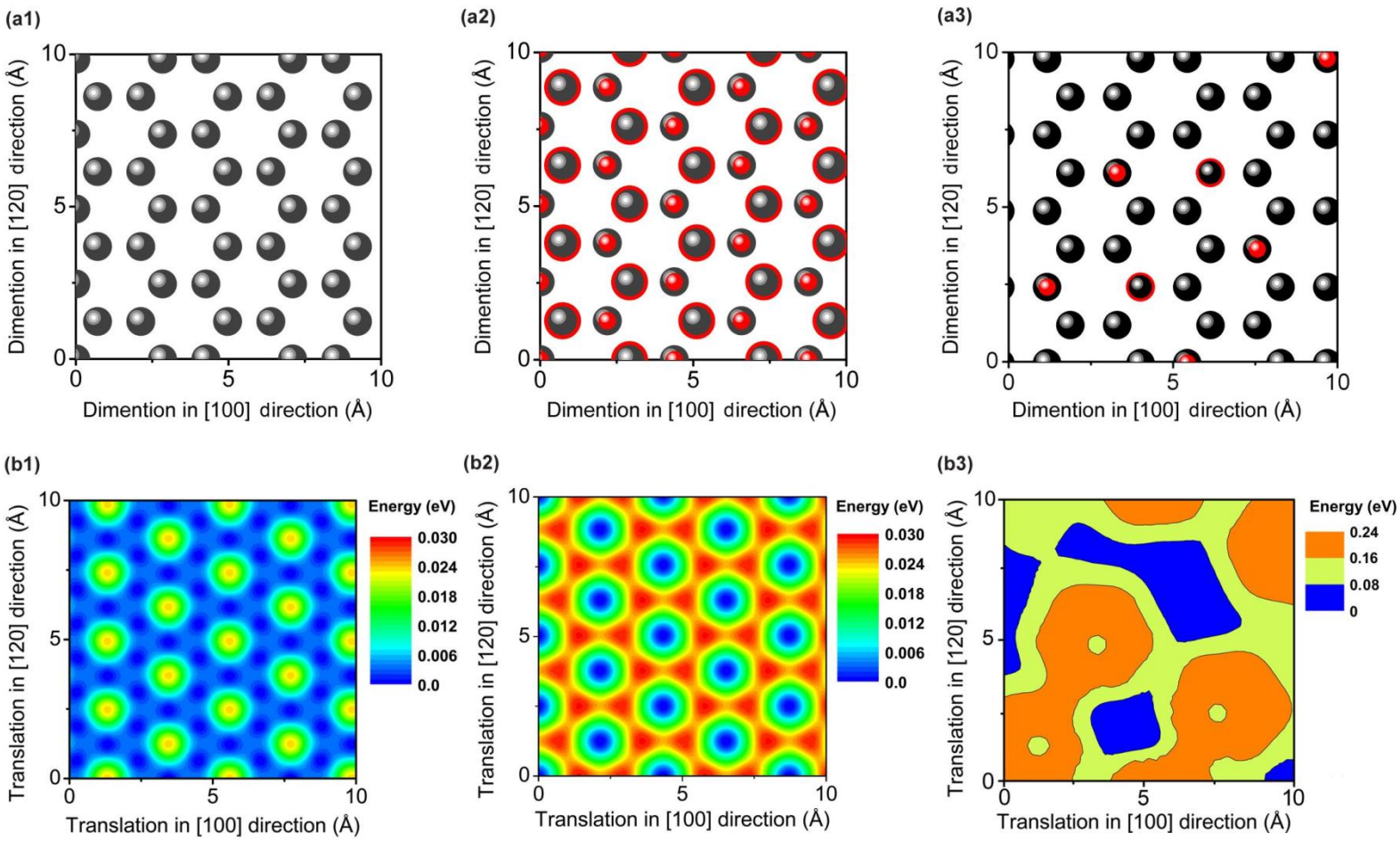

Figure 7.3 Atomic configuration of the substrates (a) and potential energy surfaces (b) of three different systems: C_{60} molecule on (1) graphene, (2) graphane, and (3) partially (15%) functionalized graphene.

First, we investigated the PES of the C_{60}/graphene system (see Figure 7.3(a1)) for the Hex.-In Phase configuration, and its contour plot is shown in Figure 7.3(b1). According to Figure 7.3(b1), the global minimum energy in C_{60}/graphene is reached when the vertical projection of the C_{60} center of mass coincides with the middle of sp^2 carbon bonds of the substrate. Meanwhile, the global maximum of this PES is reached when the vertical projection of the C_{60} center of mass coincides with the geometrical center of graphene hexagons. The difference between the minimum and maximum values of the potential energy is only 26 meV, indicating a very shallow PES arising from the Van der Waals interactions between physisorbed C_{60} molecule and graphene substrate. However, the PES of C_{60}/graphene system has another interesting feature: in this system, there exists a path parallel to the [120] crystallographic direction of the graphene (the blue channel in Figure 7.3(a1)), along which there is a negligible energy barrier of about 4 meV. Such a path provides a diffusion highway for C_{60} motion on graphene.

To examine the effect of hydrogenation on the PES, we calculated the PES of C_{60} on graphane, i.e., fully hydrogenated graphene (see Figure 7.3(a2)), for the same Hex.-In Phase configuration. The corresponding PES contour plot is shown in Figure 7.3(b2). According to the PES of C_{60}/graphane system, the global minimum energy occurs when the vertical projection of the C_{60} center of mass coincides with the position of a hydrogen atom above the substrate. In this system, if the vertical projection of the C_{60} center of mass coincides with two positions, a saddle point in the PES arises: 1) the geometrical center of the graphene hexagons, and 2) the hydrogen atoms added to the substrate in the opposite side of the C_{60} admolecule. The difference between the minimum and maximum values of the potential energy is about 30 meV, which also indicates a shallow PES.

However, there is an apparent difference between the potential energy surfaces of C_{60}/graphene and C_{60}/graphane systems: in the former system, a smooth diffusion pathway (the blue channel) exists for the C_{60} molecule (see Figure 7.3(b1)); whereas, in the later system, the potential energy wells are surrounded by high energy hills and there is no fast diffusive pathway (see Figure 7.3(b2)). Hence, although the magnitudes of PES corrugation in the C_{60}/graphene and C_{60}/graphane systems are almost the same, the difference in their topological characteristics leads to about one order magnitude difference in the mobility of C_{60} admolecule (Figure 7.2(b1, b2)).

A common feature of the PES contour plots in the C_{60}/graphene and C_{60}/graphane systems is their periodicity inherited from the periodic atomic configuration of the substrates. However, partial chemical modification of graphene destroys such periodicity, and creates large random peaks and valleys in the PES of the system. Indeed, hydrogenation of a carbon atom on graphene leads to a change in atomic bond from sp^2 to sp^3. Such bond character change introduces a change in bond length and bond angle. As a result, the hydrogenated carbon atom experiences an out-of-plane deflection. Such defection can be either positive or negative, depending on whether the location of the hydrogenation is above or below the graphene sheet. Consequently, the random hydrogenation on top and below of graphene introduces random physical roughness, which in turn alters the PES of the system. To elaborate the effect of partial hydrogenation of graphene on the PES, we plot Figure 7.3(a3) and (b3), which show the atomic configuration and its corresponding PES contour plot of a selected area of 10 x 10 $Å^2$ from a 15% randomly hydrogenated graphene, respectively. Comparing Figure 7.3(b3) and 3(b1, b2), it can be concluded that partial functionalization drastically alters the PES

of the system and introduces a heterogeneous PES profile. From Figure 7.3(b3), it can be expected that the trajectory of C_{60} in such a system will be confined along the pathways with lowest energy barriers. For example, at temperatures up to 300 K, the C_{60} molecule is unable to pass over the points where there is a positive out-of-plane roughness (a large barrier). Our analysis shows that the C_{60} bounces back from such a high energy barrier, diverting the motion of the C_{60} from its original moving path. In addition, decreasing the temperature increases the chance of trapping the C_{60} inside the potential wells.

Occurrence of subdiffusion in Figure 7.2(b3) can be related to the existence of barriers (obstacles) and traps (potential wells) in the PES of the partially hydrogenated system. The effect of random traps or barriers on the surface diffusion can be described by the random trap or random barrier models, respectively [234]. Either trapping by PES wells or blocking by PES barriers can lead to the occurrence of subdiffusion in the partially hydrogenated systems.

To analyze the effect of hydrogenation of graphene on the mobility of the C_{60} molecule in superdiffusion and subdiffusion regimes, we performed long time scale MD simulations to allow the system to reach the normal diffusion regime. We then extracted the diffusion coefficients using the best linear fit to the MSD curves at different temperatures and hydrogen coverages, and the results are presented in Figure 7.4(a). It is seen that the C_{60} mobility drastically decreases with adding/removing a small percent of hydrogen atoms (even below 5%) to/from graphene/graphane, respectively. As described in Figure 7.2, where the hydrogenation leads to subdiffusive behavior, the mobility of C_{60} is 4 to 5 orders of magnitude lower than its mobility in the C_{60}/graphane and C_{60}/graphene systems. Figure 7.4(a) also illustrates that a simple linear rule of mixtures

cannot describe the dependency of C_{60} mobility on the hydrogen coverage. Clearly, partial hydrogenation leads to the occurrence of ultrasensitivity in the molecular motion on hydrogenated graphene.

7.3.1 Random trap and barrier model

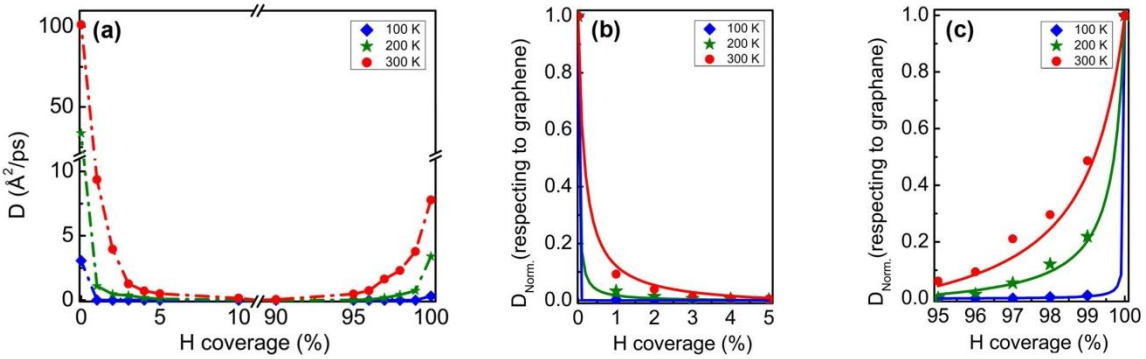

Figure 7.4 (a) Effect of hydrogenation coverage on the diffusion coefficient of C_{60} admolecule at three different temperatures. The drastic change in C_{60} mobility with the change of hydrogen coverage signifies the ultrasensitive behavior of the C_{60} motion. (b) and (c) show the comparison of the normalized diffusivities obtained from the MD simulations (scattered points), and those from our proposed model (continuous lines) at very low (< 5%) and very high (> 95%) hydrogen coverages, respectively. The normalizations of diffusion coefficients in (b) and (c) are based on the diffusivities of C_{60} on pure graphene and graphane, respectively, at the corresponding temperatures.

To reveal insights into how the hydrogen modification leads to such ultrasensitivity in the mobility of C_{60} admolecule, we develop a theoretical model considering random traps and barriers induced by random hydrogenation. For pure graphene or graphane, their PESs are shallow, leading to fast diffusion. For partially hydrogenated graphene, however, hydrogenation alters the PES of the system. If a hydrogenation occurs at the same side with the C_{60} admolecule, such hydrogenation creates a potential energy peak, leading to an energy barrier. However, if a hydrogenation occurs at the opposite side with the C_{60} admolecule, such hydrogenation creates a potential energy well, leading to an energy trap. Hence, the C_{60} performs a random motion on the hydrogenated graphene surface with a

combination of shallow energy traps and low energy barriers (on graphene/graphane regions), and deep energy traps (caused by hydrogenation/ dehydrogenation of graphene/graphane at the opposite side of C_{60} admolecule) and high energy barriers (caused by hydrogenation/dehydrogenation of graphene/graphane at the same side of C_{60}). Hence, the partially hydrogenated graphene forms an energetically heterogeneous system.

The diffusion coefficient of a homogeneous system having a periodic PES with depth of E_a, and at absolute temperature of T can be expressed as [236]:

$$D_{\text{hom}} \propto 1/ < \tau >_{\text{hom}} \propto 1/\exp(\frac{E_a}{k_B T}), \tag{7.4}$$

where $<\tau>_{hom}$ is the average dwelling time at the bottom of the energy well (E_a), and k_B is the Boltzmann constant. Based on the random trap model [234], the diffusion coefficient of a heterogeneous system which its PES contains traps with energy depth of E_t and distribution density of p_t, on the homogeneous PES with depth of E_a, can be written as:

$$D_{hett} \propto 1/ < \tau >_{hett} \propto 1/\left(p_t.\exp(\frac{E_t}{k_B T}) + (1-p_t).\exp(\frac{E_a}{k_B T}) \right), \tag{7.5}$$

where $<\tau>_{hett}$ is the average dwelling time of an admolecule at the bottom of energy wells. Hence, the normalized diffusion coefficient for this heterogeneous system can be expressed as:

$$\frac{D_{hett}}{D_{hom}} = \frac{< \tau >_{hom}}{< \tau >_{hett}} = \frac{exp(E_a / k_B T)}{p_t.exp(E_t / k_B T) + (1-p_t) exp(E_a / k_B T)}. \tag{7.6}$$

Here, it is assumed that the proportionality constants in Equations (7.5) and (7.6) are the same, independent of temperature and depth of the energy wells [236].

Next we consider the effect of random energy barriers on the surface diffusion of the partially hydrogenated system. In general, a random barrier model [234] is difficult to

handle by any analytical methods. Often, simulation techniques such as Monte Carlo (MC) methods were used to address this problem [234, 237]. Assuming a linear decay of the diffusion coefficient of C_{60} by increasing the distribution density of the random barriers p_b, the diffusion coefficient arising from random barriers, D_{hetb}, can be written based on Saxton's model as [237]:

$$D_{hetb} = (1 - p_b) D_{hom}. \tag{7.7}$$

To obtain the distribution densities of barriers or traps in terms of hydrogenation/dehydrogenation, we find that adding/removing a hydrogen atom to/from the graphene/graphane sheet, respectively, influences an area with a radius of about 5 Å on the PES of the C_{60}/graphene or C_{60}/graphane system. This influenced area corresponds to about 30 regular sites on the graphene or graphane sheet. Hence the influencing coefficient for adding or removing a hydrogen atom, a_{inf}, is taken to be 30. Since the hydrogenation/dehydrogenation is performed in a random manner, the concentrations of hydrogenation/dehydrogenation on both sides of the graphene/graphane are equal. Hence the concentrations of traps and barrier are equal:

$$\begin{aligned} c_t = c_b = 0.5 c_H \quad & \text{(hydrogen coverage < 5\%)}, \\ c_t = c_b = 0.5(1 - c_H) \quad & \text{(hydrogen coverage > 95\%)}, \end{aligned} \tag{7.8}$$

where c_t, c_b, and c_H are the concentration of traps, barriers and hydrogen atoms, respectively. The product of c_t or c_b with the influencing coefficient, i.e., $c_t.a_{inf}$ or $c_b.a_{inf}$, gives the distribution density of the traps or barriers (p_t or p_b), respectively.

Assuming traps and barriers are independent at a low concentration of hydrogenation/dehydrogenation to/from graphene/graphane, and combining Equations

(7.6) and (7.8), we obtain the normalized surface diffusion coefficient for the heterogeneous system:

$$D_{Norm} = \frac{exp(E_a / k_B T)}{c_t . a_{inf} . exp(E_t / k_B T) + (1 - c_t . a_{inf}) exp(E_a / k_B T)} \times (1 - c_b . a_{inf}). \quad (7.9)$$

Equation (7.9) can be used to predict the mobility of C_{60} on a partially hydrogenated graphene under the conditions prescribed by Equation (7.8). To do so, we performed atomistic simulations to determine the parameters E_t and E_a. In the limit of very low hydrogen coverage up to 5% (Figure 7.4(b)), we find E_t = 0.11 eV, and E_a= 0.004 eV. The normalized diffusion coefficient calculated from our model at three different temperatures (100, 200 and 300 K) are presented with continuous curves in Figure 7.4(b). In the same figure, the normalized diffusion coefficients from MD simulations at the corresponding temperatures are presented by discrete points. Here, the diffusion coefficient values obtained from MD simulations are normalized by those of C_{60} on pure graphene, which are 3.07, 33.58, and 101.16 $Å^2$/ps at 100 K, 200 K and 300 K, respectively. At very high hydrogen coverages above 95% (see Figure 7.4(c)), we find E_t=0.09 eV, and E_a= 0.03 eV. The calculated results of the model at three temperatures, i.e., 100, 200 and 300 K, are presented in Figure 7.4(c) with continuous curves, and their corresponding values from MD simulations are shown by discrete points. The diffusion coefficient values obtained from our MD simulations are normalized by those of C_{60} on graphane, which are 0.314, 3.4, and 7.78 $Å^2$/ps at 100 K, 200 K and 300 K, respectively. It is seen from Figure 7.4(b,c) that the model predictions are in good agreement with our MD simulation results, reproducing the ultrasensitivity of the molecular motion on hydrogenated graphene.

7.4 Summary

We performed MD simulations to study the effect of hydrogenation and temperature on the surface motion of a C_{60} admolecule on graphene. We showed the presence of three distinct diffusive regimes in this system: superdiffusion, normal diffusion, and subdiffusion, which are identified by their characteristic behavior in the trajectories and mean square displacement of C_{60} admolecule. A diagram of these regimes as a function of temperature and hydrogen coverage was presented. We found that the mobility of C_{60} on graphene is extremely sensitive to a minute amount of graphene hydrogenation/graphane dehydrogenation. This ultrasensitivity in surface molecular transport of the C_{60} admolecule due to minute graphene hydrogenation/graphane dehydrogenation arises from drastic changes in the PES of the system. A theoretical model was developed to describe the effect of hydrogenation at both very low and very high hydrogenation coverage on the mobility of C_{60} admolecule. The model predictions are in good agreement with the MD simulation results, reproducing the ultrasensitivity of C_{60} motion on hydrogenated graphene at very low or very high hydrogenation coverage. The present work provides fundamental insights into the ultrasensitivity of molecular mobility and a theoretical model to describe molecular motion at the nanoscale systems, and suggests that chemical functionalization of graphene can be used to control the molecular motion at the nanoscale [238, 239].

8 Conclusions and future work

8.1 Conclusions

In this thesis, we have used atomistic modeling to study the energetics and dynamics of surface diffusion and friction in the C_{60}/graphene-based system. Our present work reveals many fascinating insights into the molecular motion and frictional mechanisms in different regimes, and provides important guidance to control the dynamics of molecular motion in bottom-up approaches for building nanodevices.

1. Two distinct regimes of surface Brownian motion

For the first time, we demonstrated that a C_{60} molecule on a graphene substrate exhibits two distinct regimes of nanoscale surface Brownian motion. This is far from the traditional stick-slip picture of surface diffusion. These regimes are a quasi-continuous and a ballistic-like Brownian motion, resembling the motion of a Brownian particle in a fluid with high and low viscosity, respectively. The crossover between these two regimes takes place by merely changing the temperature. We found that the physical origin for this crossover is the effect of temperature on the mechanism of interaction between C_{60} and graphene.

2. Effect of rotational degrees of freedom on molecular mobility

Our qualitative and quantitative analysis indicated that there is an intermediate temperature range in which the rotational degrees of freedom (DOFs) enhance the molecular mobility of the C_{60}, since they provide a route for the admolecule to easily

overcome the energy barriers of the system. Consequently, the C_{60} admolecule with rotational DOFs can exhibit Brownian motion on the surface; this is absent in the system without rotational DOFs, which instead undergoes stick-slip motion. Beyond this intermediate temperature range, the contribution of rotational DOFs to the overall mobility of the admolecule is negligible. This observation provides insights into development of efficient ways to manipulate nanoscale objects with rotational DOFs.

3. Effect of temperature on kinetic nanofriction

The use of Einstein's theory of Brownian motion in analyzing the diffusion coefficient and velocity autocorrelation function of the C_{60} admolecule demonstrated that the kinetic nanofriction coefficient decreases with temperature. The temperature dependence can be described by an Arrhenius-form expression with two distinct regimes that crossover at a specific temperature, which is compatible with the mechanisms of interaction between the C_{60} admolecule and the graphene. Based on these results, a theoretical framework has been developed to study the kinetic nanofriction. In addition, the results of current work may help to tune the existing experimental setups to measure the sliding (friction) force at the nanoscale.

4. Effect of substrate chemical modification on molecular mobility

We compared the surface motion of the C_{60} admolecule on both pristine and hydrogenated graphene, and demonstrated the existence of three distinct diffusive regimes, namely, superdiffusion, normal diffusion, and subdiffusion at different temperatures and hydrogen coverages. More importantly, we presented a diffusion diagram which maps these diffusive regimes at various temperatures and hydrogen coverages. In addition, we showed that a minute hydrogenation (dehydrogenation) of the

graphene (graphane) drastically reduces the mobility of the admolecule. We developed a theoretical model, which takes the effects of both random traps and barriers into account, to predict the relation between the diffusion coefficient, temperature and hydrogen coverage. The model predictions are in good agreement with our molecular dynamics simulations. Relying on these results, we suggested a chemical route to control molecular motion at the nanoscale, but more importantly, we provided a theoretical framework to describe the molecular mobility at the nanoscale.

8.2 Future work

In this thesis, a single C_{60} admolecule on graphene was considered to study the effects of temperature, internal degrees of freedom, and chemical modification of the substrate on its diffusive and frictional behavior. However, in practical applications, a collection of C_{60} admolecules may be used for device fabrication via self-assembled structuring on the surface. For these applications, some other parameters besides temperature and internal degrees of freedom can affect the mobility of the system. For example, the C_{60}-C_{60} interactions at finite coverage and confinements of their motion can alter the diffusion characteristics. It will be interesting to explore these effects. Some interesting problems for future studies are listed below:

1. Confined Brownian motion of C_{60} on graphene nanoribbons and nanoroads

Understanding different aspects of confined Brownian motion, *e.g.* the influence of "walls" (constraints) on the dynamics of Brownian particles, is crucial in applications such as particles migration through porous media or motion along fluid-solid boundaries, diffusion of macromolecules in membranes, and interaction of cells with surfaces [240, 241].

Based on our preliminary research, the Brownian motion of C_{60} on graphene can be confined by using two different approaches: (1) by physically changing the graphene geometry and using nanoribbons or graphene flakes, (2) by chemically modifying the graphene and creating diffusive pathways. Using the former approach, we have found that the vdW interaction between C_{60} and graphene is sufficiently strong to absorb the C_{60} molecule on a finite-width GNR with a width of only 5 Å at room temperature. We have observed that the trajectory of the C_{60} admolecule is confined along the GNR length, and the edges of the GNR play a role as reflecting walls (see Figure 8.1).

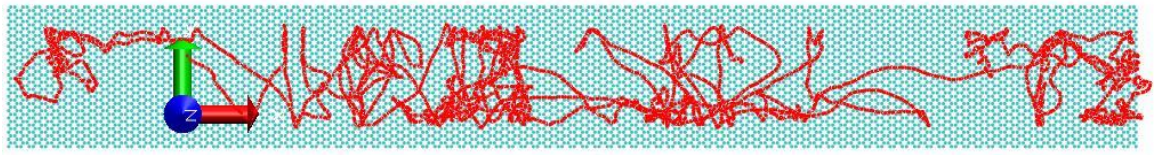

Figure 8.1 Confined Brownian motion of C_{60} on a GNR at 100 K. The width of the GNR is 50 Å. The edges confine the admolecule motion.

Regarding the latter method, we recall that the chemical functionalization of graphene provides high potential energy barriers on the surface and strongly alters the motion of the adsorbate (see Chapter 7). Theoretical [242] and experimental [243] studies revealed the possibility of constructing graphene-graphane composite sheets (see Figure 8.2(a)). Our MD simulations have indicated that the motion of a C_{60} adsorbed on the graphene domain of a graphane-graphene-graphane composite sheet is confined in the graphene area. The graphene strip between two graphane domains plays a role of a "nanoroad" for the C_{60}, and its edges adsorb the admolecule (see Figure 8.2(b)).

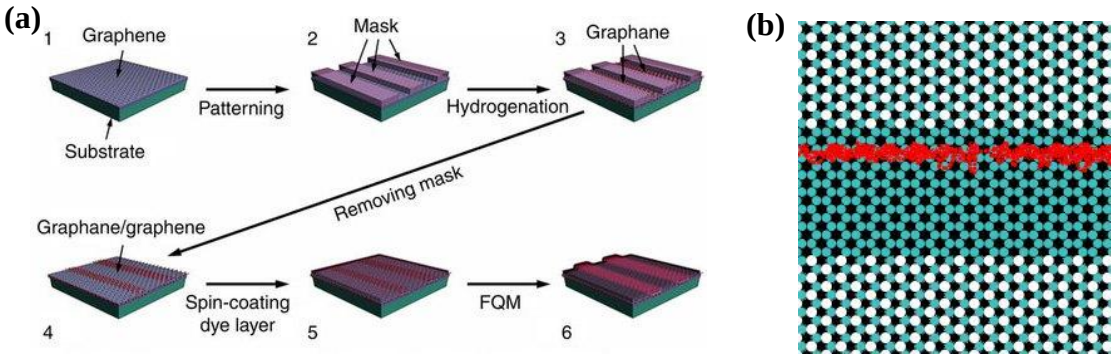

Figure 8.2 (a) Schematic illustration of fabricating the graphane/graphene composite sheet and subsequent fluorescence quenching microscopy (FQM) imaging [243].(b) Our MD simulation at 100 K reveals the confined Brownian motion of a C_{60} admolecule (red trajectory) on the 20 Å width graphene "nanoroad" confined between graphane domains in a graphane-graphene-graphane composite sheet (green and white circles represent carbon and hydrogen atoms, respectively). The PBC is applied on the simulation box. It can be seen that the edges of the "nanoroad" adsorb the C_{60} admolecule.

Continuing this research would be important for applications where confined Brownian motion is guided by patterned surface templates.

2. Coverage effects and self-assembly

In this thesis, the simulations were conducted for a single C_{60} admolecule on graphene. We investigated the admolecule-substrate interactions, independent of the effects of other admolecules. Although our case may correspond to (infinitesimally) low coverage of admolecules, in applications, a finite coverage of admolecules may be required. Therefore, the mobility of an admolecule would be dependent on the configuration of other admolecules due to the C_{60}-C_{60} interactions. Our recent MD simulations have revealed that two C_{60} molecules on graphene stay close to each other even at room temperature and diffuse as a C_{60}-dimer (see Figure 8.3). A cluster of admolecules has extra degrees of freedom compared to an isolated molecule, and studying its diffusive behavior would be interesting.

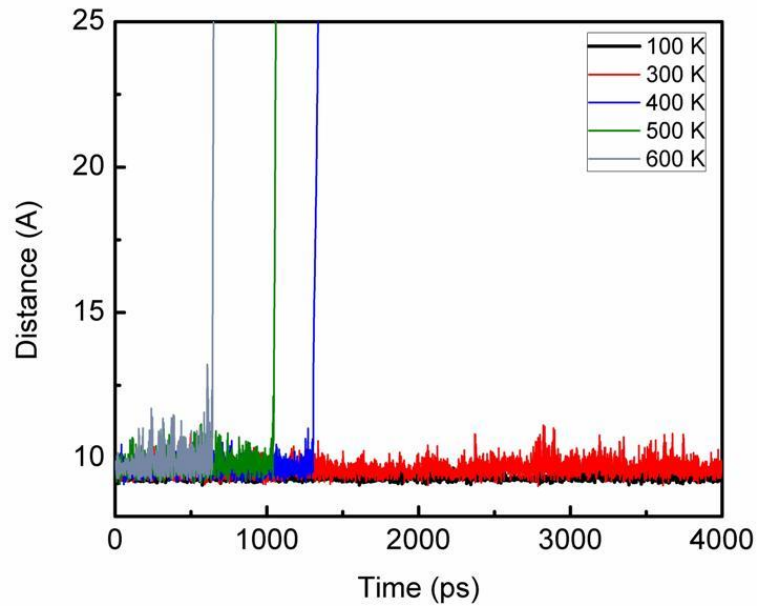

Figure 8.3 Distance between the centers of masses of two C_{60} molecules, which form a stable C_{60}-dimer, at different temperatures during their surface diffusion on graphene. Even at room temperature (300 K) the C_{60}-dimer is stable and the average distance between molecules is 9.6 Å. Higher temperatures lead to dissociation of the dimer.

At very high coverage, the C_{60} admolecules impede the motion of each other. It is expected that below a certain temperature, the motion of each C_{60} becomes very restricted, and they form a solid-like thin film. It was claimed that in contrast to the epitaxial growth of most vdW crystals, the lattice parameter of C_{60} thin films are independent of the lattice parameters of the underlying substrate [244, 245]. Understanding of these effects especially for graphene substrates, and their impact on the formation and structure of C_{60} crystalline films is another interesting objective for future research.

3. Diffusive phenomena in other systems

This thesis provides insight into the surface diffusion of C_{60} on graphene as a prototypical example of a physisorbed system. It would be interesting to apply the obtained knowledge to study the surface diffusion in other systems, for example to investigate the

possibility of controlling the mobility of graphene flakes on graphene using superlubricity [246]. It would also be fascinating to study the diffusive phenomena in benzene/graphite and other organic systems with potential applications in lubrication and photovoltaic devices [186, 247].

Bibliography

[1] R. P. Feynman, "There's plenty of room at the bottom", *Engineering and Science,* vol. 23, p. 22, 1960.

[2] R. P. Feynman, "There's plenty of room at the bottom [data storage]", *Journal of Microelectromechanical Systems,* vol. 1, p. 60, 1992.

[3] G. Binnig and H. Rohrer, "Scanning tunneling microscopy", *Surface Science,* vol. 126, p. 236, 1983.

[4] G. Binnig, C. F. Quate, and C. Gerber, "Atomic force microscope", *Physical Review Letters,* vol. 56, p. 930, 1986.

[5] E. Meyer, "Atomic force microscopy", *Progress in Surface Science,* vol. 41, p. 3, 1992.

[6] H. Aldersey-Williams, *The most beautiful molecule: The discovery of the buckyball*: John Wiley, 1995.

[7] A. Sinha, "Buckyball C_{60} - The story so far", *Resonance,* vol. 6, p. 55, 2001.

[8] A. F. Hebard, M. J. Rosseinsky, R. C. Haddon, D. W. Murphy, S. H. Glarum, T. T. M. Palstra, A. P. Ramirez, and A. R. Kortan, "Superconductivity at 18 K in potassium-doped C_{60}", *Nature,* vol. 350, p. 600, 1991.

[9] R. Saito, G. Dresselhaus, and M. S. Dresselhaus, *Physical properties of carbon nanotubes* vol. 35: World Scientific, 1998.

[10] S. Iijima and T. Ichihashi, "Single-shell carbon nanotubes of 1-nm diameter", *Nature,* vol. 363, p. 603, 1993.

[11] M. Treacy, T. Ebbesen, and J. Gibson, "Exceptionally high Young's modulus observed for individual carbon nanotubes", *Nature,* vol. 381, p. 678 1996.

[12] K. Novoselov, A. K. Geim, S. Morozov, D. Jiang, M. I. K. I. V. Grigorieva, S. Dubonos, and A. Firsov, "Two-dimensional gas of massless Dirac fermions in graphene", *Nature,* vol. 438, p. 197, 2005.

[13] A. K. Geim and K. S. Novoselov, "The rise of graphene", *Nature Materials,* vol. 6, p. 183, 2007.

[14] Y. Zhang, Y. W. Tan, H. L. Stormer, and P. Kim, "Experimental observation of the quantum Hall effect and Berry's phase in graphene", *Nature,* vol. 438, p. 201, 2005.

[15] A. H. C. Neto, F. Guinea, N. Peres, K. Novoselov, and A. Geim, "The electronic properties of graphene", *Reviews of Modern Physics,* vol. 81, p. 109, 2009.

[16] S. Stankovich, D. A. Dikin, G. H. B. Dommett, K. M. Kohlhaas, E. J. Zimney, E. A. Stach, R. D. Piner, S. B. T. Nguyen, and R. S. Ruoff, "Graphene-based composite materials", *Nature,* vol. 442, p. 282, 2006.

[17] M. Y. Han, B. Özyilmaz, Y. Zhang, and P. Kim, "Energy band-gap engineering of graphene nanoribbons", *Physical Review Letters,* vol. 98, p. 206805, 2007.

[18] W. K. Leutwyler, S. L. Bürgi, and H. Burgl, "Semiconductor clusters, nanocrystals, and quantum dots", *Science,* vol. 271, p. 933, 1996.

[19] D. Loss and D. P. DiVincenzo, "Quantum computation with quantum dots", *Physical Review A,* vol. 57, p. 120, 1998.
[20] H. B. Chan, V. A. Aksyuk, R. N. Kleiman, D. J. Bishop, and F. Capasso, "Quantum Mechanical Actuation of Microelectromechanical Systems by the Casimir Force", *Science,* vol. 291, p. 1941, 2001.
[21] H. G. Craighead, "Nanoelectromechanical Systems", *Science,* vol. 290, p. 1532, 2000.
[22] J. K. Gimzewski, C. Joachim, R. R. Schlittler, V. Langlais, H. Tang, and I. Johannsen, "Rotation of a Single Molecule Within a Supramolecular Bearing", *Science,* vol. 281, p. 531, 1998.
[23] J. Cumings and A. Zettl, "Low-friction nanoscale linear bearing realized from multiwall carbon nanotubes", *Science,* vol. 289, p. 602, 2000.
[24] Y. Yong Ju, A. Chil Seong, K. Sanghun, Y. Wan Soo, P. Byong Chon, and H. Dong Han, "Manipulation of freestanding Au nanogears using an atomic force microscope", *Nanotechnology,* vol. 18, p. 505304, 2007.
[25] R. A. van Delden, M. K. J. ter Wiel, M. M. Pollard, J. Vicario, N. Koumura, and B. L. Feringa, "Unidirectional molecular motor on a gold surface", *Nature,* vol. 437, p. 1337, 2005.
[26] J. J. Li and W. Tan, "A single DNA molecule nanomotor", *Nano Letters,* vol. 2, p. 315, 2002.
[27] J. V. Barth, G. Costantini, and K. Kern, "Engineering atomic and molecular nanostructures at surfaces", *Nature,* vol. 437, p. 671, 2005.
[28] J. C. T. Eijkel and A. van den Berg, "The promise of nanotechnology for separation devices–from a top-down approach to nature-inspired separation devices", *Electrophoresis,* vol. 27, p. 677, 2006.
[29] W. Lu and C. M. Lieber, "Nanoelectronics from the bottom up", *Nature Materials,* vol. 6, p. 841, 2007.
[30] D. J. Frank, R. H. Dennard, E. Nowak, P. M. Solomon, Y. Taur, and H. S. P. Wong, "Device scaling limits of Si MOSFETs and their application dependencies", *Proceedings of the IEEE,* vol. 89, p. 259, 2001.
[31] M. Shimomura and T. Sawadaishi, "Bottom-up strategy of materials fabrication: a new trend in nanotechnology of soft materials", *Current opinion in colloid & interface science,* vol. 6, p. 11, 2001.
[32] B. D. Gates, Q. Xu, M. Stewart, D. Ryan, C. G. Willson, and G. M. Whitesides, "New approaches to nanofabrication: molding, printing, and other techniques", *Chemical Reviews-Columbus,* vol. 105, p. 1171, 2005.
[33] I. Cosic, "Macromolecular bioactivity: is it resonant interaction between macromolecules?-theory and applications", *Biomedical Engineering, IEEE Transactions on,* vol. 41, p. 1101, 1994.
[34] D. Y. Petrovykh and F. J. Himpsel, "Self-assembled nanostructures at silicon surfaces", *Encyclopedia of nanoscience and nanotechnology,* vol. 9, p. 497, 2004.
[35] J. Tersoff, C. Teichert, and M. G. Lagally, "Self-Organization in Growth of Quantum Dot Superlattices", *Physical Review Letters,* vol. 76, p. 1675, 1996.
[36] D. Goswami, B. Satpati, P. Satyam, and B. Dev, "Growth of self-assembled nanostructures by molecular beam epitaxy", *CURRENT SCIENCE-BANGALORE-*, vol. 84, p. 903, 2003.

[37] D. Wolf and J. Villain, "Growth with surface diffusion", *EPL (Europhysics Letters),* vol. 13, p. 389, 2007.
[38] T. L. Einstein and T. J. Stasevich, "Epitaxial Growth Write Large", *Science,* vol. 327, p. 423, 2010.
[39] R. Otero, F. Rosei, and F. Besenbacher, "Scanning tunneling microscopy manipulation of complex organic molecules on solid surfaces", *Annual Review of Physical Chemistry,* vol. 57, p. 497, 2006.
[40] J. V. Barth, "Transport of adsorbates at metal surfaces: from thermal migration to hot precursors", *Surface Science Reports,* vol. 40, p. 75, 2000.
[41] A. L. Barabási, "Thermodynamic and kinetic mechanisms in self-assembled quantum dot formation", *Materials Science and Engineering: B,* vol. 67, p. 23, 1999.
[42] S. Seung-Woo, H. Meesoon, and J. Hawoong, "Anomalous scaling behavior in polymer thin film growth by vapor deposition", *Journal of Statistical Mechanics: Theory and Experiment,* vol. 2009, p. P02031, 2009.
[43] J. G. Amar, F. Family, and D. C. Hughes, "Submonolayer epitaxial growth with long-range (Lévy) diffusion", *Physical Review E,* vol. 58, p. 7130, 1998.
[44] I. Daruka and A.-L. Barabási, "Dislocation-Free Island Formation in Heteroepitaxial Growth: A Study at Equilibrium", *Physical Review Letters,* vol. 79, p. 3708, 1997.
[45] G. Medeiros-Ribeiro, A. M. Bratkovski, T. I. Kamins, D. A. A. Ohlberg, and R. S. Williams, "Shape Transition of Germanium Nanocrystals on a Silicon (001) Surface from Pyramids to Domes", *Science,* vol. 279, p. 353, 1998.
[46] A.-L. Barabasi, "Self-assembled island formation in heteroepitaxial growth", *Applied Physics Letters,* vol. 70, p. 2565, 1997.
[47] C. Ratsch, A. Zangwill, and P. Šmilauer, "Scaling of heteroepitaxial island sizes", *Surface Science,* vol. 314, p. L937, 1994.
[48] J. M. Warrender and M. J. Aziz, "Effect of deposition rate on morphology evolution of metal-on-insulator films grown by pulsed laser deposition", *Physical Review B,* vol. 76, p. 045414, 2007.
[49] D. M. Eigler and E. K. Schweizer, "Positioning single atoms with a scanning tunnelling microscope", *Nature,* vol. 344, p. 524, 1990.
[50] M. Ternes, C. P. Lutz, C. F. Hirjibehedin, F. J. Giessibl, and A. J. Heinrich, "The Force Needed to Move an Atom on a Surface", *Science,* vol. 319, p. 1066, 2008.
[51] M. Urbakh, J. Klafter, D. Gourdon, and J. Israelachvili, "The nonlinear nature of friction", *Nature,* vol. 430, p. 525, 2004.
[52] B. Bhushan, *Introduction to Tribology*: Wiley, 2002.
[53] Y. Mo, K. T. Turner, and I. Szlufarska, "Friction laws at the nanoscale", *Nature,* vol. 457, p. 1116, 2009.
[54] S. T. Nikhil and B. Bharat, "Scale dependence of micro/nano-friction and adhesion of MEMS/NEMS materials, coatings and lubricants", *Nanotechnology,* vol. 15, p. 1561, 2004.
[55] J. A. Ruan and B. Bhushan, "Atomic-scale friction measurements using friction force microscopy. I: General principles and new measurement techniques", *Journal of tribology,* vol. 116, p. 378, 1994.

[56] D. L. Sedin and K. L. Rowlen, "Influence of tip size on AFM roughness measurements", *Applied Surface Science,* vol. 182, p. 40, 2001.
[57] Z. Deng, A. Smolyanitsky, Q. Li, X. Q. Feng, and R. J. Cannara, "Adhesion-dependent negative friction coefficient on chemically modified graphite at the nanoscale", *Nature Materials,* vol. 11, p. 1032, 2012.
[58] M. Rovatti, G. Paolicelli, A. Vanossi, and S. Valeri, "Sliding onset of nanoclusters: a new AFM-based approach", *Meccanica,* p. 1, 2010.
[59] A. Schirmeisen, "Nanofriction: Surfing on graphite waves", *Nat Mater,* vol. 9, p. 615, 2010.
[60] S. Pisov, E. Tosatti, U. Tartaglino, and A. Vanossi, "Gold clusters sliding on graphite: a possible quartz crystal microbalance experiment?", *Journal of Physics: Condensed Matter,* vol. 19, p. 305015, 2007.
[61] B. C. Regan, S. Aloni, R. O. Ritchie, U. Dahmen, and A. Zettl, "Carbon nanotubes as nanoscale mass conveyors", *Nature,* vol. 428, p. 924, 2004.
[62] K. Svensson, H. Olin, and E. Olsson, "Nanopipettes for Metal Transport", *Physical Review Letters,* vol. 93, p. 145901, 2004.
[63] A. Barreiro, R. Rurali, E. R. Hernández, and A. Bachtold, "Structured Graphene Devices for Mass Transport", *Small,* vol. 7, p. 775, 2011.
[64] A. Barreiro, M. Lazzeri, J. Moser, F. Mauri, and A. Bachtold, "Transport Properties of Graphene in the High-Current Limit", *Physical Review Letters,* vol. 103, p. 076601, 2009.
[65] J. Moser, A. Barreiro, and A. Bachtold, "Current-induced cleaning of graphene", *Applied Physics Letters,* vol. 91, p. 163513, 2007.
[66] N. D. Lang and A. R. Williams, "Theory of atomic chemisorption on simple metals", *Physical Review B,* vol. 18, p. 616, 1978.
[67] C. Stadler, S. Hansen, I. Kroger, C. Kumpf, and E. Umbach, "Tuning intermolecular interaction in long-range-ordered submonolayer organic films", *Nat Phys,* vol. 5, p. 153, 2009.
[68] A. Tkatchenko, L. Romaner, O. T. Hofmann, E. Zojer, C. Ambrosch-Draxl, and M. Scheffler, "Van der Waals interactions between organic adsorbates and at organic/inorganic interfaces", *MRS Bulletin,* vol. 35, p. 435, 2010.
[69] M. Švec, P. Merino, Y. J. Dappe, C. González, E. Abad, P. Jelínek, and J. A. Martín-Gago, "van der Waals interactions mediating the cohesion of fullerenes on graphene", *Physical Review B,* vol. 86, p. 121407, 2012.
[70] Y. J. Dappe, J. Ortega, and F. Flores, "Intermolecular interaction in density functional theory: Application to carbon nanotubes and fullerenes", *Physical Review B,* vol. 79, p. 165409, 2009.
[71] M. Kisiel, E. Gnecco, U. Gysin, L. Marot, S. Rast, and E. Meyer, "Suppression of electronic friction on Nb films in the superconducting state", *Nature Materials,* vol. 10, p. 119, 2011.
[72] H. Hedgeland, P. Fouquet, A. P. Jardine, G. Alexandrowicz, W. Allison, and J. Ellis, "Measurement of single-molecule frictional dissipation in a prototypical nanoscale system", *Nat Phys,* vol. 5, p. 561, 2009.
[73] A. J. Martínez-Galera and J. M. Gómez-Rodríguez, "Surface Diffusion of Simple Organic Molecules on Graphene on Pt(111)", *Journal of Physical Chemistry C,* vol. 115, p. 23036, 2011.

[74] A. J. Oyer, J.-M. Y. Carrillo, C. C. Hire, H. C. Schniepp, A. D. Asandei, A. V. Dobrynin, and D. H. Adamson, "Stabilization of Graphene Sheets by a Structured Benzene/Hexafluorobenzene Mixed Solvent", *Journal of the American Chemical Society,* vol. 134, p. 5018, 2012.
[75] A. Hashimoto, K. Iwao, S. Tanaka, and A. Yamamoto, "van der Waals epitaxy of solid C_{60} on graphene sheet", *Diamond and Related Materials,* vol. 17, p. 1622, 2008.
[76] A. Hashimoto, H. Terasaki, A. Yamamoto, and S. Tanaka, "Electron beam irradiation effect for solid C_{60} epitaxy on graphene", *Diamond and Related Materials,* vol. 18, p. 388, 2009.
[77] K. Miura, S. Kamiya, and N. Sasaki, "C_{60} Molecular Bearings", *Physical Review Letters,* vol. 90, p. 055509, 2003.
[78] W. Harneit, "Fullerene-based electron-spin quantum computer", *Physical Review A,* vol. 65, p. 032322, 2002.
[79] J. Cho, J. Smerdon, L. Gao, Ö. Süzer, J. R. Guest, and N. P. Guisinger, "Structural and Electronic Decoupling of C_{60} from Epitaxial Graphene on SiC", *Nano Letters,* vol. 12, p. 3018, 2012.
[80] S. Naruo, I. Noriaki, and M. Kouji, "Atomic-scale ultralow friction – simulation of superlubricity of C_{60} molecular bearing", *Journal of Physics: Conference Series,* vol. 89, p. 012001, 2007.
[81] V. Balzani, A. Credi, and M. Venturi, "Molecular Machines Working on Surfaces and at Interfaces", *ChemPhysChem,* vol. 9, p. 202, 2008.
[82] F. Simon, H. Peterlik, R. Pfeiffer, J. Bernardi, and H. Kuzmany, "Fullerene release from the inside of carbon nanotubes: A possible route toward drug delivery", *Chemical Physics Letters,* vol. 445, p. 288, 2007.
[83] A. Montellano, T. Da Ros, A. Bianco, and M. Prato, "Fullerene C_{60} as a multifunctional system for drug and gene delivery", *Nanoscale,* vol. 3, p. 4035, 2011.
[84] M. Neek-Amal, N. Abedpour, S. N. Rasuli, A. Naji, and M. R. Ejtehadi, "Diffusive motion of C_{60} on a graphene sheet", *Physical Review E,* vol. 82, p. 051605, 2010.
[85] T. Ala-Nissila and S. C. Ying, "Theory of classical surface diffusion", *Progress in Surface Science,* vol. 39, p. 227, 1992.
[86] K. J. Laidler and M. C. King, "Development of transition-state theory", *The Journal of physical chemistry,* vol. 87, p. 2657, 1983.
[87] R. Gomer, "Diffusion of adsorbates on metal surfaces", *Reports on Progress in Physics,* vol. 53, p. 917, 1990.
[88] X. Zhiping and J. B. Markus, "Strain controlled thermomutability of single-walled carbon nanotubes", *Nanotechnology,* vol. 20, p. 185701, 2009.
[89] R. Ferrando, R. Spadacini, and G. E. Tommei, "The diffusion coefficient beyond TST and jump theory", *Surface Science,* vol. 287-288, p. 886, 1993.
[90] T. Ala-Nissila and S. C. Ying, "Universal properties of classical surface diffusion", *Physical Review Letters,* vol. 65, p. 879, 1990.
[91] T. Ala-Nissila, R. Ferrando, and S. C. Ying, "Collective and single particle diffusion on surfaces", *Advances in Physics,* vol. 51, p. 949, 2002.

[92] K. Lindenberg, A. M. Lacasta, J. M. Sancho, and A. H. Romero, "Unsolved Problems of Surface Diffusion at Low Friction", *AIP Conference Proceedings,* vol. 800, p. 50, 2005.
[93] J. S. Raut and K. A. Fichthorn, "Diffusion mechanisms of short-chain alkanes on metal substrates: Unique molecular features", *Journal of Chemical Physics,* vol. 108, p. 1626, 1998.
[94] R. Mahaffy, R. Bhatia, and B. J. Garrison, "Diffusion of a Butanethiolate Molecule on a Au{111} Surface", *Journal of Physical Chemistry B,* vol. 101, p. 771, 1997.
[95] D. M. Huang and P. Harrowell, "Controlling Adsorbate Diffusion on a High-Symmetry Surface through Molecular Shape Selection", *Journal of Physical Chemistry C,* vol. 115, p. 9526, 2011.
[96] J. Ou, Y. Wang, J. Wang, S. Liu, Z. Li, and S. Yang, "Self-assembly of octadecyltrichlorosilane on graphene oxide and the tribological performances of the resultant film", *Journal of Physical Chemistry C,* vol. 115, p. 10080, 2011.
[97] S. B. Legoas, R. Giro, and D. S. Galvão, "Molecular dynamics simulations of C_{60} nanobearings", *Chemical Physics Letters,* vol. 386, p. 425, 2004.
[98] A. Blumberg, U. Keshet, I. Zaltsman, and O. Hod, "Interlayer Registry to Determine the Sliding Potential of Layered Metal Dichalcogenides: The Case of 2H-MoS2", *Journal of Physical Chemistry Letters,* vol. 3, p. 1936, 2012.
[99] A. Barreiro, R. Rurali, E. R. Hernandez, J. Moser, T. Pichler, L. Forro, and A. Bachtold, "Subnanometer Motion of Cargoes Driven by Thermal Gradients Along Carbon Nanotubes", *Science,* vol. 320, p. 775, 2008.
[100] S. M. Bhattacharyya, "A mode coupling theory analysis of microscopic friction in the macroscopic limit", *Chemical Physics Letters,* vol. 386, p. 83, 2004.
[101] J. Lu, P. S. E. Yeo, Y. Zheng, Z. Yang, Q. Bao, C. K. Gan, and K. P. Loh, "Using the Graphene Moiré Pattern for the Trapping of C_{60} and Homoepitaxy of Graphene", *ACS Nano,* vol. 6 (1), p. 944, 2012.
[102] C. D. Reddy, Y. W. Zhang, and V. B. Shenoy, "Patterned graphone—a novel template for molecular packing", *Nanotechnology,* vol. 23, p. 165303, 2012.
[103] G. Zgrablich, "Surface diffusion of adsorbates on heterogeneous substrates", *Studies in Surface Science and Catalysis,* vol. 104, p. 373, 1997.
[104] F. Reif, *Fundamentals of statistical and thermal physics* vol. 11: McGraw-Hill New York, 1965.
[105] L. Y. Chen and S. C. Ying, "Theory of Surface Diffusion: Crossover from Classical to Quantum Regime", *Physical Review Letters,* vol. 73, p. 700, 1994.
[106] G. Antczak and G. Ehrlich, "Jump processes in surface diffusion", *Surface Science Reports,* vol. 62, p. 39, 2007.
[107] P. Hänggi, P. Talkner, and M. Borkovec, "Reaction-rate theory: fifty years after Kramers", *Reviews of Modern Physics,* vol. 62, p. 251, 1990.
[108] R. Ferrando, R. Spadacini, G. E. Tommei, and G. Caratti, "Correlation functions in surface diffusion: the multiple-jump regime", *Surface Science,* vol. 311, p. 411, 1994.
[109] T. R. Linderoth, S. Horch, E. Lægsgaard, I. Stensgaard, and F. Besenbacher, "Surface Diffusion of Pt on Pt(110): Arrhenius Behavior of Long Jumps", *Physical Review Letters,* vol. 78, p. 4978, 1997.

[110] R. Ferrando, "Surface Diffusion: Simulations," in *Encyclopedia of Materials: Science and Technology*, K. H. J. Buschow, W. C. Robert, C. F. Merton, I. Bernard, J. K. Edward, M. Subhash, and V. Patrick, Eds., ed Oxford: Elsevier, 2006, p. 1.
[111] L. Y. Chen, M. R. Baldan, and S. C. Ying, "Surface diffusion in the low-friction limit: Occurrence of long jumps", *Physical Review B*, vol. 54, p. 8856, 1996.
[112] R. Ferrando and G. Tréglia, "Anisotropy of diffusion along steps on the (111) faces of gold and silver", *Physical Review B*, vol. 50, p. 12104, 1994.
[113] E. Hershkovitz, P. Talkner, E. Pollak, and Y. Georgievskii, "Multiple hops in multidimensional activated surface diffusion", *Surface Science*, vol. 421, p. 73, 1999.
[114] F. Montalenti and R. Ferrando, "Jumps and concerted moves in Cu, Ag, and Au(110) adatom self-diffusion", *Physical Review B*, vol. 59, p. 5881, 1999.
[115] S. Wang, J. Wrigley, and G. Ehrlich, "Atomic jump lengths in surface diffusion: Re, Mo, Ir, and Rh on W (211)", *The Journal of Chemical Physics*, vol. 91, p. 5087, 1989.
[116] J. Kallunki, M. Dube, and T. Ala-Nissila, "Adatom dynamics in a periodic potential under time-periodic bias", *Surface Science*, vol. 460, p. 39, 2000.
[117] M. Borromeo and F. Marchesoni, "Ac-driven jump distributions on a periodic substrate", *Surface Science*, vol. 465, p. L771, 2000.
[118] J. Haus and K. Kehr, "Diffusion in regular and disordered lattices", *Physics Reports*, vol. 150, p. 263, 1987.
[119] G. L. Kellogg, "Field ion microscope studies of single-atom surface diffusion and cluster nucleation on metal surfaces", *Surface Science Reports*, vol. 21, p. 1, 1994.
[120] A. Voter and J. Doll, "Dynamical corrections to transition state theory for multistate systems: Surface self-diffusion in the rare-event regime", *The Journal of Chemical Physics*, vol. 82, p. 80, 1985.
[121] J. E. Adams and J. D. Doll, "Dynamical corrections to transition state theory adsorption rates: Effect of a precursor state", *Surface Science*, vol. 103, p. 472, 1981.
[122] J. D. Wrigley and G. Ehrlich, "Surface Diffusion by an Atomic Exchange Mechanism", *Physical Review Letters*, vol. 44, p. 661, 1980.
[123] G. L. Kellogg and P. J. Feibelman, "Surface self-diffusion on Pt(001) by an atomic exchange mechanism", *Physical Review Letters*, vol. 64, p. 3143, 1990.
[124] J. E. Black and Z.-J. Tian, "Complicated exchange-mediated diffusion mechanisms in and on a Cu(100) substrate at high temperatures", *Physical Review Letters*, vol. 71, p. 2445, 1993.
[125] D. A. Chesnut and Z. W. Salsburg, "Monte Carlo procedure for statistical mechanical calculations in a grand canonical ensemble of lattice systems", *The Journal of Chemical Physics*, vol. 38, p. 2861, 1963.
[126] L. Darken, "Application of the Gibbs-Duhem equation to ternary and multicomponent systems", *Journal of the American Chemical Society*, vol. 72, p. 2909, 1950.
[127] J. V. Barth, "Transport of adsorbates at metal surfaces: from thermal migration to hot precursors", *Surface Science Reports*, vol. 40, p. 75, 2000.

[128] J. Ma, X. Xiao, N. J. DiNardo, and M. M. T. Loy, "Diffusion of CO on Pt(111) studied by an optical diffraction method", *Physical Review B,* vol. 58, p. 4977, 1998.
[129] H. Brune, "Microscopic view of epitaxial metal growth: nucleation and aggregation", *Surface Science Reports,* vol. 31, p. 125, 1998.
[130] J. V. Barth, H. Brune, B. Fischer, J. Weckesser, and K. Kern, "Dynamics of Surface Migration in the Weak Corrugation Regime", *Physical Review Letters,* vol. 84, p. 1732, 2000.
[131] A. Bogicevic, S. Ovesson, P. Hyldgaard, B. I. Lundqvist, H. Brune, and D. R. Jennison, "Nature, Strength, and Consequences of Indirect Adsorbate Interactions on Metals", *Physical Review Letters,* vol. 85, p. 1910, 2000.
[132] S. C. Badescu, S. C. Ying, and T. Ala-Nissila, "Quantum Diffusion of H/Ni(111) through a Monte Carlo Wave Function Formalism", *Physical Review Letters,* vol. 86, p. 5092, 2001.
[133] H. Risken, *The Fokker-Planck Equation*. Berlin Springer, 1989.
[134] R. Ferrando, R. Spadacini, G. E. Tommei, and G. Caratti, "Time scales and diffusion mechanisms in the Kramers equation with periodic potentials (I)", *Physica A: Statistical and Theoretical Physics,* vol. 195, p. 506, 1993.
[135] A. M. Lacasta, J. M. Sancho, A. H. Romero, I. M. Sokolov, and K. Lindenberg, "From subdiffusion to superdiffusion of particles on solid surfaces", *Physical Review E,* vol. 70, p. 051104, 2004.
[136] A. Cucchetti and S. C. Ying, "Memory effects in the frictional damping of diffusive and vibrational motion of adatoms", *Physical Review B,* vol. 54, p. 3300, 1996.
[137] O. M. Braun and R. Ferrando, "Role of long jumps in surface diffusion", *Physical Review E,* vol. 65, p. 061107, 2002.
[138] M. Mazroui, A. Asaklil, and Y. Boughaleb, "Conductivity of two-dimensional systems of interacting Brownian particles within the effective potential description", *Surface Science,* vol. 409, p. 528, 1998.
[139] A. Cucchetti and S. C. Ying, "Diffusion of Na atoms on a Cu(001) surface", *Physical Review B,* vol. 60, p. 11110, 1999.
[140] A. F. Voter, "Classically exact overlayer dynamics: Diffusion of rhodium clusters on Rh(100)", *Physical Review B,* vol. 34, p. 6819, 1986.
[141] M. Tringides and R. Gomer, "A Monte Carlo study of oxygen diffusion on the (110) plane of tungsten", *Surface Science,* vol. 145, p. 121, 1984.
[142] C. Mottet, R. Ferrando, F. Hontinfinde, and A. Levi, "A Monte Carlo simulation of submonolayer homoepitaxial growth on Ag (110) and Cu (110)", *Surface Science,* vol. 417, p. 220, 1998.
[143] R. G. Parr, "Density functional theory", *Annual Review of Physical Chemistry,* vol. 34, p. 631, 1983.
[144] A. Kley, P. Ruggerone, and M. Scheffler, "Novel Diffusion Mechanism on the GaAs(001) Surface: The Role of Adatom-Dimer Interaction", *Physical Review Letters,* vol. 79, p. 5278, 1997.
[145] C. M. Goringe and D. R. Bowler, "Ab initio modeling of a diffusion mode for a Si ad-dimer on the Si(001) surface", *Physical Review B,* vol. 56, p. R7073, 1997.

[146] G. Boisvert, L. J. Lewis, M. J. Puska, and R. M. Nieminen, "Energetics of diffusion on the (100) and (111) surfaces of Ag, Au, and Ir from first principles", *Physical Review B,* vol. 52, p. 9078, 1995.
[147] G. Boisvert and L. J. Lewis, "Self-diffusion of adatoms, dimers, and vacancies on Cu(100)", *Physical Review B,* vol. 56, p. 7643, 1997.
[148] G. Kresse and J. Furthmüller, "Efficiency of ab-initio total energy calculations for metals and semiconductors using a plane-wave basis set", *Computational Materials Science,* vol. 6, p. 15, 1996.
[149] G. Kresse and J. Furthmüller, "Efficient iterative schemes for ab initio total-energy calculations using a plane-wave basis set", *Physical Review B,* vol. 54, p. 11169, 1996.
[150] N. Sai, M. Zwolak, G. Vignale, and M. Di Ventra, "Dynamical corrections to the DFT-LDA electron conductance in nanoscale systems", *Physical Review Letters,* vol. 94, p. 186810, 2005.
[151] R. Car and M. Parrinello, "Unified Approach for Molecular Dynamics and Density-Functional Theory", *Physical Review Letters,* vol. 55, p. 2471, 1985.
[152] V. Musolino, A. Selloni, and R. Car, "Structure and Dynamics of Small Metallic Clusters on an Insulating Metal-Oxide Surface: Copper on MgO(100)", *Physical Review Letters,* vol. 83, p. 3242, 1999.
[153] M. Harvey, G. Giupponi, and G. D. Fabritiis, "ACEMD: accelerating biomolecular dynamics in the microsecond time scale", *Journal of Chemical Theory and Computation,* vol. 5, p. 1632, 2009.
[154] D. A. Pearlman, D. A. Case, J. W. Caldwell, W. S. Ross, T. E. Cheatham, S. DeBolt, D. Ferguson, G. Seibel, and P. Kollman, "AMBER, a package of computer programs for applying molecular mechanics, normal mode analysis, molecular dynamics and free energy calculations to simulate the structural and energetic properties of molecules", *Computer Physics Communications,* vol. 91, p. 1, 1995.
[155] W. S. Young, N. A. Nystrom, and M. Schneider, "CHARMM-Molecular Dynamics", *http://www.ch.embnet.org/MD_tutorial/*.
[156] S. Plimpton, "Fast Parallel Algorithms for Short-Range Molecular Dynamics", *Journal of Computational Physics,* vol. 117, p. 1, 1995.
[157] LAMMPS-Website, *http://lammps.sandia.gov/*, 2009.
[158] H. J. C. Berendsen, D. van der Spoel, and R. van Drunen, "GROMACS: a message-passing parallel molecular dynamics implementation", *Computer Physics Communications,* vol. 91, p. 43, 1995.
[159] D. W. Cohen, "A theoretical study of the surface diffusion of large molecules. I. n-alkane-type chains on W(100)", *Journal of Chemical Physics* , vol. 97 (2), p. 1531, 1992.
[160] G. Ehrlich and F. G. Hudda, "Atomic View of Surface Self-Diffusion: Tungsten on Tungsten", *The Journal of Chemical Physics,* vol. 44, p. 1039, 1966.
[161] T. T. Tsong and R. Casanova, "Migration behavior of single tungsten atoms and tungsten diatomic clusters on the tungsten (110) plane", *Physical Review B* vol. 22, p. 4632 1980.

[162] K. D. Dobbs and D. J. Doren, "Transition state theory description of surface self-diffusion: Comparison with classical trajectory results", *Journal of Chemical Physics,* vol. 80, p. 5832, 1984.
[163] K. D. Dobbs and D. J. Doren, "Dynamical corrections to transition state theory for multistate systems: Surface self-diffusion in the rare-event regime", *Journal of Chemical Physics,* vol. 82, p. 80, 1985.
[164] K. Haug, O. Wahnistorm, and H. Metiu, "Hydrogen motion on a Cu surface: A model study of the rate of single and double site-to-site jumps and the role of the motion perpendicular to the surface", *Journal of Chemical Physics,* vol. 90, p. 540, 1989.
[165] K. D. Dobbs and D. J. Doren, "Dynamics of molecular surface diffusion: Origins and consequences of long jumps", *Journal of Chemical Physics,* vol. 97, p. 3722, 1992.
[166] M. Schunack and T. R. Linderoth, "Long jumps in the surface diffusion of large molecules", *Physical Review Letters,* vol. 88, p. 156102, 2002.
[167] W. D. Cornell, P. Cieplak, C. I. Bayly, I. R. Gould, K. M. Merz, D. M. Ferguson, D. C. Spellmeyer, T. Fox, J. W. Caldwell, and P. A. Kollman, "A second generation force field for the simulation of proteins, nucleic acids, and organic molecules", *Journal of the American Chemical Society,* vol. 117, p. 5179, 1995.
[168] W. Gropp, E. Lusk, N. Doss, and A. Skjellum, "A high-performance, portable implementation of the MPI message passing interface standard", *Parallel computing,* vol. 22, p. 789, 1996.
[169] D. W. Brenner, O. A. Shenderova, J. A. Harrison, and S. J. Stuart, "A second-generation reactive empirical bond order (REBO) potential energy expression for hydrocarbons", *Journal of Physics: Condensed Matter,* p. 783, 2002.
[170] Z. Xu and M. J. Buehler, "Geometry Controls Conformation of Graphene Sheets: Membranes, Ribbons, and Scrolls", *ACS Nano,* vol. 4, p. 3869, 2010.
[171] C. Veigel and C. F. Schmidt, "Friction in Motor Proteins", *Science,* vol. 325, p. 826, 2009.
[172] R. Guerra, U. Tartaglino, A. Vanossi, and E. Tosatti, "Ballistic nanofriction", *Nat Mater,* vol. 9, p. 634, 2010.
[173] W. D. Luedtke and U. Landman, "Slip Diffusion and Lévy Flights of an Adsorbed Gold Nanocluster", *Physical Review Letters,* vol. 82, p. 3835, 1999.
[174] I. V. Lebedeva, A. A. Knizhnik, A. M. Popov, O. V. Ershova, Y. E. Lozovik, and B. V. Potapkin, "Fast diffusion of a graphene flake on a graphene layer", *Physical Review B,* vol. 82, p. 155460, 2010.
[175] K. Tahara, S. Lei, J. Adisoejoso, S. De Feyter, and Y. Tobe, "Supramolecular surface-confined architectures created by self-assembly of triangular phenylene-ethynylene macrocycles via van der Waals interaction", *Chemical Communications,* vol. 46, p. 8507, 2010.
[176] W.-J. Lee, S.-P. Ju, and H.-C. Chen, "Effect of Surface Structure on the Dynamical Behavior of an Aromatic Carboxylic Acid Molecule on Au Surfaces", *Journal of Physical Chemistry C,* vol. 113, p. 5573, 2009.
[177] J. J. Benítez, J. A. Heredia-Guerrero, F. M. Serrano, and A. Heredia, "The Role of Hydroxyl Groups in the Self-Assembly of Long Chain Alkylhydroxyl Carboxylic Acids on Mica", *Journal of Physical Chemistry C,* vol. 112, p. 16968, 2008.

[178] W. R. Browne and B. L. Feringa, "Making molecular machines work", *Nat Nano,* vol. 1, p. 25, 2006.
[179] Q. Liu, S. Du, Y. Zhang, N. Jiang, D. Shi, and H.-J. Gao, "Surfaces: Identifying Multiple Configurations of Complex Molecules on Metal Surfaces (Small 6/2012)", *Small,* vol. 8, p. 795, 2012.
[180] I. Calvo-Almazán, S. Miret-Artés, and P. Fouquet, "A theoretical study of rotational and translational diffusion dynamics of molecules with a six-fold point symmetry adsorbed on a hexagonal lattice by neutron scattering", *Journal of Physics: Condensed Matter,* vol. 24, p. 104007, 2012.
[181] F. Buchner, J. Xiao, E. Zillner, M. Chen, M. Röckert, S. Ditze, M. Stark, H.-P. Steinrück, J. M. Gottfried, and H. Marbach, "Diffusion, Rotation, and Surface Chemical Bond of Individual 2H-Tetraphenylporphyrin Molecules on Cu(111)", *Journal of Physical Chemistry C,* vol. 115, p. 24172, 2011.
[182] A. Maiti, L. A. Zepeda-Ruiz, R. H. Gee, and A. K. Burnham, "Vapor Pressure and Sublimation Rate of Molecular Crystals: Role of Internal Degrees of Freedom", *Journal of Physical Chemistry B,* vol. 111, p. 14290, 2007.
[183] A. Idrissi, P. Damay, S. Krishtal, and M. Kiselev, "Analysis of the Effect of Translation−Rotation Coupling on Diffusion along the Molecular Axes", *Journal of Physical Chemistry B,* vol. 110, p. 18560, 2006.
[184] S. Pai and D. Doren, "Dynamics of molecular surface diffusion: energy transfer between adsorbate modes", *Surface Science,* vol. 291, p. 185, 1993.
[185] K. D. Dobbs and D. J. Doren, "Dynamics of molecular surface diffusion: Energy distributions and rotation--translation coupling", *Journal of Chemical Physics,* vol. 99, p. 10041, 1993.
[186] P. Fouquet, M. R. Johnson, H. Hedgeland, A. P. Jardine, J. Ellis, and W. Allison, "Molecular dynamics simulations of the diffusion of benzene sub-monolayer films on graphite basal plane surfaces", *Carbon,* vol. 47, p. 2627, 2009.
[187] A. S. de Wijn, "Internal degrees of freedom and transport of benzene on graphite", *Physical Review E,* vol. 84, p. 011610, 2011.
[188] M. Jafary-Zadeh, C. D. Reddy, V. Sorkin, and Y.-W. Zhang, "Kinetic nanofriction: a mechanism transition from quasi-continuous to ballistic-like Brownian regime", *Nanoscale Research Letters,* vol. 7, p. 148, 2012.
[189] J. Jellinek and D. Li, "Separation of the energy of overall rotation in any N-body system", Phys. Rev. Lett., vol. 62, p. 241, 1989.
[190] C.-A. Irene and et al., "Questions arising for future surface diffusion studies using scattering techniques—the case of benzene diffusion on graphite basal plane surfaces", *Journal of Physics: Condensed Matter,* vol. 22, p. 304014, 2010.
[191] P. Barthelemy, J. Bertolotti, and D. S. Wiersma, "A Levy flight for light", *Nature,* vol. 453, p. 495, 2008.
[192] Y. Maruyama, "Temperature dependence of Lévy-type stick-slip diffusion of a gold nanocluster on graphite", *Physical Review B,* vol. 69, p. 245408, 2004.
[193] P. A. Gravil, M. Devel, P. Lambin, X. Bouju, C. Girard, and A. A. Lucas, "Adsorption of C_{60} molecules", *Physical Review B,* vol. 53, p. 1622, 1996.
[194] S. B. Legoas, R. Giro, and D. S. Galvão, "Molecular dynamics simulations of C_{60} nanobearings", *Chemical Physics Letters,* vol. 386, p. 425, 2004.

[195] M. Porto, M. Urbakh, and J. Klafter, "Atomic Scale Engines: Cars and Wheels", *Physical Review Letters,* vol. 84, p. 6058, 2000.
[196] G. Paolicelli, M. Rovatti, A. Vanossi, and S. Valeri, "Controlling single cluster dynamics at the nanoscale", *Applied Physics Letters,* vol. 95, p. 143121, 2009.
[197] R. M. Bowman and K. B. Eisenthal, "The role of translational friction in isomerization reactions", *Chemical Physics Letters,* vol. 155, p. 99, 1989.
[198] R. M. Overney, E. Meyer, J. Frommer, D. Brodbeck, R. Luthi, L. Howald, H. J. Giintherodt, M. Fujihira, H. Takano, and Y. Gotoh, "Friction measurements on phase-separated thin films with a modified atomic force microscope", *Nature,* vol. 359, p. 133, 1992.
[199] I. V. Lebedeva, A. A. Knizhnik, A. M. Popov, O. V. Ershova, Y. E. Lozovik, and B. V. Potapkin, "Diffusion and drift of graphene flake on graphite surface", *The Journal of Chemical Physics,* vol. 134, p. 104505, 2011.
[200] A. Einstein, "On the movement of small particles suspended in a stationary liquid demanded by the molecular-kinetic theory of heat", *Annalen der Physik (Leipzig),* vol. 17, p. 549, 1905.
[201] M. Saxton and K. Jacobson, "SINGLE-PARTICLE TRACKING:Applications to Membrane Dynamics", *Annual Review of Biophysics and Biomolecular Structure,* vol. 26, p. 373, 1997.
[202] I. Gralinski and T. W. Ng, "Brownian rod scheme in microenvironment sensing", *AIP Advances,* vol. 2, p. 012180, 2012.
[203] H. Lockie, S. McLean, and R. R. Dagastine, "Hindered Diffusion of an Oil Drop Under Confinement and Surface Forces", *Journal of Physical Chemistry Letters,* vol. 2, p. 2472, 2011.
[204] M. Cappelezzo, C. A. Capellari, S. H. Pezzin, and L. A. F. Coelho, "Stokes-Einstein relation for pure simple fluids", *The Journal of Chemical Physics,* vol. 126, p. 224516, 2007.
[205] S. G. Brush, "Theories of Liquid Viscosity", *Chemical Reviews,* vol. 62, p. 513, 1962.
[206] J. E. Jones, "On the Determination of Molecular Fields. I. From the Variation of the Viscosity of a Gas with Temperature", *Proceedings of the Royal Society of London. Series A, Containing Papers of a Mathematical and Physical Character,* vol. 106, p. 441, 1924.
[207] W. Lang, S. Sokhansanj, and F. Sosulski, "Modelling the temperature dependence of kinematic viscosity for refined canola oil", *Journal of the American Oil Chemists' Society,* vol. 69, p. 1054, 1992.
[208] V. Bormuth, V. Varga, J. Howard, and E. Schäffer, "Protein Friction Limits Diffusive and Directed Movements of Kinesin Motors on Microtubules", *Science,* vol. 325, p. 870, 2009.
[209] A. Barreiro, R. Rurali, E. R. Hernández, J. Moser, T. Pichler, L. Forró, and A. Bachtold, "Subnanometer Motion of Cargoes Driven by Thermal Gradients Along Carbon Nanotubes", *Science,* vol. 320, p. 775, 2008.
[210] T. Sato, N. Iwahara, N. Haruta, and K. Tanaka, "C_{60} bearing ethylene moieties", *Chemical Physics Letters,* vol. 531, p. 257, 2012.

[211] J. M. Sancho, A. M. Lacasta, K. Lindenberg, I. M. Sokolov, and A. H. Romero, "Diffusion on a Solid Surface: Anomalous is Normal", *Physical Review Letters*, vol. 92, p. 250601, 2004.
[212] T. Li, S. Kheifets, D. Medellin, and M. G. Raizen, "Measurement of the Instantaneous Velocity of a Brownian Particle", *Science*, vol. 328, p. 1673, 2010.
[213] E. H. Cook, M. J. Buehler, and Z. S. Spakovszky, "Mechanism of friction in rotating carbon nanotube bearings", *Journal of the Mechanics and Physics of Solids*, vol. 61, p. 652, 2012.
[214] R. Huang, I. Chavez, K. M. Taute, B. Lukic, S. Jeney, M. G. Raizen, and E.-L. Florin, "Direct observation of the full transition from ballistic to diffusive Brownian motion in a liquid", *Nat Phys*, vol. 7, p. 576, 2011.
[215] P. D. Fedele and Y. W. Kim, "Direct Measurement of the Velocity Autocorrelation Function for a Brownian Test Particle", *Physical Review Letters*, vol. 44, p. 691, 1980.
[216] R. Kubo, "The fluctuation-dissipation theorem", *Reports on Progress in Physics*, vol. 29, p. 255, 1966.
[217] A. E. Filippov, A. Vanossi, and M. Urbakh, "Rotary motors sliding along surfaces", *Physical Review E*, vol. 79, p. 021108, 2009.
[218] P. Utko, R. Ferone, I. V. Krive, R. I. Shekhter, M. Jonson, M. Monthioux, L. Noé, and J. Nygård, "Nanoelectromechanical coupling in fullerene peapods probed by resonant electrical transport experiments", *Nature Communications*, vol. 1, p. 37, 2010.
[219] Y. Li Huang, Y. Lu, T. C. Niu, H. Huang, S. Kera, N. Ueno, A. T. S. Wee, and W. Chen, "Reversible Single-Molecule Switching in an Ordered Monolayer Molecular Dipole Array", *Small*, vol. 8, p. 1423, 2012.
[220] D. M. Eigler, C. P. Lutz, and W. E. Rudge, "An atomic switch realized with the scanning tunnelling microscope", *Nature*, vol. 352, p. 600, 1991.
[221] K. Y. Kwon, K. L. Wong, G. Pawin, L. Bartels, S. Stolbov, and T. S. Rahman, "Unidirectional Adsorbate Motion on a High-Symmetry Surface: "Walking" Molecules Can Stay the Course", *Physical Review Letters*, vol. 95, p. 166101, 2005.
[222] Y. Shirai, A. J. Osgood, Y. Zhao, K. F. Kelly, and J. M. Tour, "Directional Control in Thermally Driven Single-Molecule Nanocars", *Nano Letters*, vol. 5, p. 2330, 2005.
[223] K. L. Wong, G. Pawin, K. Y. Kwon, X. Lin, T. Jiao, U. Solanki, R. H. J. Fawcett, L. Bartels, S. Stolbov, and T. S. Rahman, "A Molecule Carrier", *Science*, vol. 315, p. 1391, 2007.
[224] M. Cuberes, "Room temperature repositioning of individual C_{60} molecules at Cu steps: Operation of a molecular counting device", *Applied Physics Letters*, vol. 69, p. 3016, 1996.
[225] A. J. Heinrich, C. P. Lutz, J. A. Gupta, and D. M. Eigler, "Molecule Cascades", *Science*, vol. 298, p. 1381, 2002.
[226] J. D. Meindl, Q. Chen, and J. A. Davis, "Limits on Silicon Nanoelectronics for Terascale Integration", *Science*, vol. 293, p. 2044, 2001.

[227] E. R. Kay, D. A. Leigh, and F. Zerbetto, "Synthetic Molecular Motors and Mechanical Machines", *Angewandte Chemie International Edition,* vol. 46, p. 72, 2007.
[228] M. T. Cuberes, R. R. Schlittler, and J. K. Gimzewski, "Room-temperature repositioning of individual C_{60} molecules at Cu steps: Operation of a molecular counting device", *Applied Physics Letters,* vol. 69, p. 3016, 1996.
[229] J. A. Theobald, N. S. Oxtoby, M. A. Phillips, N. R. Champness, and P. H. Beton, "Controlling molecular deposition and layer structure with supramolecular surface assemblies", *Nature,* vol. 424, p. 1029, 2003.
[230] J. Lu, P. S. E. Yeo, C. K. Gan, P. Wu, and K. P. Loh, "Transforming C_{60} molecules into graphene quantum dots", *Nature Nanotechnology,* vol. 6, p. 247, 2011.
[231] J. O. Sofo, A. M. Suarez, G. Usaj, P. S. Cornaglia, Hern, aacute, A. D. ndez-Nieves, and C. A. Balseiro, "Electrical control of the chemical bonding of fluorine on graphene", *Physical Review B,* vol. 83, p. 081411, 2011.
[232] A. Ranjbar, M. S. Bahramy, M. Khazaei, H. Mizuseki, and Y. Kawazoe, "First-principles study of structural stability, magnetism, and hyperfine coupling in hydrogen clusters adsorbed on graphene", *Physical Review B,* vol. 82, p. 165446, 2010.
[233] Q. X. Pei, Y. W. Zhang, and V. B. Shenoy, "A molecular dynamics study of the mechanical properties of hydrogen functionalized graphene", *Carbon,* vol. 48, p. 898, 2010.
[234] M. J. Saxton, "A Biological Interpretation of Transient Anomalous Subdiffusion. I. Qualitative Model", *Biophysical journal,* vol. 92, p. 1178, 2007.
[235] M. Jafary-Zadeh, C. D. Reddy, V. Sorkin, and Y. W. Zhang, "Kinetic nanofriction: A mechanism transition from quasi-continuous to ballistic-like Brownian regime", *Nanoscale Research Letters,* vol. 7:148, 2012.
[236] A. Tarasenko and L. Jastrabik, "Diffusion of particles on an inhomogeneous disordered square lattice with two non-equivalent sites", *Surface Science,* vol. 602, p. 2975, 2008.
[237] M. J. Saxton, "Lateral diffusion in an archipelago. Single-particle diffusion", *Biophysical journal,* vol. 64, p. 1766, 1993.
[238] M. Khazaei, M. S. Bahramy, A. Ranjbar, H. Mizuseki, and Y. Kawazoe, "Geometrical indications of adsorbed hydrogen atoms on graphite producing star and ellipsoidal like features in scanning tunneling microscopy images: Ab initio study", *Carbon,* vol. 47, p. 3306, 2009.
[239] C. D. Reddy, Q. H. Cheng, V. B. Shenoy, and Y. W. Zhang, "Interfacial properties and morphologies of graphene-graphane composite sheets", *Journal of Applied Physics,* vol. 109, p. 054314, 2011.
[240] T. Benesch, S. Yiacoumi, and C. Tsouris, "Brownian motion in confinement", *Physical Review E,* vol. 68, p. 021401, 2003.
[241] T. S. Kim and R. H. Dauskardt, "Molecular Mobility under Nanometer Scale Confinement", *Nano Letters,* vol. 10, p. 1955, 2010.
[242] C. D. Reddy, Q. H. Cheng, V. B. Shenoy, and Y. W. Zhang, "Interfacial properties and morphologies of graphene-graphane composite sheets", *Journal of Applied Physics,* vol. 109, p. 054314, 2011.

[243] Z. Sun, C. L. Pint, D. C. Marcano, C. Zhang, J. Yao, G. Ruan, Z. Yan, Y. Zhu, R. H. Hauge, and J. M. Tour, "Towards hybrid superlattices in graphene", *Nature Communications*, vol. 2, p. 559, 2011.
[244] K. Tanigaki, S. Kuroshima, and T. W. Ebbesen, "Crystal growth and structure of fullerene thin films", *Thin Solid Films*, vol. 257, p. 154, 1995.
[245] K. Tanigaki, T. Ichihsdhi, T. Ebbesen, S. Kuroshima, S. Iijima, H. Hiura, and H. Takahashi, "Structures and Properties of C_{60} & C_{70} Thin Films Fabricated by Organic MBE," in *MRS Proceedings*, 1992.
[246] M. Dienwiebel, G. S. Verhoeven, N. Pradeep, J. W. M. Frenken, J. A. Heimberg, and H. W. Zandbergen, "Superlubricity of Graphite", *Physical Review Letters*, vol. 92, p. 126101, 2004.
[247] R. Cantrell and P. Clancy, "A computational study of surface diffusion of C_{60} on pentacene", *Surface Science*, vol. 602, p. 3499, 2008.

Appendix: List of Publications

- **M. Jafary-Zadeh**, C.D. Reddy, Y.W. Zhang, "Effect of rotational degrees of freedom on molecular mobility and surface diffusion", *J. Phys. Chem. C*, vol. 117, p. 6800, 2013.
- **M. Jafary-Zadeh**, C.D. Reddy, Y.W. Zhang, "Effect of temperature on kinetic nanofriction of a Brownian adparticle", *Chem. Phys Lett.*, vol. 570, p. 70, 2013.
- **M. Jafary-Zadeh,** C.D. Reddy, Y.W. Zhang, "A chemical route to control molecular mobility on graphene", *Phys. Chem. Chem. Phys.*, vol. 14, p. 10533, 2012.
- **M. Jafary-Zadeh**, C.D. Reddy, V. Sorkin, Y.W. Zhang, "Kinetic nanofriction: a mechanism transition from quasi-continuous to ballistic-like Brownian regime", *Nanoscale Res. Lett.*, vol. 7, p. 148, 2012.
- C.D. Reddy, **M. Jafary-Zadeh**, Y.W. Zhang, "Tracer and collective surface diffusion of benzene on graphene and graphite", (preparation).
- **M. Jafary-Zadeh**, C.D. Reddy, Y.W. Zhang, "Molecular thermal-induced motion on graphene nanoroads", (preparation).